STUDYING LONG AND SHORT-TERM AIRBORNE PARTICULATE MATTER OVER THE ARABIAN PENINSULA

BY

MOHAMMED HAMOUD ALOTAIBI

A Thesis Presented to the

DEANSHIP OF GRADUATE STUDIES

KING FAHD UNIVERSITY OF PETROLEUM & MINERALS

DHAHRAN, SAUDI ARABIA

In Partial Fulfillment of the
Requirements for the Degree of

MASTER OF SCIENCE

In

ENVIRONMENTAL SCIENCES

FEBRUARY 2019

KING FAHD UNIVERSITY OF PERTOLEUM & MINERALS

DHAHRAN- 31261, SAUDI ARABIA

DEANSHIP OF GRADUATE STUDIES

This thesis, written by **MOHAMMED HAMOUD ALOTAIBI** under the direction of his thesis advisor and approved by his committee, has been presented to and accepted by the Dean of Graduate Studies, in partial fulfillment of the requirements for the degree of **MASTER OF SCIENCE** in **ENVIRONMENTAL SCIENCE.**

Thesis Committee

B.S. Tawabini 14/4/2019

Thesis Advisor
Dr. Bassam S. Tawabini

14/4/2019

Department Chairman
Dr. Abdullatif Al-Shuhail

Member
Dr. Ashraf M. Farahat

Dean of Graduate Studies
Dr. Salam A. Zummo

Member
Dr. Mohammad H. Omar

17/4/19

Date

[Dedicated to my lovely and supporting parents and family]

ACKNOWLEDGMENTS

This work is dedicated to all those who have at any point in time believed in me and pushed me towards the limits of excellence.

I would like first to thank Allah for his innumerable gifts and blessings upon me with. I wish to thank and express my sincere gratitude to my dear parents and my family members for their continuous support and encouragements.

I would like to acknowledge and duly express my gratitude to my academic and thesis advisor Dr. Bassam Tawabini, and the committee members Dr. Ashraf Farahat, and Dr. Mohammad Hafidz Omar who have immensely contributed to my knowledge and for engendering my keen interest in research and academic investigation.

I also wish to thank KFUPM represented by the Deanship of Graduate Studies, for giving me the opportunity to pursue my postgraduate studies. Furthermore, I would also like to acknowledge with much appreciation the assistance rendered by Dr. Abdulaziz Al-Shaibani and Dr. Mohammed Makkawi for facilitating all difficulties encountered during my study in KFUPM.

Lastly, I would like to thank Dr. Abduljamiu Amao for his wonderful support and effort for the use of KFUPM labs and research facilities. I also wish to appreciate Mr. Eyad Safi, and Mr. Tajudeen Oyehan for all the help I received during the analysis stage at the Hydrology and Environmental Science Laboratory.

TABLE OF CONTENTS

LIST OF TABLES

LIST OF FIGURES

LIST OF ABBREVIATIONS

ACF	**:**	Auto-Correlation Function
PACF	:	Partial Auto-Correlation
AE	:	Angstrom Exponent
AERONET	:	Aerosol Robotic Network
AIRS3	:	Atmospheric Infrared Sounder
AMSU-A	:	Advanced Microwave Sounding Unit
ANN	:	Artificial Neural Network
AOD	:	Aerosols Optical Depth
AOT	:	Aerosol Optical Thickness
AP	:	Arabian Peninsula
APM	:	Airborne Particulate Matter
AQG	:	Air Quality Guidelines
AQI	:	Air Quality Index
ARIMA	:	Auto-Regressive Integrated Moving Average
ASTE	:	Advanced Space Thermal Emission
CART	:	Climatology, Criteria, Classification & Regression Tree
CERES4	:	Clouds and the Earth's Radiant Energy System

EPA	:	Environmental Protection Agency
FESEM	:	Field Emission Scanning Electron Microscopy
GCC	:	Gulf Cooperation Council Countries
HSB2	:	Humidity Sounder for Brazil
ICP-MS	:	Inductively Coupled Plasma Mass Spectrometry
KAUST	:	King Abdullah University of Science and Technology
KC	:	KAUST Campus
KFUPM	:	King Fahd University of Petroleum and Minerals
KSA	:	Kingdom of Saudi Arabia
MISR	:	Multi-Angle Imaging Spectroradiometer
MODIS	:	Moderate-Resolution Imaging Spectroradiometer
MOPITT2	:	Measurements of Pollution in the Troposphere
MZ	:	Mezaira
N	:	Number of Observations
NASA	:	National Aeronautics and Space Administration
NCDC	:	National Cooperative Development Corporation
p	:	Statistical Indices
PCR	:	Principal Component Regression

PM	:	Particulate Matter
PME	:	Presidency of Meteorology and Environment
RC	:	Royal Commission
RCJY	:	Royal Commission for Jubail and Yanbu
SC	:	Solar Center
SDA	:	Spectral De-Convolution Algorithm
SV	:	Solar Village
t	:	Statistical Indices of the two-pair t-test
TN	:	Terra North
TOMS	:	Total Ozone Mapping Spectrometer
TS	:	Terra South
UAE	:	United Arab Emirates
VOC	:	Volatile Organic Compound
WHO	:	World Health Organization
XRD	:	X-Ray Diffraction Spectrometer
XRF	:	X-Ray Fluorescence Spectrometer

ABSTRACT

Full Name : [MOHAMMED HAMOUD ALOTAIBI]

Thesis Title : [STUDYING LONG AND SHORT-TERM AIRBORNE PARTICULATE MATTER OVER THE ARABIAN PENINSULA]

Major Field : [ENVIRONMENTAL SCIENCES]

Date of Degree : [FEBRUARY 2019]

In recent years, air pollution has been of special importance because of its potential danger to the environment. This study investigates the distribution of long and short-term airborne particulate matter over the Arabian Peninsula using data gathered from AERONET Ground-Based Stations, Space-Borne Sensors, and Real-Time Ground Monitoring stations. The study also examines the morphological and chemical characteristics of APM using SEM/EDXS; XRD; XRF; FTIR and ICP instruments. Importantly, the study predicts the future trends of PM using mathematical models. Results from ground monitoring stations (AERONET) and satellite (Terra/ MODIS) analysis showed that the increase in particulate matter concentration over the East and Center of the Arabian Peninsula can be attributed to the increase in natural particles; while the increase in the particulate matter over the West and South of the Peninsula can be attributed to the increase in man-made particles. It showed that the trend for particulate matter concentration over the five regions increased with time, although in uneven percentages. The percentages are 58%, 15%, 13%, 8%, and 6% in the Central, Western, Southern, Northern and Eastern regions, respectively. However, the same results also showed that the trend for man-made particulate matter decreased over time by 29%, 28% and 21% in the Northern, Central and Eastern Regions, respectively. Conversely, it increased significantly in the Western (72%)

and Southern (18%) regions. SEM showed that the average size of particles in Jubail city (1.4 - 2.8 µm) is smaller than Ras Tanura (5 - 7 µm). Although, in both cities, the particle shape is irregular and spherical, it is accompanied by many clusters deposited in different spots on the Jubail filters. XRF showed that the APM collected over Jubail Industrial City contains zinc, barium, sulfur, sodium, and potassium in higher concentrations than the APM collected over Ras Tanura. Conversely, Ras Tanura APM samples have a higher concentration of calcium, chlorine, aluminum, iron, and magnesium. The XRD analysis revealed that the APM is composed of silica, koktaite, mascagnite, and calcium carbonate. The analysis of trace metals using the ICP-MS showed that the levels of lithium, cobalt, vanadium, arsenic, silver, manganese, nickel molybdenum, copper, chromium, cadmium, and lead, are within the regulatory authority limits. R-Studio showed that particulate matter concentration over the Central region is increasing. This will be followed by a decrease until the end of 2030. However, over the north area, the predicated values indicated that there was an overall increase in the particulate matter concentration followed by a significant drop in 2020 which will continue until 2030. Lastly, over the south area during 2019, a rise in particulate matter concentration was followed by a decrease starting from mid-2019 until the fourth quarter of the same year. After that, the mean values will keep fluctuating as we move forward to 2030.

ملخص الرسالة

الاسم الكامل: محمد حمود العتيبي

عنوان الرسالة: دراسة الجسيمات طويلة وقصيرة المدى المنقولة جواً فوق شبه الجزيرة العربية

التخصص: علوم البيئة

تاريخ الدرجة العلمية: فبراير 2019]

خلال السنوات العشرون الماضية، اكتسب تلوث الهواء أهمية بالغة؛ وذلك بسبب الخطورة التي قد يتسبب بها على كل من البيئة وصحة الإنسان. ولهذا أُجرِيت هذه الدراسة للتحقيق في التوزيع المكاني والزماني للجسيمات المحمولة جواً – الطويلة وقصيرة المدى – وذلك فوق شبة الجزيرة العربية باستخدام بيانات تم الحصول عليها من خلال شبكة محطات قياس الهباء الجوي الروبوتيك "ايرونت"، وأجهزة استشعار التصوير الطيفي الراديو مترية المحمولة فوق أقمار فضائية صناعية تعرف بـ "تيرا"، بالإضافة الى أجهزة قياس أرضية تعتمد في عملها على المرشحات حيث يتم تمرير الهواء عبرها ليترسب كل ما هو محمول جواً فيها. ويتركز هذا البحث – أيضاً – على دراسة الخصائص الشكلية والكيميائية، وذلك باستخدام أجهزة تحليل عدة وهي: المجهر الإلكتروني الماسح، حيود الأشعة السينية، فلورية الأشعة السينية وطيف الانبعاث الذري/ بلازما. بالإضافة إلى أنه تم التنبؤ بتراكيز هذه الجسيمات على مدار السنوات القادمة حتى عام 2030 وذلك بالاستعانة ببرامج رياضية تعتمد على الانحدار المتوسط المتحرك المتكامل والذي يعرف بـ "أريما". أظهرت نتائج تحليل بيانات شبكة محطات قياس الهباء الجوي الروبوتيك "ايرونت" وأجهزة استشعار التصوير الطيفي الراديو مترية المحمولة فوق أقمار فضائية صناعية تعرف بـ "تيرا" أن هناك ارتفاعًا في تراكيز الجسيمات فوق كل من المنطقتين الشرقية والوسطى من شبة الجزيرة، وتعزى هذه الزيادة الى زيادة الجسيمات ذات النشأ الطبيعي. بالإضافة لذلك، فقد كان هناك – أيضاً – ارتفاع في تراكيز هذه الجسيمات على كل من المنطقتين الغربية والجنوبية، ولكن هذه المرة فقد عزى هذا الارتفاع إلى الزيادة في الجسيمات ذات النشأ البشري "الناتج عن الأنشطة البشرية المختلفة". وبصورة عامة، فإن تراكيز الجسيمات في كل مناطق شبة الجزيرة التي شملتها هذه الدراسة هي في ارتفاع، ولكن بنسب مئوية متفاوتة. النسب هي 58 ٪، 15 ٪، 13 ٪، 8 ٪ و6 ٪ في كل من المناطق الوسطى، الغربية، الجنوبية، الشمالية والشرقية، وذلك على التوالي. غير

أن النتائج نفسها أظهرت أن هناك انخفاضًا في تراكيز الجسيمات ذات النشأ البشري وذلك بنسب 29٪، 28٪ و21٪ في كل من المناطق الشمالية، الوسطى والشرقية على التوالي. وعلى العكس فقد لوحظ زيادة كبيرة في التراكيز على كل من المناطق الغربية (72 ٪) والجنوبية (18 ٪). وتظهر نتائج تحليل العينات باستخدام جهاز المجهر الإلكتروني الماسح أن متوسط حجم الجسيمات فوق مدينة الجبيل يتراوح ما بين 1.4 و2.8 ما يكرون، وهي أصغر من نظائرها فوق مدينة رأس تنورة حيث تراوحت ما بين 5 و7 ما يكرون وذلك على الرغم من أن أشكال الجسيمات غير منتظم، بل كروي ومصحوب بعديد من التكتلات على أماكن متفرقة من المرشحات خاصة في منطقة الجبيل. وبرهنت نتائج التحليل باستخدام جهاز فلورية الأشعة السينية على وجود عناصر الزنك، الباريوم، الكبريت، الصوديوم، والبوتاسيوم وذلك بتراكيز أعلى في مدينة الجبيل منها في رأس تنورة. وبالمقابل، فإن تراكيز عناصر الكالسيوم، الكلور، الألومنيوم، الحديد والمغنيسيوم هي الأعلى في مدينة رأس تنورة. وباستخدام جهاز حيود الأشعة السينية اتضح أن العينات في كلتا المدينتين تحتوي على السليكا، كوكتايت، الماسكجنيت وكربونات الكالسيوم. وتوصلت – أيضاً – نتائج التحاليل باستخدام جهاز طيف الانبعاث الذري/ بلازما إلى أن تراكيز العناصر الثقيلة: الليثيوم، الكوبالت، الفناديوم، الزرنيخ، الفضة، المنغنيز، النيكل، الموليبديوم، النحاس، الكروم، الكادميوم والرصاص هي في حدود التعرض المسموح بها من قبل السلطات التنظيمية "الهيئة الملكية بالجبيل وينبع". وفيما يتعلق بالتكهن بالنتائج المستقبلية، فإن نتائج التنبؤ باستخدام برامج رياضية تعتمد على الانحدار المتوسط المتحرك المتكامل تعرف بـ "أريما" أشارت إلى أن تراكيز الجسيمات في المنطقة الوسطى ازداد بمرور الوقت ولكنها سوف تنخفض وذلك حتى أواخر عام 2030. وفي المنطقة الشمالية سيكون هناك زيادة في التراكيز ومن ثم انخفاض كبير وذلك بحلول عام 2020 وسيستمر هذا الانخفاض حتى عام 2030. وفي المنطقة الجنوبية وخلال عام 2019، سيكون هناك – أيضاً – ارتفاع يتبعه انخفاض، حيث سيبدأ في منتصف عام 2019 حتى الربع الرابع من نفس العام، وتبقى القيم المتوسطة متقلبة بمرور الوقت حتى وصولنا عام 2030.

CHAPTER 1

INTRODUCTION

1.1 The Particulate Matter (PM) or Aerosols

Pollution is a major concern for environmentalists and professionals working in industry. This is due to the growing industrialization level and the impact it has on air, land, and water. Saudi Arabia is located between (17°N–30°N) and (36°E–55°E) covering an area of more than two million km^2 or roughly 80% of the Arabian Peninsula's total area. It is one of the countries that is heavily affected by massive industrial activity, especially in the petrochemical industries and the refining sectors. The country's location within the sub-tropical belt is known for its harsh climate and arid lands with an average rainfall of 92 mm per year, excluding the region of Jizan (El-Askary, and Al-Shaibani, 2015). Keeping this in mind, it is considered as a major source of atmospheric dust due to the presence of extended desert areas where sandstorms are very frequent, especially during certain seasons of the year.

The vast drylands and dune spans present an immense source of atmospheric dust and Aerosols or Particulate Matter (PM). Often, PM mix to form complex mixtures of different particles that have different chemical compositions containing sea salt, organic carbon, dust, sulfate, black carbon, etc. Power and water desalination plants, intensive construction activities, and the increasing number of vehicles are the most common factors accelerating man-made emissions. In addition, sulfur dioxide (SO_2) and nitrogen oxides

(NO_x) emitted from industrial sites react with water vapor to produce sulfuric and nitric acids and thus result in acid rain that can destroy buildings, rocks, streets, soil, etc. Consequently, these increase the rate of corrosion. Moreover, a major concern associated with PM released into the air is their small size, which enables suspension into the atmosphere englobing dirt, dust, smoke, liquid droplets, and soot, which are mostly generated from industrial activities. These are mixed with heavy toxic materials and pollutants capable of being transferred from one place to another. In addition, the frequent and common sandstorms and particle mixing scenarios could strongly contribute to the change of the PM characteristics and to the weather conditions over the Arabian Peninsula. Aina and Alshuwaikhat (2014) revealed that biomass and coal burning activities are adding more aerosol particles (organic components and absorbing soot) into the air in Asia. In the Arabian Peninsula, the issue is not only related to the nature of the land in many areas but also to the rapid development of industries and petrochemical plants in various areas, especially in the Eastern and Western regions of Saudi Arabia. Many human activities have led to an increase in the pollutants in the atmosphere such as cement production, oil refining, power, and desalination plants (Farahat, 2016; Al-Jeelani, 2013). In addition, ship movement in the Arabian Gulf and the discharge of volatile organic compounds (VOC) contribute to the spread of pollutants in the air (Farahat et al., 2016; Farahat, El-Askary, and Al-Shaibani, 2015). It is worth mentioning that the Particulate Matter levels have always influenced by precipitation and monsoon circulation. These events play a major role in transporting dust loaded in the air during later summer from East Africa and the Arabian Peninsula (Zhao, 2015). More so, favorable climatic and geospatial factors, along with the nature of winds in the Arabian Peninsula, are

factors that aggravate the suspended particles and volatile compounds. Shamal wind is generated due to cold cyclones and fronts over the high mountains in Turkey, which then travel through Iraq to the north of Saudi Arabia. Shamal wind is present frequently during the summer season and produces about 3m to 4m of wind waves that transport massive amounts of particles and decrease visibility (Teller at al., 2008).

1.1.1 Effects of the Particulate Matter

The PM aggravates the adverse effects on human health. It can easily travel deep into the body through inhalation and cause various respiratory problems such as lung irritation and asthma. Naturally induced particles are seasonally present due to sea salt and dust storms that happen very frequently (El-Askary and Al-Shaibani, 2015). The growing pace of industrialization in areas such as the petrochemical and refining industries, in addition, to other man-generated aerosols has increased the adverse impact on humans and their environment. However, despite the importance of this subject, only a few studies have been conducted to evaluate the PM in different regions of Saudi Arabia (TAIWO, 2016) and the Arabian Peninsula at large. According to (McCarthy, 2016), the World Health Organization (WHO) reported that the highest levels of small particles were recorded in Asia, the Southeast, and the Mediterranean. The cities of Riyadh and Al-Jubail in Saudi Arabia have recorded PM_{10} levels almost 18 times the WHO recommended level of 20 µg/ m^3, while Dammam City reached almost 14 times.

1.1.2 PM Standards

The official publicized standards of PM_{10} around the world can be summarized in the global guidelines presented by the World Health Organization (WHO), like the Air Quality Guidelines on Air Quality for Particulate Matter (2006). The WHO limit for

PM_{10} is less than 20 μg/m^3 for the annual mean and 50 μg/m^3 over a 24-hour mean. The standards established by the United States Environmental Protection Agency (U.S. EPA) set the levels in 1997 and then revised them in 2006.

These standards "limited PM_{10} concentrations to 50 μg/m^3 based on an annual average and 150 μg/m^3 based on a 24-hour average." (EPA, 2018).

Also, the local regulatory authorities in Saudi Arabia, which are represented by the Royal Commission (RC) and the Presidency of Meteorology and Environment (PME), specify the limits of PM_{10} to not exceed 50 μg/m^3 for the annual mean and 150 μg/m^3 for the 24-hour mean, while the PME set a higher limit not exceeding 340 micrograms/m^3 more than once at any location and 80 microgram/m^3 of annual means (RCER-2015, PME).

1.2 Significance of the Study

A study of air pollution over the Arabian Peninsula is imperative to understand the distribution and potential sources of Particulate Matter over the Arabian Peninsula and to evaluate their adverse impact on the environment and human health. Indeed, such studies help to obtain the necessary and beneficial information about the air quality in the Arabian Peninsula. Thus, a database has been built up which later can be used to prevent and reduce the pollution in all its types.

Along with Saudi Arabia's 2030 vision and the expected industrial rise in the country, it is very important to maintain high standards of air quality, conserve human health, and avoid an economic burden that may result from people being affected by poor air quality.

1.3 Research Objectives

The main objective of this research is to study the Particulate Matter over different geographical locations in the Arabian Peninsula based on long-term and short-term measurements. The following are the specific objectives:

1. Determine physical, optical and seasonal Particulate Matter characteristics over several geographical locations in the Arabian Peninsula based on long-term space-borne and ground-based observations.
2. Assess the morphological and mineralogical characteristics of the Particulate Matter over two different cities within the Arabian Peninsula.
3. Predict the future trend of the Particulate Matter using historical data gathered from space-borne and ground-based stations.

CHAPTER 2

LITERATURE REVIEW

2.1 Definition of Particulate Matter and its types

According to Jacobson et al. (2000) and Mohammed et al. (2015), Atmospheric Aerosols (or Particulate Matter) are tiny liquid or solid particles suspended in air. These vary in their origin, shape, formation, and size, as well as the duration of their existence. This has been further explained by Mohammed et al. (2015) in Grivas et al., (2008) and Hering et al. (2003). They confirmed that "the size distribution and chemical compositions of atmospheric particles play significant roles in the transport, transformation, and removal mechanisms of particulate matters. It is therefore understood that Aerosols differ in their nature, measurement techniques, and methods. Yet aerosols are broadly classified into two main categories namely- PM_{10} and $PM_{2.5}$. These particulate matters possess several characteristics and origins, and are of a different size of 10 micrometers or less for PM_{10}, also called Coarse Particulate Matter. While the size of 2.5 micrometers or less for $PM_{2.5}$ is called fine. According to the Australian Department of the Environment and Energy (2018), the chemical nature of these particles or aerosols varies according to their energy. Aerosols can be liquid droplets or industrial dust or gases that are suspended in the air. Aerosols can travel long distances and can be inhaled into the lungs easily.

2.2 Methods of Estimating PM_{10} in Urban Areas

Various methods and techniques are used to estimate the concentration, size, and origin of airborne particles over urban, rural and desert areas and these include ground-based monitoring stations. Other methods use satellite gathered information, complex remote sensing spectrometry, and photometry. These networks monitor and provide a continuous long-term public domain database of microphysical aerosol properties, whether in optical or in radiation terms. Because of these stations, it is possible to have perceptible water and inversion products, as well as the worldwide spread of observations of aerosol optical depth (AOD).

The data generated by the Aerosol Robotic Network is mostly related to three main categories, although it yields more than these. It provides data about the AOD, the Perceptible Water, and the Angstrom Parameter. Han et al. (2015) conducted research to evaluate regional background Particulate Matter. They used various methods for estimating the PM_{10} concentration and chemical characteristics in China. For example, in the year 2009, three-dimensional ultrasonic anemometers were used to measure hourly turbulent fluxes. PM_{10} filter samples were collected at the mentioned heights.

Furthermore, to estimate the chemical composition of PM_{10}, "24 h PM_{10} filter samples were collected using medium-volume PM_{10} at the heights of 10, 40, 120, and 220 m with an automatic sampling system using constant-flow control at a flow rate sampling of 100 L/min." (Han et al. 2015). The PM_{10} filters had two different "samplers for chemical analysis of inorganic composition on polypropylene filters and for organic composition analyses on quartz-fiber filters. Elements such as Si, Ti, Al, Mn, Ca, Mg, Na, K, Cu, Zn,

Pb, Cr, Ni, Co, Fe, and V were identified by Inductively Coupled Plasma atomic emission spectroscopy (ICP/AES). Blank filters were processed simultaneously with sampled filters." (Han et al. 2015).

Other sources, like the EPA (2010) particulate matter urban-focused study on visibility assessment used the Light Extinction Method in estimating PM_{10} and used the Win Haze algorithm to evaluate the impact of different levels of PM concentration on a clear image. "Win Haze analysis synthetically superimposes a uniform haze on a digitized, actual photograph. The Win Haze computer algorithm evaluates the extent of extinction level on the appearance of each individual portion of the photograph." (EPA, 2010).

2.3 Methods of Measuring PM_{10} Using Satellite Data

Remote sensing using satellite measurements of Particulate Matter in the air has been widely accepted as one of the most efficient methods. Most studies use spatiotemporal records of airborne sensors, especially the Multi-Angle Imaging Spectro-radiometer (MISR) and the Moderate Resolution Imaging Spectro-radiometer (MODIS), or the CALIPSO and the LANDSAT ETM^{+} which all use different algorithms according to the targeted particulate matter and other criteria are explained by Othman et al. (2010) who said that "each component such as the path radiances/atmospheric reflectance at different wavelengths and satellite viewing geometries were calculated and archived in a look-up table. During the retrieval process, the path radiances/atmospheric reflectance of each aerosol mixture is calculated and compared with the in-situ data." (Othman et al. 2010).

One research study that was found within Saudi Arabia is that of Al-Harbi et al. (2014) who conducted a study in the Riyadh Area over a period of six years from 1999 to 2004

using a Multi-Angle Imaging Spectro-radiometer (MISR) and a Moderate Resolution Imaging Spectro-radiometer (MODIS). Another study over Saudi Arabia was conducted by Farhat et al. (2016). They used data from airborne sensors/ satellites like MODIS and CALIPSO, along with the AERONET (Aerosol Robotic Network) ground stations measurements, to examine aerosol characteristics from March to May between 2003 and 2010.

Nevertheless, Donkelaar et al. (2010) explain that these satellites have different advantages and limitations. They claim that "the MODIS instrument measures a wide range of spatial and spectral information from its orbit aboard the Terra satellite which is advantageous due to the frequency of measurements." (Donkelaar et al. 2010). As for the MISR, it only allows for much more limited spectral and spatial ranges. This, however, allows it to be more accurate and focused since it offers perspectives of the land spots from nine distinct angles. This helps in minimizing "algorithmic assumptions and retrieval bias" (Donkelaar et al. 2010). The problem, however, is that none of these satellite tools can retrieve AOD information when the weather is cloudy. Other researchers have raised the issue that certain algorithmic adjustments often have to be done, especially in bright areas with high reflection rates such as deserts and arid lands where the deep blue algorithm set-up is used. In addition, Gupta et al. (2009) revealed that satellites can only generate columnar spot, and surface values of PM concentration cannot be obtained unless there is a clear vertical distribution of the aerosols. This means that if the PM is suspended in the air and the satellite registers AOD values, this might not be captured by the ground monitors.

Higgs et al. (2015) investigated the connection of aerosol presence and asthma issues in Athens, Greece and highlighted that out of 366 days in 2004, they were only able to get

99 MODIS generated images that were suitable for the study. This was due to inappropriate attitudinal aspects of the MODIS tool and the non-availability of images. They revealed that "the list of useful images is often less than the number of theoretically possible observations for a variety of technical and physical reasons. For example, such factors as technical problems with sensor systems, characteristics of the air mass itself, and intervening media such as cloud cover have traditionally contributed to limitations on the completeness of remotely sensed data." (Higgs et al., 2015). In addition, the algorithms which interpret satellite images can in many ways handicap accurate analysis of the available images due to resolution limitations and computational capacity.

2.4 Models Used to Calculate and Predict the Concentration of PM_{10}

According to Daly and Zanetti (2007), two approaches were used to calculate PM: a statistical approach and a deterministic one. "The statistical approach relays on the excessive historical measurement of air quality at monitoring stations that are spatially distributed while the deterministic only requires information on meteorological conditions and pollutant sources." (Daly & Zanetti, 2007).

In the prediction of future trends, several methods and approaches are available. These include climatological information, classification, and regression analysis, in addition to neural networks and 3D air quality approaches. The Artificial Neural Network (ANN) model can be explained through the following equation between the neuron input and the output Liu & Li (2015).

$$a = f(wp + b) \qquad (2.1)$$

Where:

a = Neuron output, f = Transfer function, w = Input weight, p = Neuron input, and b = a constant for one-unit input.

Another model "The Regression" allows calculating the interdependence between one or more dependent variables and one independent variable. It can create data for an input layer of ANN (Badoghpour, Hashemi, and Haghshenas, 2009). This model is generally used with a statistical framework to give indicators on the origins and the causes of the different types of aerosols. Liu & Li (2015) presented a more focused version of this under the name of the Autoregressive Integrated Moving Average (ARIMA) Model. The stochastic sequence also called the time series data to study the prediction of an object. This sequence is fitted with some mathematical models. Once this model is identified, the future values would be predicted by the time series of past and present values." (Liu & Li, 2015). The third model is called the "Time Series" and is based on the retrieval and analysis of stored data to predict trends, forecast climatic and weather changes, in addition to being used to predict trends in Aerosol transfer and range. It is also widely used for extending hydrologic data records. Furthermore, it is used to estimate and generate missing data. (Soltani, Modarres and Eslamian, 2007). The time series model often reveals close observations in terms of time. Close observations are usually more closely related than distant observations.

Furthermore, the models will overwhelmingly make use of the natural one-way ordering of time, so that values for a given period will be expressed as deriving in some way from past values rather than future values (Soni, Parmar and Kapoor, 2014). Sigrid and Teigen (2015) claimed that the prediction of future trends can be described in probabilistic

terms and could lead to different expectations for future expansions. Also, based on trends that people have observed in the past, they can at best make predictions about the future. This method can be used in econometrics, statistics, weather forecasting, signal processing, earthquake prediction, trajectory forecasting, intelligent transport pattern recognition, and many other applications. In their study, they mainly used "Linear Regression" to describe the relationships between independent variables indicated by X and a scalar dependent variable Y. Also, they used Multilayer Perceptron to plot sets of input data into a set of suitable outputs. Their prediction shows that PM levels are going to increase by 45.90% in the future. Kumar and Goyal (2011) have used the principal component regression (PCR) technique, which was developed using a multilayer perceptron neural network, to forecast a short–term daily Air Quality Index (AQI) using previous data (2000 to 2005) and meteorological info. The study targeted different seasons (winter, spring, summer, and fall). The authors verified that the used model gave better results in winter than in the other seasons.

In Tehran city, Bahari, Abbaspour and Pahlavani (2014) also used the multilayer perceptron neural network. They used a novel method with a history of data from 2012 to 2013 to predict particulate matter (PM2.5) concentration during the next 72 hours. Input data included PM2.5 concentration, temperature inversion strength, ambient temperature, wind speed, relative humidity, wind direction, and cloud cover which was collected from the Mehrabad synoptic station. Their result indicated the capability of the model to predict the future trend of particles. García et al. (2016) validated the estimated ANN AOD time series from 1941 to 2001 against coincident AOD measurements obtained during

the period from 2004–2009 and 1984–2009 from different devices. The analysis shows a good agreement daily.

Using MODIS long-term AOD_{550} observations from March 2000 to December 2012, Soni, Singh, Bano, Tanwar, and Nath (2011) carried out an assessment of air quality by targeting the coal mines in India. They forecasted the AOD values for a three_year period from January 2013 to December 2015. The authors claimed that many studies were conducted to predict the concentrations of air pollutants in the future such as sulfate dioxide, nitrogen dioxide, ozone, and carbon monoxide instead of AOD loading. An Auto-Regressive Integrated Moving Average (ARIMA) model was fitted to time series data to forecast the values during the upcoming years.

2.5 Using AOD and AE to Calculate PM_{10}

2.5.1 The Aerosol Optical Depth (AOD)

This is an effective tool to estimate quantities of pollution in the atmosphere. AOD is usually used as a quantitative index to indicate aerosol concentrations in the atmosphere using ground-based stations, and satellites (Yu et al., 2013). AOD surveys the extinction of direct-beam radiation over different wavelengths and then restores the contribution of aerosol to total extinction (Hamasha, Abu Mostafaa, and Alexander, 2012). Aerosol Robotic Network (AERONET) is one of the most important tools to measure AOD. AERONET is a reliable ground-based AOD measurement source that is designed to gain more accurate air quality evaluations by verifying the generated results with data gathered by satellites (Holben et al., 1998). Data sets of AOD can also be retrieved using OMI, MISR, MODIS, and SeaWiFS. These are spaceborne sensors with different re-

trieval instruments, viewing geometry, and instrument design which have been developed to retrieve density and aerosol property data in the atmosphere. Khalil et al. (2015) said that these sensors give different measurements which are suitable for cross verification, and therefore, better results. Again, the Aerosol Optical Depth (AOD) can be defined as the quantitative measure of solar radiation extinction through aerosol absorption and dispersion between the upper atmospheric boundaries and the observation point by both the Ground-Based Sun-Photometry technique and satellite intercommunication systems. Broadly, over desert regions, higher AOD values indicate high concentrations of dust particles, and therefore, they increase impairment visibility events (Hamasha, Abu Mostafaa, and Alexander, 2012). Usually, Optical Depth is measured downwards from the top of the atmosphere, so that $T_{top} = 0$ and an Aerosols Optical Depth greater than 1 indicates high aerosol loadings in the atmosphere / severe pollution. Table 1 shows the values of AOD and what the values indicate.

Work carried out by Salinas, Chew, and Liew (2009) explained that the Atmospheric Optical Depth (columnar) can be measured based on the direct Sunlight intensity using a Sun-Photometer and AOD. This is explained by the law of Beer/Lambert and Bourger:

$$F(\lambda) = Fo(\lambda) \times 10Ke(\lambda)\, m(\xi) \qquad (2.2)$$

Where:

$F(\lambda)$= the solar irradiance that is monochromatic and which reaches the sensor at wavelength, F_o = Irradiance at the top of the atmosphere (Used also to set the device), K_e = Total attenuation (or extinction) coefficient, and m = Optical air mass (a function of the solar zenith angle ξ).

Salinas, Chew, and Liew (2009) continued to explain that the calculation of the AOD can be affected by the different wavelengths or bands selected during the measurements. They explained that a Sun-photometer was conducted over of several spectrum ranges, where every band has a well-defined central wavelength.

2.5.2 The Angstrom Exponent (AE)

Analysis of the Angstrom Exponent (AE) describes the AOD dependency at different wavelengths to identify particle size; the smaller the particles are, the higher the exponent indicator. However, when the Angstrom value is greater than or equal to one, the particle refers to "Fine Mode Aerosols" and to "Coarse Mode Aerosols" if the value is smaller than one (Dayou, Chang, and Sentian, 2014). Table 2 below shows the relationship between each mode and the Angstrom Exponent value which explain how sources, formation, composition, solubility, travel distance and the lifetime of particles can be estimated (Wilson and Suh, 1997).

Table 1. Optical Depth Value and its relationship with Aerosols

Optical Depth	Aerosol Loadings	Pollution	Example
Greater than one	High	Severe	SA storms, Heavy Emissions
Less than one	Low	Moderate	Mixed Aerosol

Table 2. Relationship between particle modes and Angstrom Exponent

Angstrom Exponent	Aerosol Size Distribution (Diameter)	Mode	Example
Values near ZERO	Greater than 2.5 µm	Coarse	Desert dust
Equal or greater than One	Smaller than 2.5 µm	Fine	Smoke particles and sulfates

2.6 Previous works on PM 0ver the Arabian Peninsula

King Müller et al. (2016), along with Farahat, ElAskry and Dogan (2016), and many others, have conducted field studies over Saudi Arabia, and the Middle East in general, to find out the concentrations, characteristics and sources of Aerosol or "Particulate Matter" during different periods and events. Many other research works have also been done in this area, but more focused on a single city or isolated events like sand storms or the Shamal Wind. For example, Saeed, Dashti and Spyrou (2014) studied the aerosol's optical and physical characteristics and direct radiative forcing during a Shamal dust storm on the 26th and 27th of March of 2003. In the following section, more specific literature is reviewed for Saudi Arabia.

Many studies have been conducted over Saudi Arabia because of the preoccupying nature and concentration of air pollution and Particulate Matter in the vast deserts of the kingdom or over highly industrialized cities like Jubail and Yanbu. Several studies have been done on air quality in the Riyadh region like Rushdi, Mutlaq & Simoneit, (2013) and in

Makkah and the Jeddah region like Othman, Jafri & San, (2010), as well as Shaltout et al., (2013) who studied Taif city among many others.

King Müller et al. (2016) used the MODIS instrument over the period between 2000 and 2015 and found out that the AOD trend over the Arabian Peninsula and Saudi Arabia was high, as shown in "Figure 1".

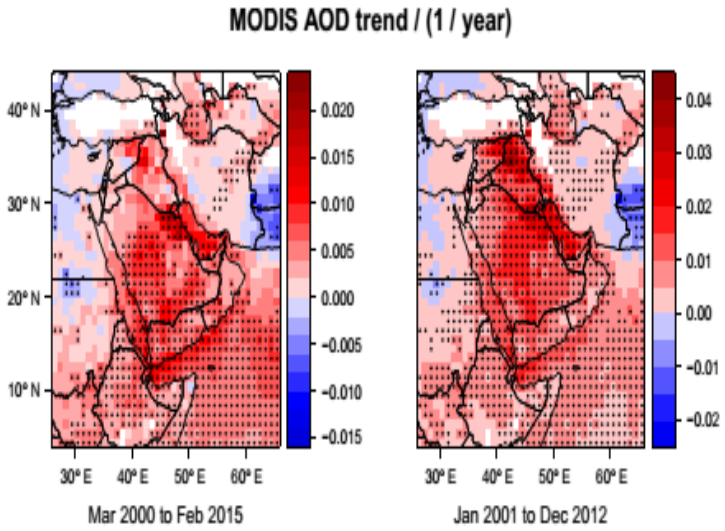

Figure 1. MODIS AOD trend over the Middle East (2000-2015) KingMüller et al. (2016)

Other research works like Saeed et al. (2014), who specifically targeted the Shamal Wind driven sand storm event of the 26th and 27th of March of 2003, found out that during this particular event "dust concentrations reached 4800 µg m^3 on 26 March and fluctuated around 1000 µg/m^3 throughout the following day. Ground-based measurements of AOT reached 3.617 on the 26th March and 4.17 on the 27th March with the corresponding Angstrom coefficient $\alpha = 870/440$ dropping to −0.0234 and −0.0318 respectively reflecting the dominance of coarse-sized particles PM_{10}." (Saeed et al. 2014)

Farahat, Askary, and Dongan (2016), also studied the Aerosols' size distribution characteristics and the role of precipitation during dust storm formation over Saudi Arabia. They focused their observations using MODIS and CALIPSO, along with AERONET ground observations to study aerosol characteristics during the March–May season over the span of eight years from 2003 to 2010 in Saudi Arabia. Their study showed that the levels of Particulate Matter were rather stable until 2009. They found out that "the mean angstrom exponent during March–May 2003 to 2008 was found to be ~17% higher than the same period during 2009." (Farahat, Askary & Dongan, 2016). This is mainly due to the huge dust storm that occurred on the 9^{th} and 10^{th} of March 2009. In the study, the angstrom exponent observed in 2004 indicated the dominance of fine-mode particles $PM_{2.5}$, while the angstrom exponent decreased in the years 2005, 2006, 2007, and 2008. The aerosols' size distribution measured by sun-photometer indicates a maximum value of ~47% higher in 2009, suggesting the domination of coarse mode particles PM_{10}." (Farahat, Askary & Dongan, 2016)

Farahat (2016) presented a more comprehensive study on air pollution; its causes and effects, as well as aerosol categorization in the Arabian Peninsula (Saudi Arabia, the United Arab Emirates, Kuwait, Qatar, Bahrain, and Oman). He concluded that the mentioned countries share several characteristics and their sources of pollution are mainly climate related. This is mainly due to the presence of frequent seasonal large-scale sandstorms during the spring season facilitating fine particle transport. In addition, the growing anthropogenic sources are due to the growing industrialization in this area and massive "fossil fuel burning, water desalination, and heavy traffic near big cities are some of the

major factors that contribute to the sulfur and nitrogen dioxide emissions in addition to the fine particulate matter".

Another study by Al-Harbi assessed the CO, O_3, SO_2, H_2S, $PM_{2.5}$ and NO_2 concentration levels over Riyadh city for six consecutive years (1999-2004). He found that all these pollutants increased with time except Hydrogen Sulfide (H_2S) and Sulfur Dioxide (SO_2) (Alharbi, Pasha and N, 2014). However, the study showed that inhabitants were affected 29% of the time mostly by Particulate Matters (PM_{10}) and Sulfur Dioxide (SO_2), while O_3 and CO made a smaller contribution.

In an earlier study of Aerosol Optical Depth (AOD) efficiency by Yu et al. (2013), the team performed an assessment of spatial-temporal variations in atmospheric dust over Saudi Arabia from 2000 to 2010 using qualitative station dust observations, ground-based AOD measurements, and remotely sensed AOD. They claimed that the dust loading spatial and temporal variations have always been a concern for society and that there was no way to reduce or prevent the negative impact of dust storms. This might be traced back to a lack of understanding the variations of AOD that take place due to a limited number of weather stations distributed over the country since the 1980s. Moreover, they mentioned that many studies used a Total Ozone Mapping Spectrometer (TOMS) and proved that dust aerosols are higher over eastern Saudi Arabia during the spring and summer seasons. In addition, this study confirmed the reliability of AOD, especially over desert regions.

In fact, the authors started examining the seasonal cycle by identifying favorable wind conditions and dust activities over the east and center of the peninsula. The authors obtained data from the MISR instrument database from March 2000 to December 2010, the

MODIS instrument from May 2002 to December 2010, the NCAR database, the NCDC database, and ground-based stations AOD at 500 nm.

These ground-based stations are Solar Village, Hamim, Sde Boker, Mezaira, Kuwait University, and Dhadnah. Data was collected starting from January 2000 to December 2010, June 2004 to July 2007, November 1996 to July 2011, March 2004 to November 2008, November 2007 to June 2010, April 2004 to June 2010, for the aforementioned stations, respectively.

Also, from the NCDC database weather observations were collected for the period of January 2000 to December 2010 from 26 weather stations distributed in Saudi Arabia.

The results reflect the similarity of AOD values between the MODIS AOD and the MISR AOD. However, in desert regions the MISR showed higher values and this might be due to low sensitivity to the properties of APM over bright surfaces.

Rub'al Khali was observed to be higher in dust levels among the remaining areas, while in Makkah and Jeddah there was moderate station dust frequency, which might be due to rare experiences of dust storms, or to the low number of available observations by MODIS and MISR.

When it comes to seasonal comparisons, a higher AOD was observed in the spring season across the northwest of Saudi Arabia. Lower levels were found in the central region during the summer season and then in the southern deserts.

Over a nine-year period (2001 to 2010), Munir et al. (2016) detailed and clearly quantified temporal trends and the spatial variability of $PM_{2.5}$. At the regional level, the western and eastern coastal borders of Saudi Arabia had higher levels of AOD, followed by the south-east region, and then the north region.

In a similar way to the western and eastern coastal borders, the southwest region had higher levels of $PM_{2.5}$ and the reason is expected to be because of the proximity of the region to particles sources that include seawater where salt aerosols are constantly emitted into the atmosphere, and vast Saudi deserts, commercial and industrial areas, along with the busiest areas, and volcanoes. At the city level, Dammam City is highly affected by Particulate Matter ($PM_{2.5}$), while Tabuk City has the lowest concentration of $PM_{2.5}$.

In like manner, many other studies investigated the chemical composition of the atmospheric particulate matter ($PM_{2.5}$) that travels over Taif city to identify the origins of these particles and formation methods (e.g. primary or secondary). As a result, Black Carbon (BC), urban industrial operations, wealthy merchant families, pilgrims, vehicle emissions, metallurgical activities, blacksmithing, and the non-optimal management of solid waste facilities were the main sources identified (Hamasha, Abu Mostafaa, and Alexander, 2012). Another work was conducted by TAIWO (2016). His work was limited to the Eastern Province of Saudi Arabia and aimed to examine the elemental composition, and the morphological and mineralogical characteristics of PM_{10} in three different cities (Dhahran, Khobar, and Dammam). PM_{10} samples over two months (October – December 2015) were collected using an Ecotech HiVol-3000 sampler with a PM_{10} size selective inlet and analyzed through multiple analyzers. Consequently, it was proved that the size and shape of the particles varied from one location to another, and this denotes the expected influences of spatial and temporal variations. Exceeding the maximum allowable limit was noticed also. Different standards were used after obtaining the data to evaluate compliance, as shown in the result of his study.

CHAPTER 3

RESEARCH METHODOLOGY

3.1 Description of Study Area

According to Engel et al. (2011), "The Arabian Peninsula encompasses a total area of 2.7 million km^2 and is thus the largest peninsula on Earth." Its boundaries are made of the Red Sea on the western and southwestern parts and the Arabian Sea in the south and southeastern parts, while the Arabian Gulf limits it from the northeastern side. The northern border of the Arabian Peninsula (part of Saudi Arabia) shares a land border with Iraq and Jordan. The peninsula is made of Yemen, Oman, the United Arab Emirates, Qatar, Kuwait and Bahrain in the center, while the major part of it is Saudi Arabia with an area of about 2.1 million Km^2. Figure 2 illustrates the different parts of the Arabian Peninsula, as well as the political borders between the states. Saudi Arabia is the largest country within the Peninsula and covers more than two thirds of it. Because it is located directly on the Tropic of Cancer in the subtropical high-pressure belt, the peninsula has one of the most arid and most extensive deserts in the world with the dominance of "monotone sand and rock deserts with extremely few water resources, as well as numerous oases and elevated regions with lush vegetation." (Engel et al. 2011). In the Middle East, Saudi Arabia possessed the highest number of minerals (Mehdi, Reza, Ahmad, & Omid, 2016). In addition, the western region of Saudi Arabia is the home of various minerals including; iron, aluminum, zinc, copper, silver, chromium tungstate, manganese, tin, and gold etc.

More so, the eastern part of the country contains minerals including salt, sulphur, mica, and feldspar. Saudi Arabia is also a source of highly prized rare earth elements such as tantalum - of which it has a quarter of the world's reserves - and niobium." (Industrial Investors' Guide, 2016). However, for the time being, the most important commodity that Saudi Arabia has in abundance is fossil fuel (oil) which was discovered in the early 1930s, since it sits on about 25% of the world's known recoverable oil reserves that reach up to 266.4 billion barrels (Oamen Festus, 2019). In addition, the kingdom enjoys a very advanced industrial network of plants and factories in various fields, especially in the petrochemical sector. Saudi Arabia has developed over 40 industrial cities comprising around 7000 factories and plants mostly active in the petrochemical sector under the MODON authority. The Royal Commission for Jubail and Yanbu (RCJY) manages four world class industrial cities located in Saudi Arabia; Jubail, Ras Alkhair on the East coast, Jazan Economic City and Yanbu on the West coast. Jubail and Yanbu are fully developed, stand-alone cities, hosting widely diversified industries from petrochemical, mineral and synthetic material producers to downstream and finished products." (Industrial Investors' Guide, 2016).

Figure 2. Map showing the Arabian Peninsula.

3.2 Approaches Followed for PM_{10} Assessment over the Arabian Peninsula

To fulfill the first and second objectives, two approaches have been followed:

1. Approach 1: to understand the trends, physical, optical, and seasonal characteristics of the airborne particulate matter (PM_{10}), satellite data was obtained and analyzed over the South, North, East, West, and Center of the Arabian Peninsula.
2. Approach 2: to assess the morphological and chemical characteristics of the airborne particulate matter (PM_{10}), samples were collected in two industrial areas in the Eastern part of Saudi Arabia, namely: Jubail and Ras Tanura.

3.2.1 Approach 1: Trends and Levels of PM_{10} Using Satellite Data

3.2.1.1 The Centre of Arabian Peninsula (Solar Village Station)

The Solar Village Station has 15.288 years (5580 days) of operational time at the site. It exists in the center of the Arabian Peninsula at a latitude of 24.90693° north, and a longitude of 46.39729° east, and is posted at an elevation of 764.0 meters. This instrument is located 50 km northwest of the city of Riyadh. It is worth noticing that it has the largest powered electricity generating system among all the stations around the world. The Solar Village station is operated and monitored by the laboratories of the King Abdul-Aziz City for Science and Technology. This station covers the center of the Arabian Peninsula and continuously monitors the particles passing through the area. The present map "Figure 4" shows its location. The following pictures "Figure 3" give more detail on the exact location of the solar village.

Figure 3. Aerial View of the Solar Village (Google Maps, 2018) and Location map of the Solar /Village showing the distance from Riyadh. (Google Maps, 2018)

Figure 4. Location Map of AERONET Station (Google Maps, 2018)

3.2.1.2 East of Arabian Peninsula (Mezaira Station)

The Mezaira is another station located in the Arabian Peninsula. The station is operated and monitored by the Department of Water Resources Studies in the United Arab Emirates (UAE). It continuously monitors the particles passing over the instrument area. The station location is shown in "Figure 4".

3.2.1.3 West of Arabian Peninsula (KAUST Campus Station)

The King Abdullah University for Science and Technology (KAUST) AERONET station exists in the western region of Saudi Arabia with a latitude of 22.30483° north, and a longitude of 39.10283° east, and has spent about 5.079 years (1854 days) of operational time on the site. Its elevation is around 11.2 meters and it is located on the rooftop of the seashore building in a rural region of the King Abdullah University of Science and Technology Campus.

In 2010, the project received a ranking by the American Committee on the Environment as “one of the top ten Green Projects” (Wikipedia, 2018). The following map shows the location of the Solar Center (KSC) "Figure 4".

3.2.1.4 North and South of Arabian Peninsula

Due to the unavailability of AERONET ground-based stations, satellite data were used to obtain the data for the **Northern** and **Southern** parts of the Arabian Peninsula. The satellites are ***Terra and Aqua / MODIS*** and have sixty-three bands of different primary uses. The bands from three to seven were targeted in this study, since they are designated to collect information about the land, cloud and aerosols properties over the Earth.

Terra and Aqua were launched in 1999 and 2002, respectively (Tatem, Goetz and Hay, 2004). In the morning, Terra passes around the Earth from north to south across the equator, whilst the Aqua passes in the afternoon in the opposite direction (south to north) to view the whole Earth's surface every two days and to get data from sixty-three spectral bands. The principle for measurements will be as of ground-based stations in which the AOD is measured. This helps to understand the process of global changes and aggravate the accuracy of our future predictions.

Terra basically passes at an altitude of 705 km (within sun-synchronous orbit; 200 to 1000 km) and an orbital period of 99 minutes which allows for comparing images for a different period over many years. It takes 14 days to cover the whole globe and completely views the Earth's surface. Terra carries five sensors/ instruments; MISR[1] (Multi-angle Imaging Spectroradiometer), MOPITT[2] (Measurements of Pollution in the Troposphere), MODIS[3] (Moderate Resolution Imaging Spectroradiometer), and MODIS[6] (Moderate Resolution Imaging Spectroradiometer). These sensors work continually obtaining information about the Earth and its complex system. Aqua also moves at a latitude of 702 kilometers and an orbital period of 99 minutes (Tatem, Goetz and Hay, 2004).

3.2.2: Approach 2: Morphological and Chemical Characteristics of PM_{10}

3.2.2.1 Jubail and Ras Tanura Cities

Al-Jubail is one of the major industrial cities in Saudi Arabia. It lies on the east coast of Saudi Arabia as part of the Eastern Province "Figure 5". It is directly situated on the Arabian Gulf coast and enjoys a great infrastructure. It is one of the world's largest industrial cities, if not the largest, with a complex of companies and plants including the fourth

largest petrochemical company. The city has the world's largest independent water and power project with a total capacity of 2743.6 MW of electrical power and 800,000 m^3 of desalinated fresh water daily. The major companies present in the city include SABIC with over 20 affiliates, including Saudi Kayan and HADEED (which employ more than 13,000 employees), SADARA, SATORP and SASREF which are two refineries involving a joint venture between Saudi ARAMCO, TOTAL and SHELL. The coordinate of the sampling point is 26.922175, 49.726379 and the map below shows the exact location of Jubail. The importance of Jubail for this study stems from the intensive industrial activity in the area and the high levels of emissions into ambient air.

Ras Tanura is another important city on the eastern coast of Saudi Arabia that enjoys great importance in terms of oil refining and exporting given its outstanding port "Figure 6". It is about 60 km south of Jubail City and north across the Tarut Bay from Dammam. The area has been developed by Saudi ARAMCO due to the abundance of oil reserves in the area. Several offshore and onshore rigs make it one of the most important port cities for oil exports by ARAMCO. Similarly, this city has a high PM indicator and would be interesting for the present study. The coordinate of sampling point in this city is 26.700510, 50.061519.

Figure 5. Location Map of Jubail Industrial City (Google Maps, 2018)

Figure 6. Location Map of Ras Tanura. (Google Maps, 2018)

As for the south, north, center, west, and east of AP, the data were obtained using two means which included ground-based stations (Solar Village, Mezaira, and Kaust-Camp) and satellites sensors (Terra and Aqua / MODIS). All data are readily accessible and available on two websites; (https://aeronet.gsfc.nasa.gov) and (https://modis.gsfc.nasa.gov). However, below is the procedure followed to extract the data: AERONET website:

1. Enter the homepage of AERONET (https://aeronet.gsfc.nasa.gov/).
2. Click on Download Tool of Aerosols Optical Depth Version 2.
3. Change the geographic location to the Middle East and pressed on get country or state.
4. Select the desired station from the list. Solar Village, Mezaira, and KAUST-Camp have been selected individually.
5. Select the start and end dates of the data download. Periods downloaded for each station and satellite as the following
    - Solar Village (Center), 2001 - 2013
    - Mezaira (East), 2004 - 2017
    - KAUST-Campus (West), 2012 - 2018
    - MODIS (North & South), 2000- 2018
6. In Direct Sun Products table, Aerosol Optical Depth (AOD) level 2 with Precipitable Water and Angstrom Parameter Box was checked
7. Daily Average Box was checked and then pressing download.
8. Using the Microsoft Excel program, all downloaded files were extracted and prepared to start the analysis.

3.3 Methods and Procedures of Samples and Data Collection

Air samples were collected from Jubail and Ras Tanura using (i) Thermo Scientific 5030i "Figure 7", a Synchronized Hybrid Ambient Real-time Particulate Monitor and (ii) the Ecotech HiVol-3000 Sampler "Figure 8". The thermo scientific 5030i is easy to operate. To calibrate data using this equipment, the monitor light-scattering nephelometry is checked against the mass concentration of the beta attenuation. The device also offers several advantages such as increased data storage, a large and easy to read interface screen, and superior accuracy and precision. However, the use of other instruments can be attributed to the breakdown of the Thermo Scientific 5030i sampler after two weeks of monitoring in Jubail city. Furthermore, the time and procedures to repair the equipment is another constraint to consider the alternative Ecotech HiVol-3000 Sampler. Hence, the monitoring was continued in Ras Tanura using the Ecotech HiVol-3000 Sampler. The Ecotech HiVol 3000 sampler possessed advanced features which include: electronic volumetric flow control that permits consistent flow and collects a real sample of particulate matters. Furthermore, the device incorporates programming functions.

The collection of Particulate Matter (PM_{10}) samples from Jubail and Ras Tanura was carried out over a two-week period in each city.

Figure 7. Thermo Scientific 5030i

Figure 8. Ecotech HiVol-3000

In Jubail City, particulate matter (PM_{10}) samples were collected from the 19th of May to the 1st of June 2018 as per the following procedure:

1. Identify a safe and suitable location of sampling, in addition to the availability of reliable electrical power source.
2. Prepare the site and install the unit using its installation manual, which includes providing a portable cooling unit connected to a continuous water flow source, power source and shielding to protect from direct sunlight.
3. Operate the unit for 24 hours to stabilize before collecting the samples.
4. The filter was automatically moved over tape for every 24 hours.
5. After 2 weeks of sampling, the filter was extracted from the unit and packed into different plastic bags.
6. Transfer all filters to KFUPM laboratories for characterization.

In Ras Tanura City, particulate matter (PM_{10}) samples were collected from the 23rd of June to the 2nd of July 2018 as per the following steps:

1. Identify a safe and suitable location of sampling, in addition to the availability of reliable electrical power source.
2. Prepare the site and install the unit following the installation manual.
3. Operate the unit for 24 hours to make sure the unit is clear from pervious sampling particles/ impurities.
4. Obtain the initial filter weight.
5. Insert the filter into the unit and being collect samples.
6. Remove the filter manually from the sampler head and packed it into plastic bags.
7. Transfer the filters to KFUPM laboratories for characterization.

3.3.1 Samples Characterization

Field Emission Scanning Electron Microscopy (FESEM) was used to study the morphological characteristic because it has excellent sensitivity for PM filter samples (Watson et al., 1999). A Rigaku MiniFlex600 X-ray diffraction phase/composition identification (XRD) was used for identifying the mineral composition of the PM_{10} particles. In addition, a PerkinElmer Optima 8000 inductively coupled plasma optical emission spectroscopy (ICP-MS) was utilized to determine the trace metal levels in the samples. Elemental constituents of the PM were carried out using X-Ray Fluorescence Spectrometer (XRF) techniques (Walter M. Gibson, Z. W. Chen, and Danhong Li, 2008).

3.3.1.1 Data Analysis

Numerous approaches have been adopted to characterize the Particulate Matter (PM_{10}) including the identification of morphology, elemental and mineralogical information. A 24-hour mean of ambient air PM_{10} mass concentration during the monitoring period was used by comparing daily averages with the PME, WHO, USEPA and RC Standards.

3.3.1.2 Data Analysis of Ground-Based Stations and Satellites

These data are daily average measurements of the Angstrom Exponent ($\alpha_{440-870}, \alpha_{380-500}, \alpha_{500-870}$) at AOD_{500} between 2001 and 2017 for different geographical locations in the Arabian Peninsula. To study the Particulate Matter (PM_{10}) characteristics, the daily average measurements of Angstrom Exponents at AOD_{500} have been divided based on the available data. Table 3 shows the periods and frequencies used in the analysis. However, to determine the relationship significance and to ensure accurate in-

terpretation of the data, most common statistical indices are applied during the analysis including the mean, median, p- value, t-test, and confidence level.

Table 3. Periods and Frequencies Subjected to the Analysis

	Observation Frequency				
Station/ Sensor Name	Daily	Monthly	Yearly	Seasonally	Two Periods
Solar Village	2001 - 2013				2001- 2006 2007 - 2013
Mezaira	2004 – 2017				2004 - 2011 2012 - 2017
KAUST-Campus	2012 - 2018				2012 - 2014 2015 - 2018
MODIS - Terra	2000- 2018				2000 – 2010 2011 - 2018

During the study period, trend analysis using the **linear regression** of the monthly **mean** and **median** of ($\alpha_{440-870}, \alpha_{380-500}, \alpha_{500-870}$) was also used. Since the air-borne Particulate Matter over the Arabian Peninsula is made of a combination of natural elements and other anthropogenic components in various seasons.

We analyzed the statistical tendencies of fine particles and coarse ones through the analysis of the changes in the Angstrom Exponent (AE) at AOD_{500} for all the available data series ($\alpha_{440-870}$, $\alpha_{380-500}$, and $\alpha_{500-870}$)

Linear regression analysis was used for the period in question based on the mean values for each day, month, year etc.

To describe changes and calculate the percent variation for a sample N (days, months, years) of any of the trend analysis parameters, we applied the formula:

$$Fx(\%) = \frac{a\,N}{\bar{x}} * 100\% \qquad (3.1)$$

Where:

[x**]** is the variable, **[a]** is the slope calculated from the linear regression, **[N]** is the whole number of records in the given period, and [$\bar{x}$] is the average.

Moreover, to avoid outliers, especially for dates where the particle size is minimal or limited, the **median-based analysis** will also be applied, while the linear regression is computed based on the medians. Thus, if the outlier bias is minimal, then the trends from both the median and mean methodologies would not differ significantly.

Median regression analysis is important to catch data outliers during certain periods with limited available data. If there are few data outliers, there will not be a significant discrepancy between the mean and median trends. This technique aims to make results more robust by filtering data outliers.

The statistical significance of the slope was checked by imposing a 95 % confidence level (P-value < 0.05) on all data trends to determine if the study results are statistically significant or not. Moreover, to distinguish how significant the differences are between two groups and to find out if the difference could have happened by chance, we will apply the t-test. In detail, this linear regression result is summarized under the "P-Value" and helps to either accept or reject the null hypothesis based on the threshold value.

Usually, 5% or 1% (0.05 or 0.01) was the level at which the hypothesis was rejected and the observed result would be inconsistent with the assumption. Table 4 below shows an interpretation of different possible p-values.

In our case, if the null hypothesis appears invalid, accordingly, the data denotes having an abnormality.

Table 4. Interpretation of Different Possible p-Values

Level	The presumption against the null hypothesis
$p > 0.1$	NO
$0.05 > p \geq 0.1$	Low
$0.01 > p \geq 0.05$	Strong
$p \leq 0.01$	Very Strong

Another test called the "t-test" helps to compare the means of two sets of data. The big t-value means there is a difference between the groups, but the small value indicates that there is similarity between the groups. If the difference between the two groups is equal or close to zero, the data is not significant statistically. The equation for the t-test works as follows:

$$t = \frac{Difference\ between\ groups}{Sampling\ variability} \tag{3.2}$$

Moreover, to avoid outliers, especially for dates where the sample size is minimal or limited, a median-based analysis is also applied and for that reason, the linear regression is computed based on the medians. In this way, if the outlier bias is minimal, then the trends from both the median and mean methodologies would not differ significantly.

Median regression analysis is important to catch data outliers during certain periods with the limited available data. If there are not many data outliers, there will not be a significant discrepancy between the mean and the median trends. This technique helped to make the results more robust by filtering the data outliers. The statistical significance of the slope was checked by imposing a 95% confidence level (P value < 0.05) on all data trends.

3.3.1.3 Concept of Data Analysis of future trend prediction:

In this study, we used the RStudio Software that becamme available for use in December 2011. RStudio software, like MATLAB, is a programming language for statistical computing and graphics. The **Autoregressive Integrated Moving Average (ARIMA) Model** which regards "the time series data of the prediction object are regarded as a stochastic sequence, and this sequence is fitted with some mathematical models".

The Autoregressive Integrated Moving Average (ARIMA) Model is a tool, which is integrated into RStudio and is always available to download and called upon whenever necessary.

Using the ARIMA, a prediction of the future trend was performed. **Monthly Average Values** for each station/sensor were used individually. Accordingly, anthropogenic and natural trends for Particulate Matter in each geographical location were discovered.

3.3.2 Procedure of Samples and Data Analysis

3.3.2.1 Procedure for Determining the PM_{10} Concentration

For samples collected from Jubail city, the procedure below was followed:

1. Obtaining an hourly average concentration of PM_{10} in microgram/m^3 over the monitoring period. A Thermo Scientific 5030i Monitor was used, and because of that, we were able to extract the data immediately after monitoring from the system with no further calculations or steps required. The data included PM_{10} concentration, ambient and air flow temperature, humidity, vacuum and volume flow rate, nephelometer, and barometric pressure, in addition to other data.

For samples collected from Ras Tanura city, the procedure below was followed:

1. Obtaining the difference between initial and final corrected volumes.
2. Getting the difference between the initial and final weights of used membrane filters using digital balance (Mettler). This step is performed before and after the filters change.
3. Multiply the difference of the filter weights by 10^6.
4. Divide the weight by the change in the corrected volume to obtain PM_{10} concentration in microgram/m^3

For data collected from AERONET Stations and Satellites, the below procedure was followed: (**Note: Each station data was analyzed individually)**

1. Using the Excel Program, data were imported as follows:
    - Data > Get External Data > From Text > Select files downloaded from AERONET website for each year. This step was repeated for each station individually. Data imported include daily average readings of AOT_500, 440-870Angstrom, 380-500Angstrom, 500-870Angstrom, and 340-440Angstrom as well as the Julian date.
2. Data imported were according to the following periods due to availability:
    - Solar Village Station: 2001 – 2013.
    - Mezaira Station: 2004 – 2017.
    - KAUST_Campus Station: 2012 – 2017.
    - Terra Satellite: 2000- 2018.
3. Developing a summary sheet that contains the monthly mean and median for the observation's values during the entire period. This varies from one station and satellite to another based on data availability.
4. In the summary sheet, the actual number of observation days was counted.
5. Data were separated as follows:
    - Daily mean for the whole period.
    - Monthly mean and median for the whole period.
    - Yearly mean and median for the whole period.
    - Two groups (first and second half of the series)
6. Create graphs for all data mentioned in step #4 separately to obtain the slope value.

7. Calculate the following for data mentioned in step #4.
    - Variation percentage using equation 3.
    - P value (Data > Data Analysis > Regression).
    - t- test (Data > Data Analysis > t test: two samples assuming unequal variances). This step has been applied for two groups only.
    - An actual number of observation days.

3.3.2.2 Determining Morphology of the PM samples

To identify the morphology information (size and shape) of the samples collected from Jubail and Ras Tanura, a Field Emission Scanning Electron Microscopy (FESEM) was utilized (Fig. 9).

Figure 9. Field Emission Scanning Electron Microscopy (FESEM) located at KFUPM

For the FESEM/EDX characterization, the following procedure was followed:

1. Select a representative sample for each area (e.g. one for Jubail and another for Ras Tanura).
2. Cut the filters of the selected samples from the middle in 1 mm^2 size to avoid areas where the deposition of PM_{10} is null.
3. Mount the samples on stubs and add colloidal graphite to release earthing for the electrons that are going to be discharged while coating (Fig. 10)
4. Then the samples were coated with a thin layer of gold using a "Gold Sputter Coater" to make the sample conductive (Fig. 11).
5. Immediately after the coating, all samples were transferred to the FESEM to look at the size and shape of the deposited PM_{10}.
6. Images of size and shape were taken 10 times from different spots for each sample.

3.3.2.3 Determining Elemental Composition of PM Samples

To identify the elemental composition of the samples collected from Jubail and Ras Tanura, ann X-Ray Fluorescence Spectrometer (XRF) was employed for this purpose (Fig. 12)

For the XRF characterization, the following procedure was followed:

1. Load the samples into the XRF analyzer.
2. Select five different spots for each loaded sample.
3. Elemental composition was obtained after the analysis and transferred to an excel file.

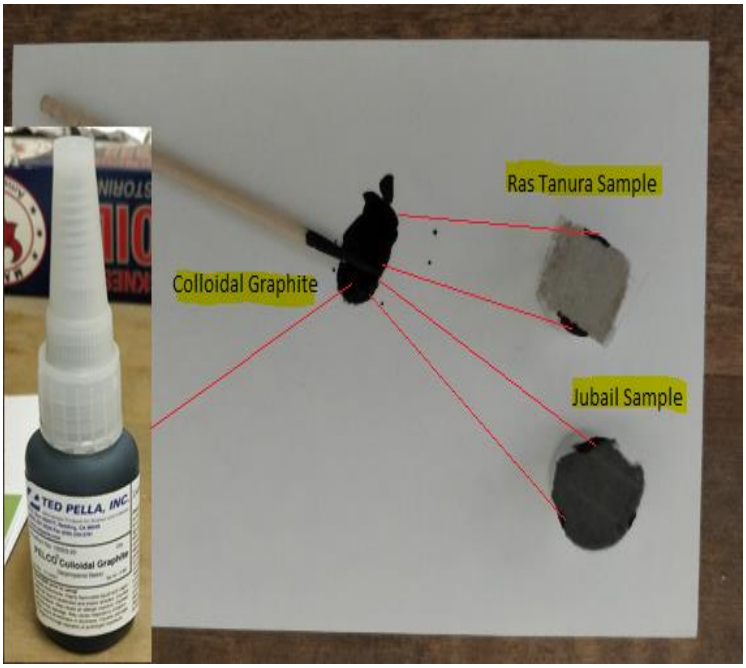

Figure 10. Samples mounted with Colloidal Graphite

Figure 11. Gold Sputter Coater located at KFUPM

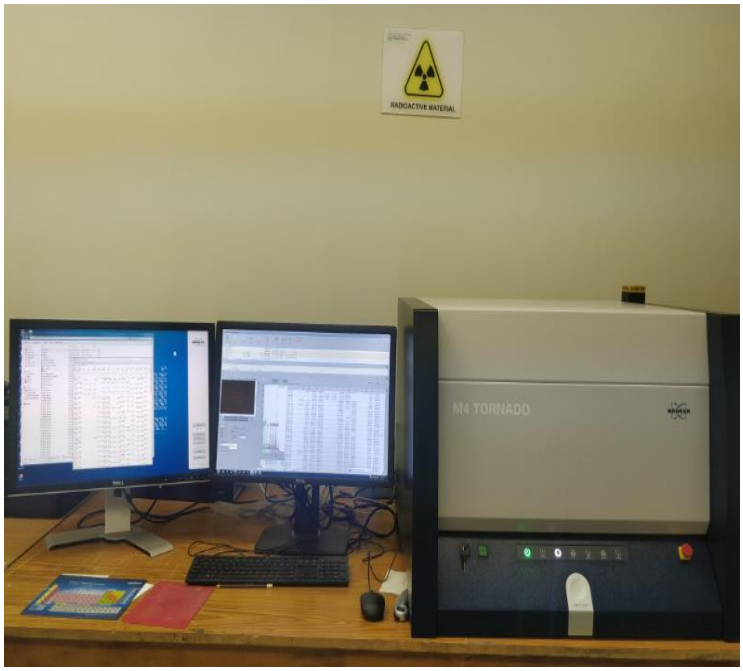

Figure 12. X-Ray Fluorescence Spectrometer (XRF) at KFUPM

3.3.2.4 Determining the Mineral Composition of the PM Samples

To obtain the mineral composition of the samples collected from Jubail and Ras Tanura, an X-ray Diffractometer (XRD was employed (Fig. 13). Steps followed are:

1. Prepare the samples by attaching/ loading them to a flat aluminum holder.
2. A samples holder that contains the loaded filters was placed into the XRD instrument.
3. Run the analysis using the attached PC.
4. Obtain results, which showed different peaks and positions.
5. After obtaining the graphs of the results, the background was adjusted.
6. During mineral identification, the results of the XRF analysis were utilized to come up with a meaningful interpretation.
7. The process was repeated for all samples collected.

Figure 13. X-ray Diffractometer (XRD)

3.3.2.5 Determining the Trace Metal Levels in the PM Samples

PerkinElmer Optima 8000 inductively coupled plasma optical emission spectroscopy (ICP-MS) was for this purpose.

In addition, and before doing the analysis, a microwave digestion system (mars 6) was used to digest all of the samples as required (Fig. 14).

Steps for the ICP/MS analysis were as follows:

1. Prepare all samples (Ras Tanura samples) (Fig. 15).
2. Use mars 6, all samples were digested.
3. Filters were cut out into small pieces in a 100ml glass beaker and wet with some water.

4. Add a 1:3 ratio of distilled HNO3 and concentrated HCl solution with distilled water.
5. Place the breakers on a heater. Heating took 4 hours at 130ºC.
6. Cool the breakers down for a while.
7. Filter all content with another filter paper (size 42).
8. Make the filtrate up to 50ml of volume.
9. Use an acid digest (filtrate) to determine the trace metal using the ICP-MS.

Figure 14. Inductively coupled plasma and microwave digestion system

Figure 15. Samples prepared for ICP analysis

3.3.3 Procedure for Developing ARIMA Model

To forecast future trends based on historical data, a proper model should be selected.

"Figure 16" below reflects the steps required to begin the forecast.

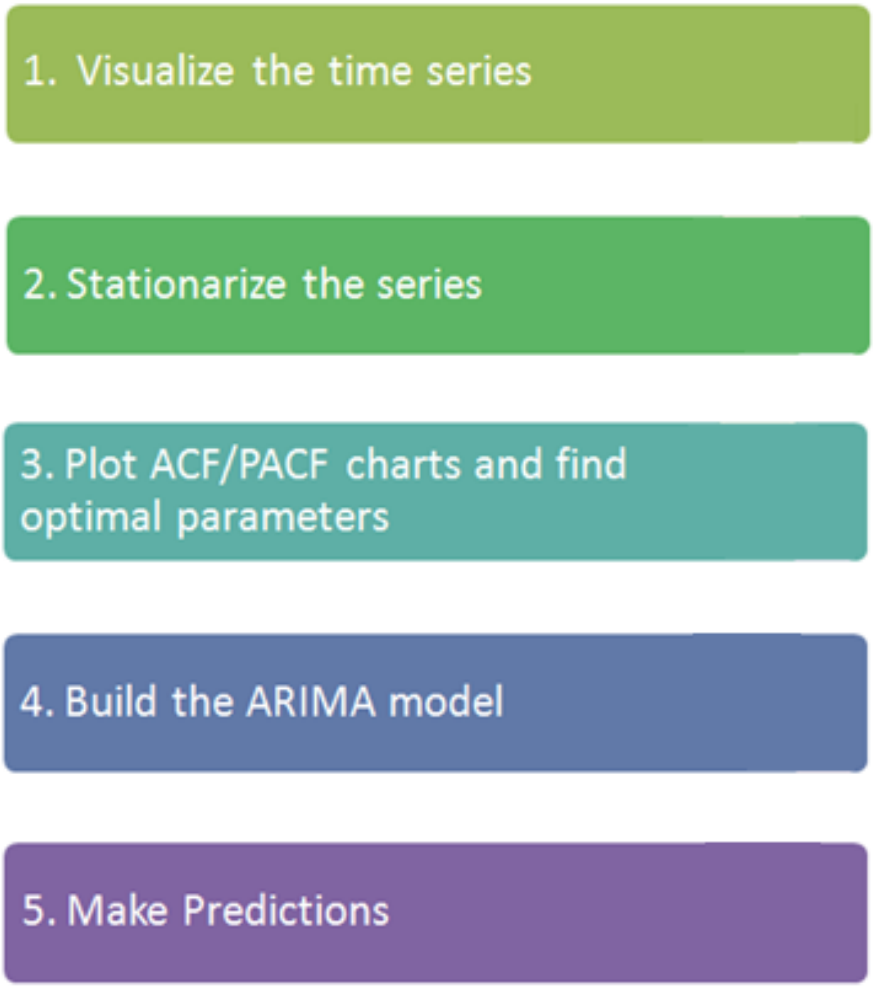

Figure 16. Framework shows systematic approach on 'How to build-up a Time Series Analysis Model (analyticsvidhya.com, 2018)

3.3.3.1 Solar Village Forecasting Steps:

The steps below were implemented during the forecasting process:

1. **Visualize the time series:**

1.1. Decide what data frequency should be selected for the forecasting process. This was achieved by looking at the number of missing (NAs) data in the series.

1.2. Based on step #1, a monthly time series was selected as it has the lowest number of missing (NAs) daily data values.

1.3. Extract the AOD monthly values from the EXCEL file into a txt file in which the series is arranged in one column. A file named Solar.txt contains this data.

1.4. Locate the TimeSeriesData.txt file in a path that the *R Studio* software would look for it later to begin loading the data.

1.5. Launch the *R Studio* software program and load the data from the Solar.txt file. To load the data we typed: Solar <- scan("Solar.txt").

1.6. Because the data, where used, was comprised of monthly observations, we defined the frequency as 12 months and the start date to help the program recognize the data as a time-series formatted data, in addition to giving a specific name to this defined series. Hence, we typed: Solar time-series <- ts (Solar, frequency=12, start=c (2001,1)).

1.7. Produce the plot and visualize the data by writing: plot.ts (Solar time-series).

2. **Stationarize the series:**

2.1. Applying unit root testing (**Dickey Fuller**) to check if the series is stationary or not. This test was carried out by typing:

- library(t-series). Loading the tools required.

- adf.test (Solar time-series, alternative = c ("stationary", "explosive"), k = trunc ((length (Solar time-series)-$12^{1/3}$

2.2. Another test was performed to confirm the stationarity condition. This test is called Kwiatkowski-Phillips-Schmidt-Shin (KPSS). We typed:

- kpss.test (Solar time-series, null = c ("Level", "Trend"), lshort = TRUE)

3. Finding optimal parameters of the ARIMA model:

3.1. To obtain the optimal parameters of the ARIMA model that fit the time series, three different procedures were selected. The procedures include:

- **Partial Autocorrelation Function (PACF).** PACF helps to find how many autoregressive (AR) terms are required to model the time series. By typing: pacf (Solar time-series, plot = T), the procedure is executed.
- **Autocorrelation Function (ACF)**. ACF tells you how many Moving Average (MA) terms are required to eliminate the remaining autocorrelation from a time series. The procedure is accomplished by typing: acf (Solar time-series, plot = T).
- **Extended Autocorrelation Function (EACF).** This additional procedure determined that the PACF and ACF may not be enough in some cases with mixed autoregressive and moving average components. The procedure is accomplished by writing eacf (Solartimeseries, ar.max = 7, ma.max = 13)

3.2. Based on the results of the Dicky-Fuller test and the KPSS test, the time series needed to be Stationarize by differencing. Differencing the time series two times

was required. We also performed all the procedures mentioned above to decide which model is possible to fit the time series.

- First, the differencing and tests were done by typing the following:
    i. Solarseriesdiff1 <- diff (Solarseries, differences=1)
    ii. plot.ts (Solarseriesdiff1)
    iii. pacf (Solarseriesdiff1, lag.max=20)
    iv. acf (Solarseriesdiff1, lag.max=20)
- Second, the differencing was by Solarseriesdiff2 <- diff (Solarseries, differences=2) and the orders were the same as the first differencing steps, taking into account replacing the defined series to be Solarseriesdiff2.

4. The building of the ARIMA Model:

4.1. The values which resulted from carrying out different procedures in step 3 were used to guide the selection of the proper ARIMA model that fits the series, and in selecting optimal parameters.

4.2. Look at the results of BIC and AIC.

- Compare the values of BIC and AIC among all results.
- Select the model that has the lowest values of BIC and AIC.

4.3. Deciding on the model that is going to be used. This model was ARIMA (0,1,0).

5. Make Prediction:

5.1. The prediction is accomplished by typing the following:

- a=arima (Solartimeseries, order=c (0,1,0))
- summary(a)
- f=forecast (a, h=80)

- plot(f)

5.2. Prediction results and graphs were obtained.

5.3. In addition to the ARIMA (0,1,0) model used, another prediction was carried out using the Neural Network Autoregression (NNAR) model as follows:

- Look again at the seasonality of the series by typing:
    i. fit1 <- tbats (Solartimeseries)
    ii. seasonal <-! is.null (fit1$seasonal)
    iii. seasonal
- Start the Neural Network Time Series Forecasting of the data by typing:
    i. fit <- nnetar (Solartimeseries, lambda=0)
    ii. autoplot (forecast (fit, h=200))
- Obtain the forecasted values and graphs.

3.3.3.2 KAUST & Mezaira Stations - Forecasting Steps (W & E):

Because the data extracted from the KAUST_Campus and Mezaira stations was plagued by a huge number of missing daily data values, it is hard to produce a reliable model to do the prediction. This is a limitation that was faced during the work. Hence, no prediction is provided in this sub-section.

3.3.3.3 Terra Satellite - Forecasting Steps (N & S):

The same steps as the solar village time series were followed to do the forecast with some changes based on the number of observations and the results of the model building procedures and tests.

CHAPTER 4

RESULTS AND DISCUSSIONS

4.1 Types and Levels of PM_{10} based on AOD and AE values

As mentioned earlier, the total number of sub-objectives are three (3). However, the section 4.1 (below) is completely related to the first objective "**Determine physical, optical and seasonal Airborne Particulate Matter characteristics over several geographical locations in the Arabian Peninsula based on long-term space-borne and ground-based observations**".

4.1.1. Central Region - Particulate Matter Trend and Variation Percent

Yearly, monthly, daily and seasonal data were used in this study. In all cases, the mean values of τ_{500} represent the concentration of the particulate matter suspended in the atmosphere, $\alpha_{440-870}$ represents the size of both particles including the fine and coarse, while the $\alpha_{380-500}$ and $\alpha_{500-870}$ represent the fine and course size particles, respectively. Percentage difference, p values, and t tests are also listed. Differences that are statistically significant ($P < 0.05$) are highlighted in bold in all tables under this section.

The annual trend at τ_{500} "Figure 17" shows an overall increase in PM_{10} concentration by (37%), while the trend at $\alpha_{440-870}$ showed a reduction in anthropogenic emission by (35%) over time. Based on these facts, we can say that most of the emission is probably generated naturally rather than being man-made. Further, the results at $\alpha_{380-500}$ and $\alpha_{500-870}$ "Fig-

ure 18" suggest that there is a decrease in the fine and coarse particles over time by (58%) and (42%), respectively, which indicates that the major contributor to the rise of particulate matter concentration is natural emissions. Statistical significance is at the 95% confidence level with ($p < 0.05$) of the results are also listed in "Table 5".

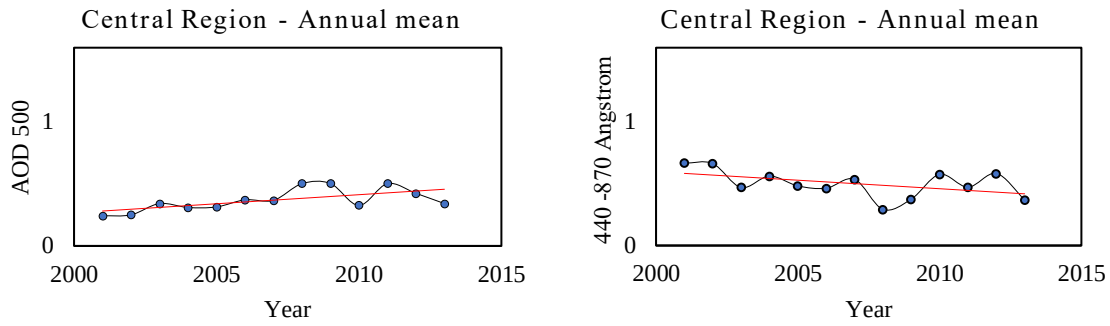

Figure 17. Trend of τ_{500} & $\alpha_{440-870}$ over Solar Village, Saudi Arabia for 2001 to 2013 using annual mean values.

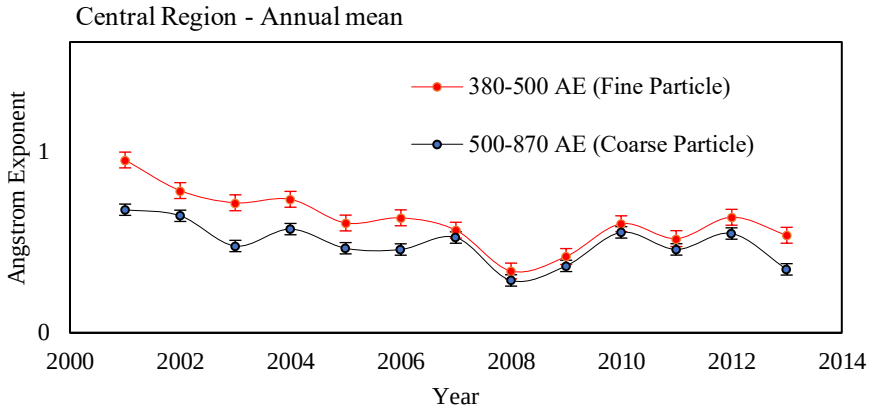

Figure 18. Trend of $\alpha_{380-500}$ & $\alpha_{500-870}$ over Solar Village, Saudi Arabia for 2001 to 2013 using annual mean values.

Table 5. Yearly Statistical Comparison over Solar Village, Saudi Arabia during the periods 2001 and 2013.

	Mean			Median		
N:13	Slope	Percentage	P-Value	Slope	Percentage	P-Value
τ500	0.0146	37	**1.94×10^{-02}**	0.0109	39	**4.28×10^{-02}**
α 440-870	-0.0138	35	9.74×10^{-02}	-0.0181	46	6.04×10^{-02}
α 380-500	-0.0279	58	**9.24×10^{-03}**	-0.0304	63	**1.19×10^{-02}**
α 500-870	-0.0162	42	**4.59×10^{-02}**	-0.0187	48	**3.27×10^{-02}**

The monthly trend at τ_{500}, $\alpha_{440\text{-}870}$, $\alpha_{380-500}$ and $\alpha_{500-870}$ "Figures 19 and 20" "Table 7" also showed the same results as the annual trends with a difference in variation percent, especially in the fine particles. Although they are all agreed on the descending trend, the decline in the trend for fine particles was much higher in the monthly values analysis. The decrease over time was about (92%) "Table 6".

A comparison was made between the two periods (2001 - 2006) and (2007 - 2013) for size distribution in each month separately "Table 8". "Figure 21" indicates that the rising trend for the natural particles is high compared to the anthropogenic one during the second period (2007 - 2013) in all months. However, during March and June, the ratio is equal between the two periods. Nevertheless, during the month of September natural particles were higher in the first period (2001-2006), which was not observed in any other month over the central region. We also noticed a rise in anthropogenic particles from August to December in both periods, in addition to February, but in lower concentrations.

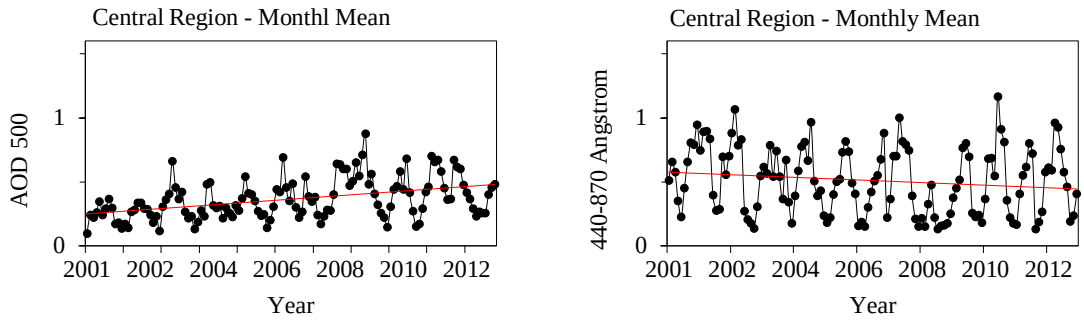

Figure 19. Trend of τ_{500} & $\alpha_{440-870}$ over Solar Village, Saudi Arabia for 2001 to 2013 using monthly mean values.

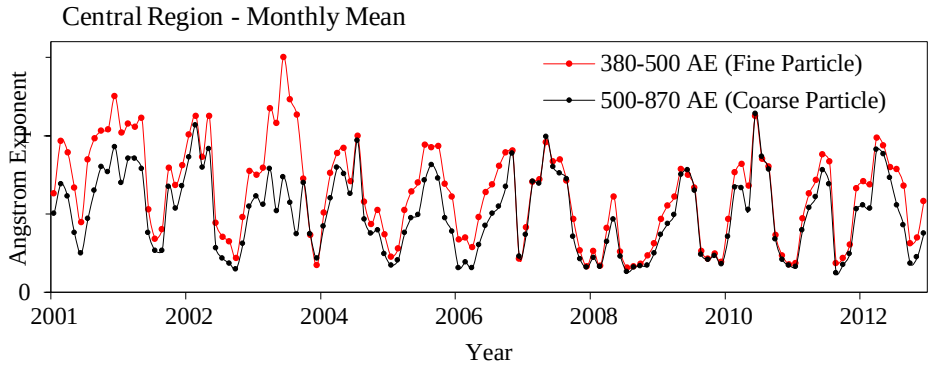

Figure 20. Trend of $\alpha_{380-500}$ & $\alpha_{500-870}$ over Solar Village, Saudi Arabia for 2001 to 2013 using monthly mean values.

Table 6. Monthly Statistical Comparison over Solar Village, Saudi Arabia during the periods 2001 and 2013.

	Mean			Median		
N:130	Slope	Percentage	P-Value	Slope	Percentage	P-Value
τ500	0.0017	53	**2.03×10^{-02}**	0.0014	50	7.19×10^{-02}
α 440-870	-0.001	39	**1.43×10^{-10}**	-0.0012	39	**3.54×10^{-11}**
α 380-500	-0.0027	92	**3.27×10^{-07}**	-0.0027	92	**9.62×10^{-09}**
α 500-870	-0.0012	46	**9.44×10^{-10}**	-0.0014	46	**9.63×10^{-11}**

Table 7. Monthly Statistical Comparison over Solar Village, Saudi Arabia during the periods 2001 and 2013.

	Mean			Median		
N: 10 (Jan)	Slope	Percentage	P-Value	Slope	Percentage	P-Value
τ500	0.0114	58	**1.99×10^{-02}**	0.0098	56	1.11×10^{-01}
α 440-870	-0.0221	3	1.95×10^{-01}	-0.0268	37	2.13×10^{-01}
α 380-500	0.0451	50	**2.63×10^{-02}**	-0.0496	56	**9.96×10^{-03}**
α 500-870	-0.0308	43	1.18×10^{-01}	-0.0366	52	1.25×10^{-01}
N: 11 (Feb)	Slope	Percentage	P-Value	Slope	Percentage	P-Value
τ500	0.0117	42	1.07×10^{-01}	0.0108	45	1.82×10^{-01}
α 440-870	-0.0234	62	9.21×10^{-02}	-0.0184	52	1.82×10^{-01}
α 380-500	-0.0498	92	**4.00×10^{-02}**	-0.0364	73	7.41×10^{-02}
α 500-870	-0.0258	7	5.24×10^{-02}	-0.0208	62	1.11×10^{-01}
N: 11 (Mar)	Slope	Percentage	P-Value	Slope	Percentage	P-Value

τ500	0.0218	63	**1.49×10^{-02}**	0.0164	56	**1.44×10^{-02}**
α 440-870	-0.0293	15	**2.56×10^{-02}**	-0.0271	107	**4.27×10^{-02}**
α 380-500	-0.0447	121	**4.47×10^{-03}**	-0.0426	122	**1.30×10^{-02}**
α 500-870	-0.0317	116	**2.14×10^{-02}**	-0.0287	116	**3.64×10^{-02}**
N: 12 (Apr)	Slope	Percentage	P-Value	Slope	Percentage	P-Value
τ500	0.0267	66	**4.31×10^{-03}**	0.0266	71	**1.43×10^{-03}**
α 440-870	-0.0104	57	**3.48×10^{-02}**	-0.0103	60	**6.27×10^{-03}**
α 380-500	-0.0232	93	**1.47×10^{-02}**	-0.0222	97	**1.83×10^{-02}**
α 500-870	-0.0128	67	**1.87×10^{-02}**	-0.0112	66	**2.43×10^{-03}**
N: 11 (May)	Slope	Percentage	P-Value	Slope	Percentage	P-Value
τ500	0.0153	3	1.12×10^{-01}	0.0164	36	6.49×10^{-02}
α 440-870	0.0049	26	4.10×10^{-01}	0.0023	14	6.47×10^{-01}
α 380-500	-0.0002	1	9.84×10^{-01}	-0.0043	19	6.70×10^{-01}
α 500-870	0.0024	13	6.52×10^{-01}	0.0002	1	9.60×10^{-01}
N: 10 (Jun)	Slope	Percentage	P-Value	Slope	Percentage	P-Value
τ500	0.0399	76	**3.67×10^{-03}**	0.0336	70	**3.01×10^{-03}**
α 440-870	-0.0131	47	1.67×10^{-01}	-0.021	84	**2.70×10^{-02}**
α 380-500	-0.0377	99	**3.05×10^{-02}**	-0.0484	134	**1.52×10^{-02}**
α 500-870	-0.0156	54	1.12×10^{-01}	-0.0235	93	**1.61×10^{-02}**
N: 11 (Jul)	Slope	Percentage	P-Value	Slope	Percentage	P-Value
τ500	0.0219	58	**2.54×10^{-03}**	0.0229	65	**1.16×10^{-03}**
α 440-870	-0.0191	44	1.11×10^{-01}	-0.0226	52	5.35×10^{-02}

α 380-500	-0.0348	62	**2.50×10^{-02}**	-0.0372	65	**1.16×10^{-02}**
α 500-870	-0.0204	49	7.47×10^{-02}	-0.0246	57	**2.88×10^{-02}**
N: 11 (Aug)	Slope	Percentage	P-Value	Slope	Percentage	P-Value
τ500	0.0183	47	**4.07×10^{-02}**	0.0153	42	**3.71×10^{-02}**
α 440-870	-0.0106	19	3.42×10^{-01}	-0.0088	16	4.97×10^{-01}
α 380-500	-0.0185	28	1.12×10^{-01}	-0.0184	27	1.40×10^{-01}
α 500-870	-0.0125	24	2.82×10^{-01}	-0.0108	20	4.29×10^{-01}
N: 9 (Sep)	Slope	Percentage	P-Value	Slope	Percentage	P-Value
τ500	0.0114	4	**6.41×10^{-03}**	0.0113	32	**2.54×10^{-03}**
α 440-870	-0.0034	5	7.57×10^{-01}	-0.0031	4	8.00×10^{-01}
α 380-500	-0.015	17	1.96×10^{-01}	-0.0166	18	2.07×10^{-01}
α 500-870	-0.0049	7	6.54×10^{-01}	-0.0048	7	6.80×10^{-01}
N: 11 (Oct)	Slope	Percentage	P-Value	Slope	Percentage	P-Value
τ500	0.012	47	**1.57×10^{-03}**	0.0112	47	**3.49×10^{-02}**
α 440-870	-0.0143	18	3.21×10^{-01}	-0.0221	28	1.50×10^{-01}
α 380-500	-0.0336	36	**2.28×10^{-02}**	-0.0422	44	**8.75×10^{-03}**
α 500-870	-0.0156	2	2.68×10^{-01}	-0.0219	29	1.47×10^{-01}
N: 10 (Nov)	Slope	Percentage	P-Value	Slope	Percentage	P-Value
τ500	-0.0003	1	9.51×10^{-01}	0.0002	1	9.52×10^{-01}
α 440-870	0.0206	22	2.42×10^{-01}	0.0289	31	9.47×10^{-02}
α 380-500	-0.0078	7	5.85×10^{-01}	-0.0041	4	7.43×10^{-01}
α 500-870	0.0198	22	2.80×10^{-01}	0.0276	31	1.17×10^{-01}

N: 11 (Dec)	Slope	Percentage	P-Value	Slope	Percentage	P-Value
τ500	0.0062	28	2.21×10^{-01}	0.0056	29	2.24×10^{-01}
α 440-870	-0.0023	3	7.81×10^{-01}	-0.0024	3	8.02×10^{-01}
α 380-500	-0.0345	32	7.92×10^{-02}	-0.0248	23	3.51×10^{-01}
α 500-870	-0.0048	5	5.54×10^{-01}	-0.0041	4	9.05×10^{-01}

Table 8. Monthly Statistical Comparison over Solar Village, Saudi Arabia during the sub-periods 2001 – 2006 (G1) and 2007 -2013 (G2).

Jan	G1 (N:141)	G2 (N:121)	P	t
τ500	0.164	0.230	**2.9×10^{-04}**	**2**
α 440-870	0.744	0.715	5.7×10^{-01}	2
α 380-500	0.994	0.779	**3.0×10^{-04}**	**2**
α 500-870	0.769	0.675	7.7×10^{-02}	2
Feb	G1 (N:136)	G2 (N:132)	P	t
τ500	0.267	0.319	**3.4×10^{-02}**	**2**
α 440-870	0.476	0.361	**2.3×10^{-03}**	**2**
α 380-500	0.781	0.424	**6.5×10^{-08}**	**2**
α 500-870	0.469	0.336	**3.4×10^{-04}**	**2**
Mar	G1 (N:153)	G2 (N:174)	P	t
τ500	0.303	0.457	**2.8×10^{-06}**	**2**
α 440-870	0.402	0.213	**1.5×10^{-11}**	**2**
α 380-500	0.560	0.252	**1.7×10^{-19}**	**2**
α 500-870	0.409	0.204	**6.5×10^{-13}**	**2**
Apr	G1 (N:155)	G2 (N:138)	P	t

τ500	0.362	0.594	1.34×10^{-13}	2
α 440-870	0.262	0.181	1.77×10^{-05}	2
α 380-500	0.410	0.203	4.07×10^{-14}	2
α 500-870	0.274	0.180	4.22×10^{-07}	2
May	G1 (N:173)	G2 (N:155)	P	t
τ500	0.517	0.631	**1.4×10^{-03}**	**2**
α 440-870	0.189	0.196	6.1×10^{-01}	2
α 380-500	0.291	0.227	**2.2×10^{-03}**	**2**
α 500-870	0.199	0.194	6.8×10^{-01}	2
Jun	G1 (N:147)	G2 (N:161)	P	t
τ500	0.374	0.652	**3.3×10^{-18}**	**2**
α 440-870	0.335	0.238	**7.6×10^{-06}**	**2**
α 380-500	0.521	0.271	**5.6×10^{-15}**	**2**
α 500-870	0.343	0.236	**3.6×10^{-07}**	**2**
Jul	G1 (N:163)	G2 (N:178)	P	t
τ500	0.342	0.495	1.1×10^{-14}	2
α 440-870	0.533	0.406	**2.1×10^{-08}**	**2**
α 380-500	0.741	0.482	**6.8×10^{-21}**	**2**
α 500-870	0.529	0.394	**1.1×10^{-09}**	**2**
Aug	G1 (N:165)	G2 (N:144)	P	t
τ500	0.376	0.469	**7.9×10^{-06}**	**2**
α 440-870	0.607	0.578	2.7×10^{-01}	2

α 380-500	0.761	0.656	**1.6×10^{-04}**	**2**
α 500-870	0.598	0.563	1.8×10^{-01}	2
Sep	G1 (N:146)	G2 (N:123)	P	t
τ500	0.285	0.384	**4.6×10^{-11}**	**2**
α 440-870	0.625	0.643	4.9×10^{-01}	2
α 380-500	0.828	0.727	**3.5×10^{-04}**	**2**
α 500-870	0.609	0.622	6.1×10^{-01}	2
Oct	G1 (N:177)	G2 (N:129)	P	t
τ500	0.218	0.288	**4.8×10^{-08}**	**2**
α 440-870	0.801	0.760	2.0×10^{-01}	2
α 380-500	1.029	0.816	**4.8×10^{-11}**	**2**
α 500-870	0.783	0.736	1.4×10^{-01}	2
Nov	G1 (N:158)	G2 (N:108)	P	t
τ500	0.235	0.201	**2.4×10^{-02}**	**2**
α 440-870	0.787	0.917	**4.6×10^{-04}**	**2**
α 380-500	0.956	0.920	2.7×10^{-01}	2
α 500-870	0.769	0.891	**1.2×10^{-03}**	**2**
Dec	G1 (N:129)	G2 (N:117)	P	t
τ500	0.201	0.221	3.0×10^{-01}	2
α 440-870	0.847	0.814	4.8×10^{-01}	2
α 380-500	1.004	0.812	**1.4×10^{-05}**	**2**
α 500-870	0.835	0.785	2.9×10^{-01}	2

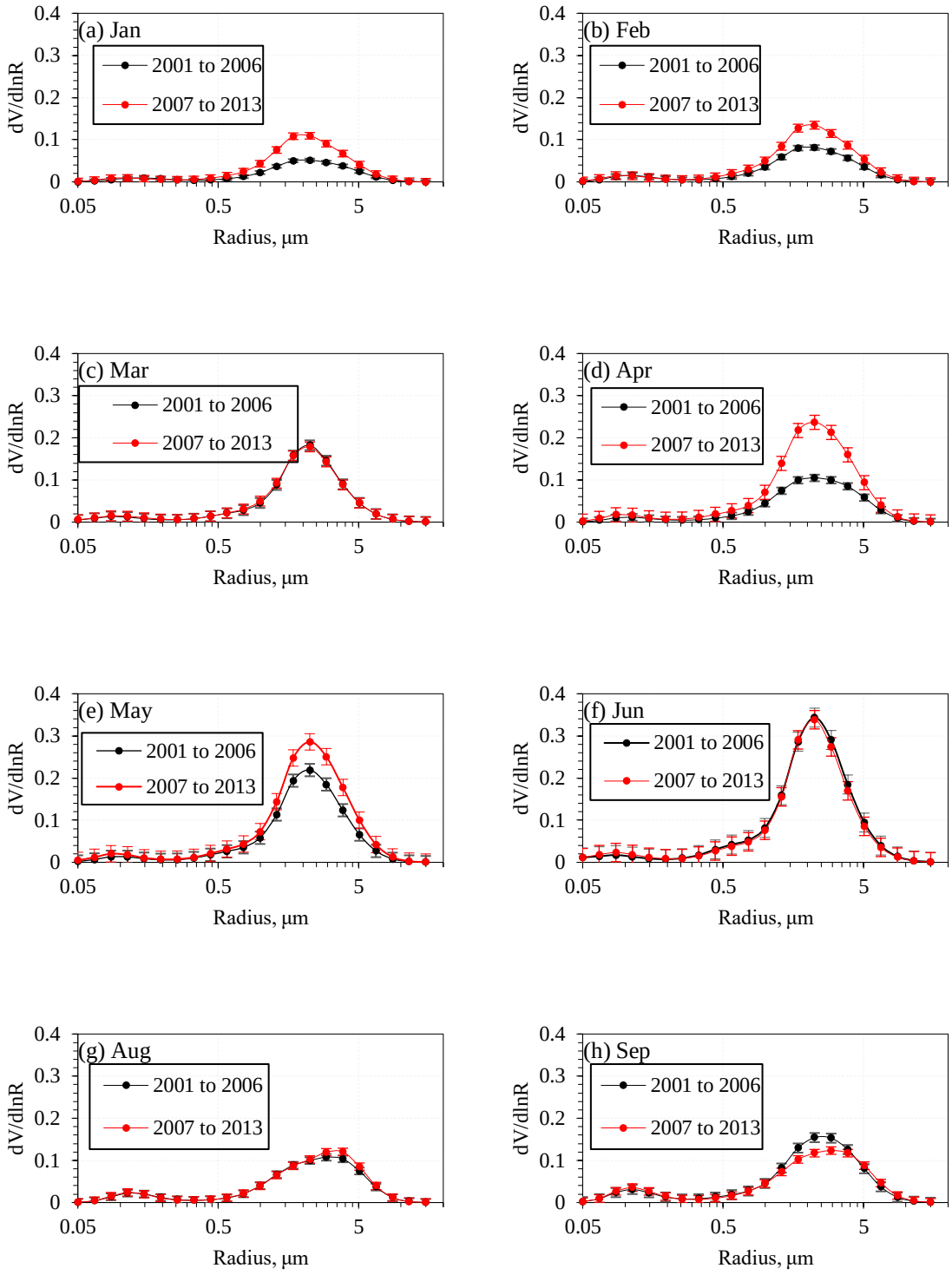
(a) Jan
(b) Feb
(c) Mar
(d) Apr
(e) May
(f) Jun
(g) Aug
(h) Sep
2001 to 2006
2007 to 2013
dV/dlnR
Radius, μm
0.4
0.3
0.2
0.1
0
0.05
0.5
5

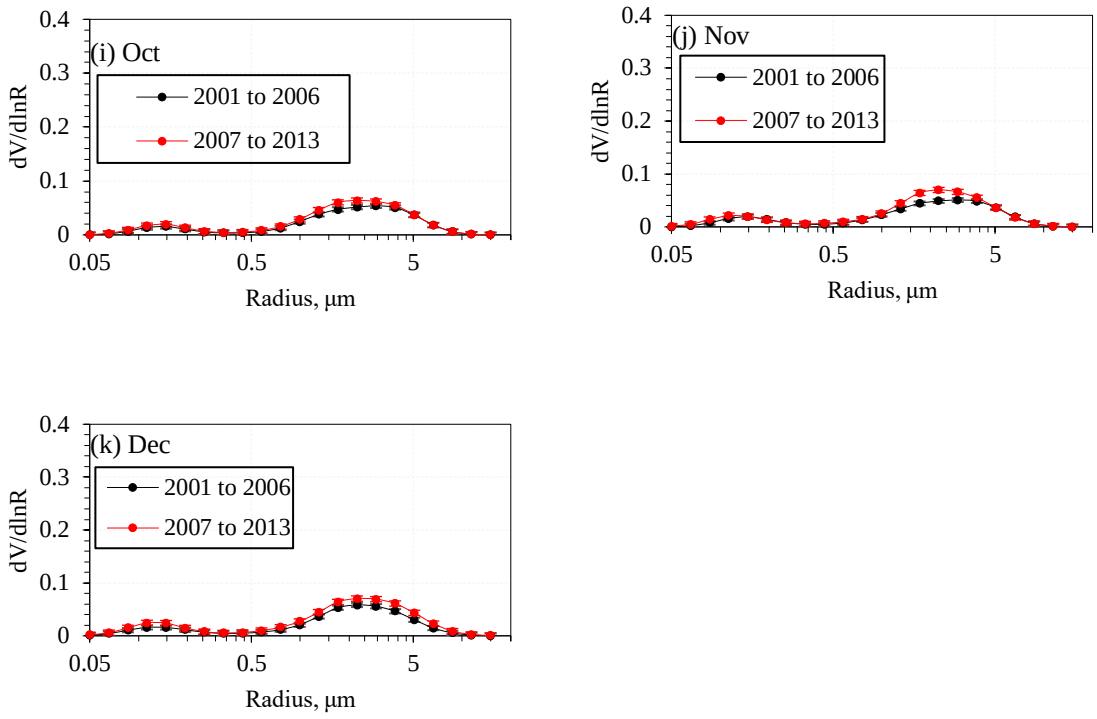

Figure 21. Monthly variation using size distribution data over Solar Village, Saudi Arabia during the sub-periods 2001 – 2006 (G1) and 2007 -2013 (G2).

Daily values analysis in "Figure 22" "Table 9" showed similar results to the annual results just discussed. The overall increasing trend at τ_{500} was by (58%), while the decreasing trend at $\alpha_{440\text{-}870}$ was (28%). Also, the variations associated with $\alpha_{380\text{-}500}$ and $\alpha_{500\text{-}870}$ dropped by (56%) and (28%), respectively. Results in "Table 10" showed that the increasing trend at τ_{500} was during February by (860%), along with another slight rising trend in October. While a strong decreasing trend was in May by (700%), there were other slight decreasing trends during the months of August and December. The results representing trends during Jan, Mar, Apr, Jun, Jul, and Dec are not statistically significant. Analysis at $\alpha_{440\text{-}870}$ showed that there is an overall drop in anthropogenic emission during February and a rise between May and Aug that is confirmed by the results obtained at $\alpha_{380\text{-}500}$. In addition, the coarse particles (at $\alpha_{500\text{-}870}$) were also increasing and decreasing the same as during the period mentioned for the fine particles ($\alpha_{380\text{-}500}$). The highest increase in the fine particles ($\alpha_{380\text{-}500}$) trend was during Aug by (460%), while the decrease was in Feb by (550%). The same procedure was done using daily values. The analysis focused on each month separately to investigate the variations during every month over the whole period. The results as shown indicated also that there is a continuous increase in the trend at τ_{500} of different proportions from January to December, except for November. However, the values analyzed in February, May, November, and December are not statistically significant. Based on the P values at $\alpha_{440\text{-}870}$ and $\alpha_{500\text{-}870}$, we find that high levels of confidence are only associated with the results for March and April, which show declining trends in fine particles ($\alpha_{380\text{-}500}$) and an increase of the coarse one ($\alpha_{500\text{-}870}$) during the two months. This has been confirmed by the values obtained at $\alpha_{380\text{-}500}$ where there was a decrease in all months except during January in which an increasing trend

was observed. All the values at the $\alpha_{380\text{-}500}$ wavelength enjoyed a high level of confidence with ($p < 0.05$).

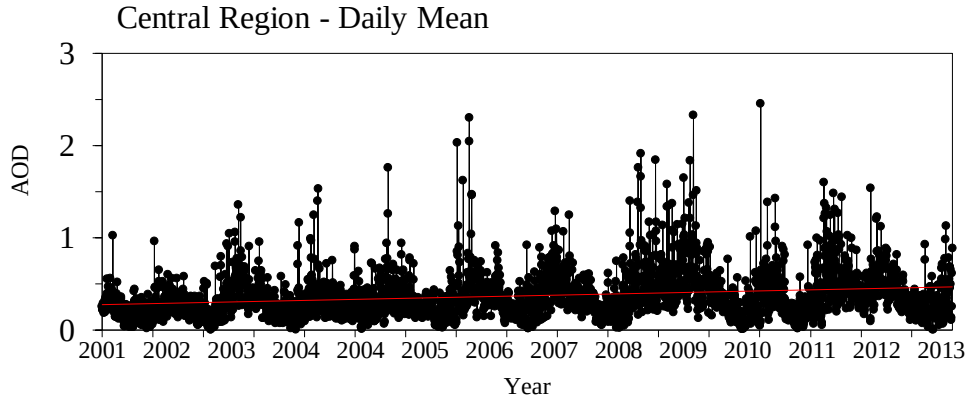

Figure 22. Aerosols Optical Depth over the center of AP

Table 9. Daily Statistical Comparison over Solar Village, Saudi Arabia during the periods 2001 and 2007 -2013.

	Mean		
N: 3523	Slope	Percentage	P-Value
τ500	0.00006	58	$\mathbf{9.7\times10^{-16}}$
α 440-870	-0.00004	28	$\mathbf{1.05\times10^{-144}}$
α 380-500	-0.0001	56	$\mathbf{1.665\times10^{-93}}$
α 500-870	-0.00004	28	$\mathbf{2.9\times10^{-134}}$

Table 10. Monthly Statistical Comparison using daily values over Solar Village, Saudi Arabia during the periods 2001 and 2013.

Mean	Jan (N: 262)			Mar (N: 327)		
	Slope	Percentage	P-Value	Slope	Percentage	P-Value
τ500	0.0018	182	6.84×10^{-02}	0.0032	307	8.96×10^{-02}
α 440-870	-0.0044	181	1.41×10^{-01}	-0.0028	176	8.70×10^{-02}
α 380-500	-0.004	113	2.55×10^{-01}	-0.0038	180	$\mathbf{4.71\times10^{-02}}$
α 500-870	-0.0028	111	3.56×10^{-01}	-0.0025	154	1.14×10^{-01}
Mean	Feb (N: 268)			Apr (N: 293)		
	Slope	Percentage	P-Value	Slope	Percentage	P-Value
τ500	0.0078	860	$\mathbf{1.71\times10^{-07}}$	0.0011	110	5.55×10^{-01}
α 440-870	-0.0089	374	$\mathbf{2.42\times10^{-04}}$	0.001	54	3.57×10^{-01}
α 380-500	-0.0163	552	$\mathbf{7.10\times10^{-05}}$	-0.0001	4	9.34×10^{-01}
α 500-870	-0.0088	387	$\mathbf{1.15\times10^{-04}}$	0.0006	32	6.11×10^{-01}
Mean	May (N: 328)			Jul (N: 341)		
	Slope	Percentage	P-Value	Slope	Percentage	P-Value
τ500	-0.007	700	$\mathbf{4.72\times10^{-04}}$	-5×10^{06}	1	9.97×10^{-01}
α 440-870	2.20×10^{03}	145	$\mathbf{3.08\times10^{-03}}$	0.0059	376	$\mathbf{3.42\times10^{-06}}$
α 380-500	0.0041	224	$\mathbf{3.99\times10^{-04}}$	0.0057	344	$\mathbf{4.41\times10^{-04}}$
α 500-870	0.0022	150	$\mathbf{1.31\times10^{-03}}$	0.0055	358	$\mathbf{8.81\times10^{-06}}$
Mean	Jun (N: 308)			Aug (N: 309)		
	Slope	Percentage	P-Value	Slope	Percentage	P-Value
τ500	-0.0034	282	8.36×10^{-02}	-0.0038	258	$\mathbf{1.01\times10^{-03}}$

α 440-870	0.0058	430	**3.10×10^{-06}**	0.0062	501	**1.94×10^{-05}**
α 380-500	0.0066	332	**5.00×10^{-04}**	0.0063	462	**6.55×10^{-05}**
α 500-870	0.0055	411	**6.75×10^{-06}**	0.006	494	**3.94×10^{-05}**
Mean	Sep (N: 269)			Nov (N: 266)		
	Slope	Percentage	P-Value	Slope	Percentage	P-Value
τ500	-0.0026	152	**2.66×10^{-03}**	-0.0021	184	**1.85×10^{-03}**
α 440-870	-0.001	62	5.09×10^{-01}	0.0032	181	7.10×10^{-02}
α 380-500	0.0013	73	4.13×10^{-01}	0.0006	33	7.41×10^{-01}
α 500-870	-0.0015	95	2.97×10^{-01}	0.0035	205	**4.39×10^{-02}**
Mean	Oct (N: 306)			Dec (N: 246)		
	Slope	Percentage	P-Value	Slope	Percentage	P-Value
τ500	0.0028	131	**1.40×10^{-03}**	-0.0011	79	3.06×10^{-01}
α 440-870	-8×10^{04}	63	7.10×10^{-01}	-0.0048	193	5.42×10^{-02}
α 380-500	-0.0042	244	**3.19×10^{-02}**	-0.0025	87	3.20×10^{-01}
α 500-870	-0.0009	62	6.90×10^{-01}	-0.0051	218	**4.49×10^{-02}**

Seasonal variation was also part of the investigation but it used a different way of analysis. The analysis was based on two sub-periods (2001-2006 and 2007- 2012). Changes in the AOD and AE values, beside the size distribution, were calculated for all seasons. The results are represented in "Figures 23 and 24."

In the second sub-period (2007- 2012), an increase in the trend of particulate matter concentration (at τ_{500} was noticed in all seasons except during the fall season. At $\alpha_{440\text{-}870}$ (fine and coarse), there were decreasing trends, although not during the fall season where

there was an increasing trend. These results indicate that the natural emission is higher than the anthropogenic one in all seasons except the fall; however, the trend at $\alpha_{440-870}$ during the fall season is not statistically significant at the 95% confidence level with ($p <$ 0.05) where the p value is 0.454. The other wavelength ($\alpha_{380-500}$, and $\alpha_{500-870)}$ results have shown a declining trend in anthropogenic emission during the second-sub period during all seasons. Upward trends during the spring and summer seasons "Figure 23" might be because during these seasons the AP is encountering frequent dust storms, which aggravate the particles in the atmosphere for a while. "Table 11" show the significance levels for all the data discussed in the seasonal sub-section. It indicates a high confidence level for most of the results. The size distribution of the particles is shown in "Figure 24". The results here represent man-made (from 0.05 to 0.5) and the natural (from 0.5 to 5) emissions. It showed that the natural emission increase in the order: spring, summer, winter, and fall, respectively. While the man-made one is higher during the summer and then the spring, followed by the fall and lastly the winter. This could be because during the summer people tend to consume more government-supported energy. Since the energy is based-oil energy (requires burning of oil to produce energy), we expect a higher emission rate from a lot of sources including mobile and stationary sources.

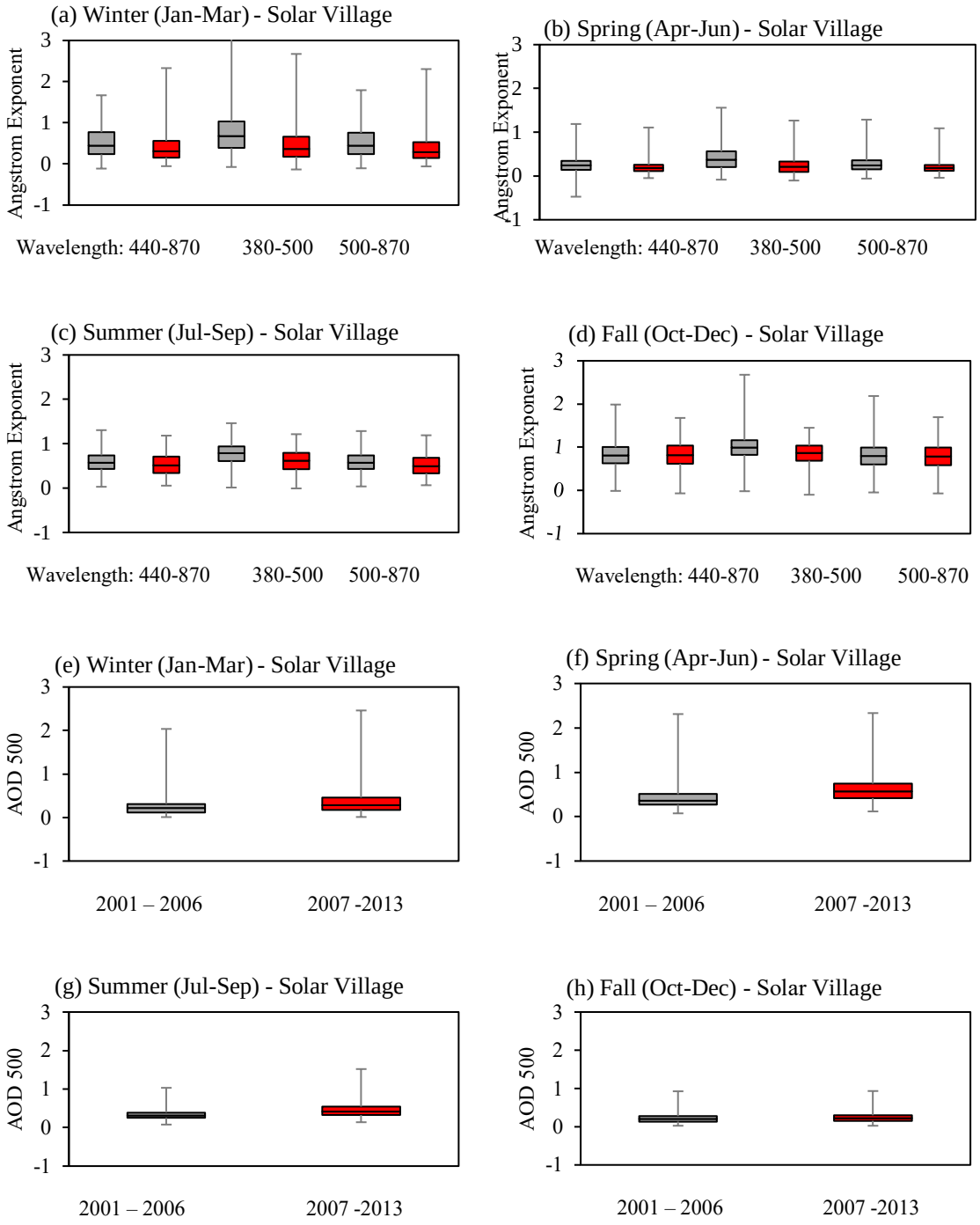

Figure 23. Seasonal Variation using daily mean values of τ_{500}, $\alpha_{440-870}$, $\alpha_{380-500}$ & $\alpha_{500-870}$ over Solar Village, Saudi Arabia during the sub-periods 2001 – 2006 (G1) and 2007 - 2013 (G2).

Table 11. Seasonal Statistical Comparison over Solar Village, Saudi Arabia during the sub-periods 2001 – 2006 (G1) and 2007 -2013 (G2).

		τ500	α440-870	α380-500	α500-870	N
Winter	p	**5.30×10^{-10}**	**6.32×10^{-08}**	**1.17×10^{-21}**	**5.90×10^{-11}**	430
	t	2	2	2	2	427
Spring	p	**5.44×10^{-26}**	**1.89×10^{-06}**	**4.23×10^{25}**	**1.45×10^{-09}**	475
	t	2	2	2	2	454
Summer	p	**1.52×10^{-25}**	**8.25×10^{-05}**	**1.64×10^{-23}**	**1.02×10^{-05}**	474
	t	2	2	2	2	445
Fall	p	**2.37×10^{-02}**	4.54×10^{-01}	**6.29×10^{-13}**	7.66×10^{-01}	464
	t	2	2	2	2	354

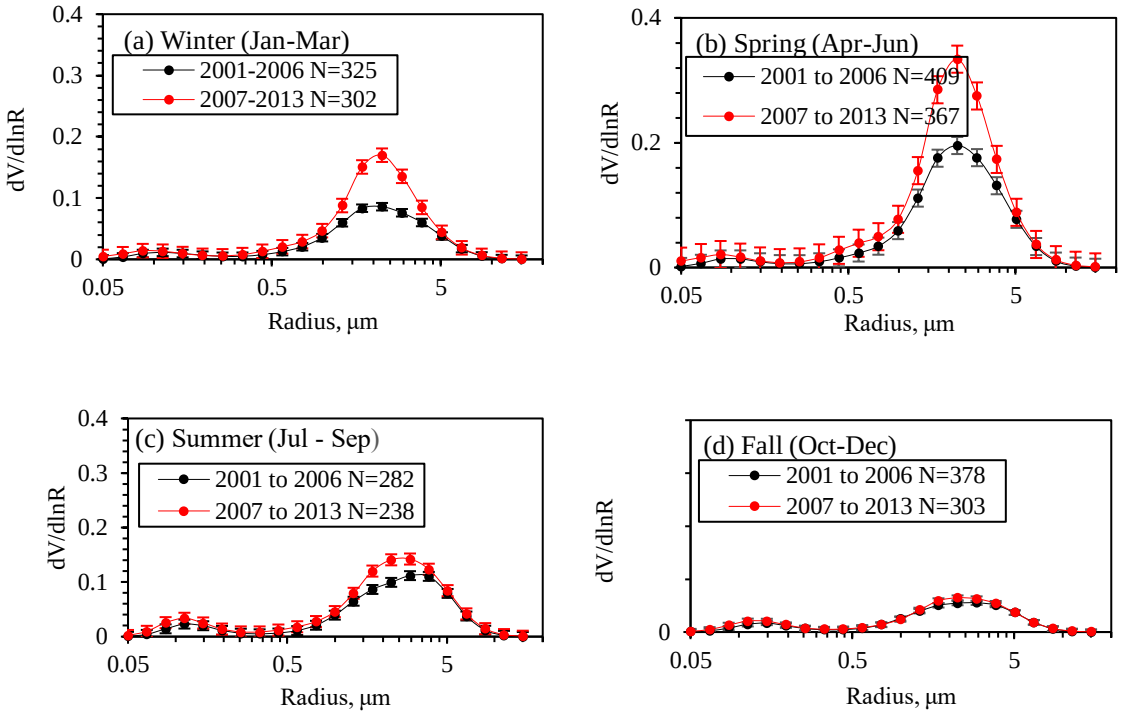

Figure 24. Seasonal Variation using size distribution data over Solar Village, Saudi Arabia during the sub-periods 2001 – 2006 (G1) and 2007 -2013 (G2).

4.1.2. Eastern Region - Particulate Matter Trend and Variation Percent

The second area was investigated is the Eastern Region. Many tables and graphs are listed below which show the yearly monthly, daily and seasonal variations, the same as for the case in the previous sub-section. The results include the percentage difference, the p values, and the t-tests. The frequencies in this section are daily, monthly, seasonal, and annual. The values were calculated using observations measured over the Mezaira Station during the period 2004 to 2017. The number of daily, monthly, and annual values here are 2043, 93, 12, respectively. The mean values corresponding to different frequency variations are represented, along with the percentage difference and the p values in tables attached. The annual trend at τ_{500} "Figure 25" show that there is an increase in PM_{10} concentration by (9%) and a decreasing trend at $\alpha_{440\text{-}870}$ by (35%). This the same as the case with the Central Region results with some differences in the percent variation. This indicates lower anthropogenic emission rates over the eastern region of the Arabian Peninsula compared to the western and southern regions, which is going to be discussed in the upcoming sub-sections. The P values for both are not statistically significant at the 95% confidence level with ($p < 0.05$) where the values are 0.6 and 0.2. Further, the results at $\alpha_{380\text{-}500}$ and $\alpha_{500\text{-}870}$ "Figure 26 " propose that there are decreasing trends in fine and coarse particles over time by (23%) and (29%), respectively, which shows that the increase in PM_{10} concentration over time was due to natural emissions being higher than man-made emissions, although not significantly "Table 12". Almost like what is happening over the central region but with lower trends.

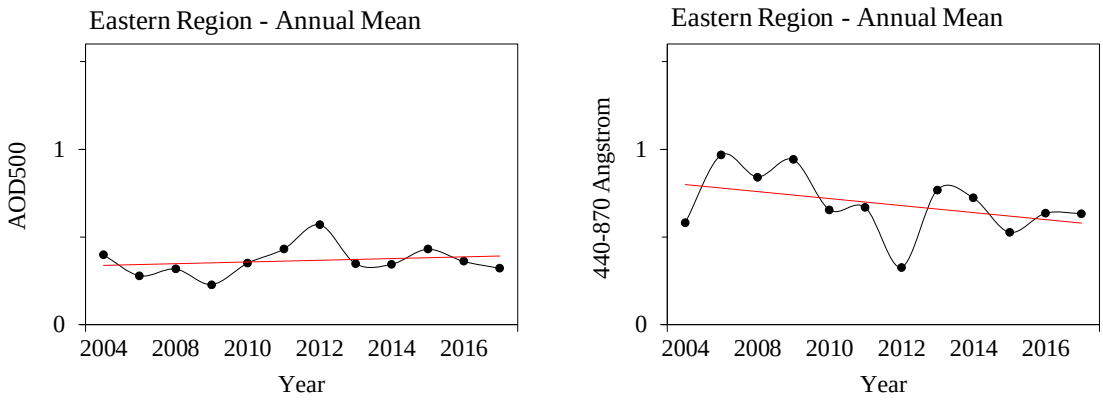

Figure 25. Trend of τ_{500} & $\alpha_{440-870}$ over Mezaira, UAE for 2004 to 2017 using annual mean values

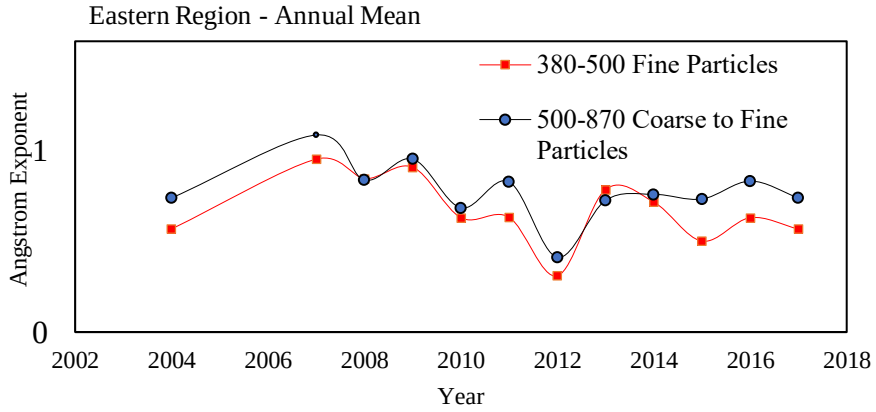

Figure 26. Trend of $\alpha_{380-500}$ & $\alpha_{500-870}$ over Mezaira, UAE for 2004 to 2017 using annual mean values

Table 12. Yearly Statistical Comparison over Mezaira, UAE during the periods 2004 and 2018.

	Mean			Median		
N:12	Slope	Percentage	P-Value	Slope	Percentage	P-Value
τ500	0.0048	9	6.02×10^{-01}	0.0022	7	8.36×10^{-01}
α 440-870	-0.0200	35	2.72×10^{-01}	-0.0239	42	2.41×10^{-01}
α 380-500	-0.0150	23	3.48×10^{-01}	-0.0179	28	3.36×10^{-01}
α 500-870	-0.0214	39	2.45×10^{-01}	-0.0253	46	2.15×10^{-01}

Trends using monthly mean values "Figure 27" show dissimilar trend results discussed in the annual mean values when it comes to variation percentage. The trend at τ_{500} over the months is increasing by (101%). In "Table 13", results showed that overall there is a decreasing trend at $\alpha_{440-780,}$ $\alpha_{380-500}$, and $\alpha_{500-870}$ by 30%, 5%, and 33%, respectively. "Figure 28" also shows an overall declining trend at AE denoting that there is a decrease in anthropogenic emissions with time over the eastern region. The results of the annual and monthly mean values at τ_{500} are not statistically significant at the 95% confidence level with ($p < 0.05$) because the p values are higher than 0.05.

Using monthly mean values to analyze every month separately, "Table 14" represents the slope, percentage difference and the P values, and indicates that there was an increasing trend at τ_{500} during Feb, Mar, Jun, Jul, Aug, Oct and Nov with high values of p (low confidence level). The results for AE also have high values of p except in Aug where the values for the median readings at $\alpha_{440-870}$ and $\alpha_{500-870}$ are 0.02 and 0.05 respectively, which proposes a decrease in the trend over time. Also, during Feb at $\alpha_{380-500}$ the p value

of the average reading is 0.04 and here it suggests an increase in the AE trends over time (higher in fine particles). By making a comparison between the two the sub-periods (2004 - 2011) and (2012 - 2017) when it comes to size distribution "Figure 29" "Table 15", we can conclude that there was an increasing trend of the coarse particles ($\alpha_{440\text{-}870)}$ over time is higher than the anthropogenic one ($\alpha_{380\text{-}500}$) during the second sub-period (2012 - 2017) in all months except Feb, Aug, and Dec. In January and October, the ratio between the two sub-periods is equal. Another thing is that during the month of February the increasing trend of the coarse particles was higher in the first sub-period (2004-2011) over the eastern region.

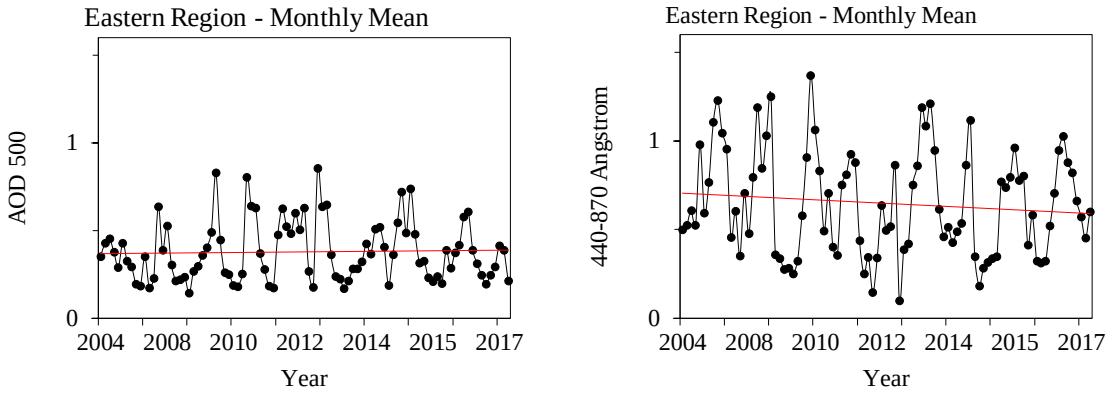

Figure 27. Trend of τ_{500} & $\alpha_{440-870}$ over Mezaira, Saudi Arabia for 2004 to 2018 using monthly mean values

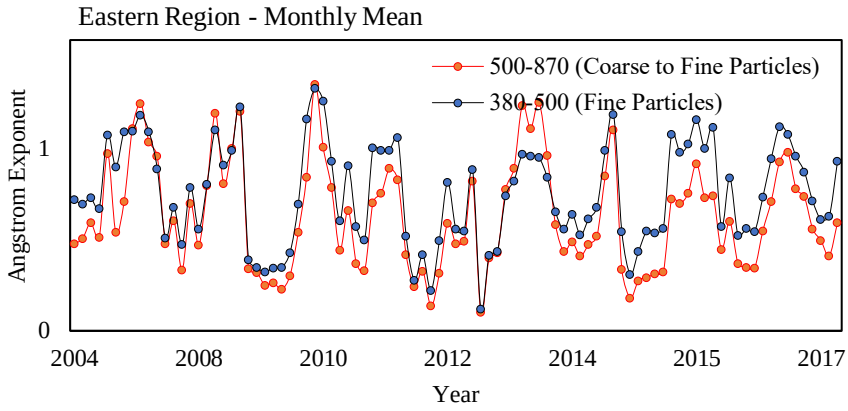

Figure 28. Trend of $\alpha_{380-500}$ & $\alpha_{500-870}$ over Mezaira, Saudi Arabia for 2004 to 2018 using monthly mean values.

Table 13. Monthly Statistical Comparison over Mezaira, UAE during the periods 2004 – 2017.

	Mean			Median		
N:13	Slope	Percentage	P-Value	Slope	Percentage	P-Value
τ500	0.0040	101	4.54×10^{-01}	0.0001	2	6.67×10^{-01}
α 440-870	-0.0012	30	**3.73×10^{-05}**	-0.0013	33	**4.76×10^{-05}**
α 380-500	-0.0002	5	**2.49×10^{-06}**	-0.0005	13	**7.00×10^{-06}**
α 500-870	-0.0013	33	**3.16×10^{-05}**	-0.0013	33	**3.01×10^{-05}**

Table 14. Monthly Statistical Comparison over Mezaira, UAE during the periods 2004 and 2017.

	Mean			Median		
N: 7 (Jan)	Slope	Percentage	P-Value	Slope	Percentage	P-Value
τ500	-0.0039	7	6.43×10^{-01}	-0.0043	14	6.03×10^{-01}
α 440-870	-0.0225	26	5.17×10^{-01}	-0.0253	19	5.18×10^{-01}
α 380-500	-0.0059	5	8.12×10^{-01}	-0.0055	4	8.42×10^{-01}
α 500-870	-0.0274	33	4.68×10^{-01}	-0.0308	24	4.63×10^{-01}
N: 8 (Feb)	Slope	Percentage	P-Value	Slope	Percentage	P-Value
τ500	0.0016	5	9.08×10^{-01}	0.0007	2	9.32×10^{-01}
α 440-870	0.0475	36	7.51×10^{-02}	0.0429	58	1.25×10^{-01}
α 380-500	0.058	43	**4.04×10^{-02}**	0.0538	61	9.88×10^{-02}
α 500-870	0.0381	29	1.77×10^{-01}	0.0343	49	2.5×10^{-01}
N: 7 (Mar)	Slope	Percentage	P-Value	Slope	Percentage	P-Value
τ500	0.0097	24	5.86×10^{-01}	0.0137	28	4.41×10^{-01}
α 440-870	0.0007	1	9.74×10^{-01}	0.0012	2	9.61×10^{-01}
α 380-500	0.0106	9	6.3×10^{-01}	0.0123	16	6.39×10^{-01}
α 500-870	-0.0016	1	9.33×10^{-01}	-0.0011	2	9.63×10^{-01}
N: 6 (Apr)	Slope	Percentage	P-Value	Slope	Percentage	P-Value
τ500	-0.0102	17	6.25×10^{-01}	-0.0067	10	7.22×10^{-01}
α 440-870	0.0232	28	3.94×10^{-01}	0.025	44	3.23×10^{-01}
α 380-500	0.0514	61	1.58×10^{-01}	0.0484	61	1.81×10^{-01}
α 500-870	0.0237	30	4×10^{-01}	0.0289	52	2.76×10^{-01}

N: (May)	Slope	Percentage	P-Value	Slope	Percentage	P-Value
τ500	-0.0278	46	5×10^{-01}	-0.0287	43	4.39×10^{-01}
α 440-870	0.0444	37	1.65×10^{-01}	0.036	81	2.32×10^{-01}
α 380-500	0.0788	59	8.10×10^{-02}	0.0738	114	1.01×10^{-01}
α 500-870	0.0493	43	1.06×10^{-01}	0.0406	93	1.66×10^{-01}
N: 7 (Jun)	Slope	Percentage	P-Value	Slope	Percentage	P-Value
τ500	0.0018	3	9.23×10^{-01}	0.0034	5	8.62×10^{-01}
α 440-870	-0.0141	15	3.86×10^{-01}	-0.0221	40	2.34×10^{-01}
α 380-500	-0.0137	12	4.59×10^{-01}	-0.0239	29	2.73×10^{-01}
α 500-870	-0.0113	12	4.57×10^{-01}	-0.0193	35	2.73×10^{-01}
N: 7 (Jul)	Slope	Percentage	P-Value	Slope	Percentage	P-Value
τ500	0.0086	15	5×10^{-01}	0.0074	11	5.44×10^{-01}
α 440-870	-0.0081	18	4.54×10^{-01}	-0.0092	21	3.05×10^{-01}
α 380-500	-0.006	12	6.40×10^{-01}	-0.0064	10	5.91×10^{-01}
α 500-870	-0.0065	13	5.10×10^{-01}	-0.0068	16	3.87×10^{-01}
N: 9 (Aug)	Slope	Percentage	P-Value	Slope	Percentage	P-Value
τ500	0.0138	45	1.17×10^{-01}	0.0093	17	2.44×10^{-01}
α 440-870	-0.0179	17	6.54×10^{-02}	-0.0231	43	$\mathbf{2.18\times10^{-02}}$
α 380-500	-0.0175	19	1.76×10^{-01}	-0.0215	30	10×10^{-02}
α 500-870	-0.0152	14	1.4×10^{-01}	-0.0209	40	$\mathbf{5\times10^{-02}}$
N: 9 (Sep)	Slope	Percentage	P-Value	Slope	Percentage	P-Value
τ500	-0.0029	6	6.43×10^{-01}	-0.0038	8	4.91×10^{-01}

α 440-870	0.0199	28	8.79×10^{-02}	0.0212	24	1.53×10^{-01}
α 380-500	0.0215	25	2.46×10^{-01}	0.026	23	2.55×10^{-01}
α 500-870	0.0213	31	5.01×10^{-02}	0.0221	26	10×10^{-02}
N: 8 (Oct)	Slope	Percentage	P-Value	Slope	Percentage	P-Value
τ500	0.001	2	7.24×10^{-01}	-0.0001	0	9.76×10^{-01}
α 440-870	-0.0133	19	2.86×10^{-01}	-0.0207	18	7.65×10^{-02}
α 380-500	-0.0023	2	8.56×10^{-01}	-0.008	6	6.02×10^{-01}
α 500-870	-0.0149	22	2.92×10^{-01}	-0.0212	19	9.87×10^{-02}
N: 8 (Nov)	Slope	Percentage	P-Value	Slope	Percentage	P-Value
τ500	0.0034	7	2.25×10^{-01}	0.0024	9	4.22×10^{-01}
α 440-870	-0.025	40	3.13×10^{-01}	-0.0319	24	2.19×10^{-01}
α 380-500	-0.0107	12	5.08×10^{-01}	-0.0122	9	5.17×10^{-01}
α 500-870	-0.0286	44	3×10^{-01}	-0.0351	26	2.18×10^{-01}
N: 9 (Dec)	Slope	Percentage	P-Value	Slope	Percentage	P-Value
τ500	-0.0006	2	9.74×10^{-01}	0.001	4	9.61×10^{-01}
α 440-870	-0.0088	10	7.27×10^{-01}	-0.0123	12	6.34×10^{-01}
α 380-500	-0.0006	1	9.81×10^{-01}	-0.0024	2	9.32×10^{-01}
α 500-870	-0.0131	16	6.23×10^{-01}	-0.0154	15	5.61×10^{-01}

Table 15. Monthly Statistical Comparison over Mezaira, UAE during the sub-periods 2004 – 2011 (G1) and 2012 -2017 (G2).

Jan	G1 (N:58)	G2 (N:111)	P	t
τ500	0.255	0.240	5.61×10^{-01}	2
α 440-870	1.088	0.852	**6.07×10^{-04}**	**2**
α 380-500	1.007	0.864	**1.17×10^{-02}**	**2**
α 500-870	1.072	0.823	**3.98×10^{-04}**	**2**
Feb	G1 (N:32)	G2 (N:89)	P	t
τ500	0.287	0.273	7.01×10^{-01}	2
α 440-870	0.399	0.785	**1.88×10^{-08}**	**2**
α 380-500	0.412	0.835	**4.48×10^{-09}**	**2**
α 500-870	0.384	0.749	**5.56×10^{-08}**	**2**
Mar	G1 (N:44)	G2 (N:118)	P	t
τ500	0.311	0.428	**6.46×10^{-03}**	**2**
α 440-870	0.434	0.436	9.66×10^{-01}	2
α 380-500	0.449	0.517	2.00×10^{-01}	2
α 500-870	0.420	0.416	9.30×10^{-01}	2
Apr	G1 (N:29)	G2 (N:128)	P	t
τ500	0.395	0.413	5.28×10^{-01}	2
α 440-870	0.306	0.400	**6.79×10^{-03}**	**2**
α 380-500	0.324	0.550	**7.77×10^{-08}**	**2**

α 500-870	0.290	0.389	**4.12×10^{-03}**	**2**
May	G1 (N:18)	G2 (N:89)	P	t
τ500	0.441	0.434	8.71×10^{-01}	2
α 440-870	0.280	0.397	**6.68×10^{-03}**	**2**
α 380-500	0.359	0.569	**2.50×10^{-04}**	**2**
α 500-870	0.258	0.403	**4.50×10^{-04}**	**2**
Jun	G1 (N:44)	G2 (N:94)	P	t
τ500	0.474	0.465	8.17×10^{-01}	2
α 440-870	0.424	0.351	5.12×10^{-02}	2
α 380-500	0.598	0.533	1.95×10^{-01}	2
α 500-870	0.399	0.348	1.44×10^{-01}	2
Jul	G1 (N:62)	G2 (N:100)	P	t
τ500	0.562	0.632	7.90×10^{-02}	2
α 440-870	0.466	0.372	**4.30×10^{-04}**	**2**
α 380-500	0.631	0.528	**2.11×10^{-03}**	**2**
α 500-870	0.443	0.370	**4.17×10^{-03}**	**2**
Aug	G1 (N:107)	G2 (N:101)	P	t
τ500	0.503	0.570	**2.29×10^{-02}**	**2**
α 440-870	0.547	0.464	**9.25×10^{-03}**	**2**
α 380-500	0.709	0.613	**6.75×10^{-03}**	**2**
α 500-870	0.520	0.467	8.85×10^{-02}	2

Sep	G1 (N:107)	G2 (N:85)	P	t
τ500	0.390	0.380	6.38×10^{-01}	2
α 440-870	0.652	0.764	**2.47×10^{-03}**	**2**
α 380-500	0.853	0.894	3.08×10^{-01}	2
α 500-870	0.620	0.770	**4.91×10^{-05}**	**2**
Oct	G1 (N:111)	G2 (N:93)	P	t
τ500	0.294	0.293	9.36×10^{-01}	2
α 440-870	0.893	0.849	2.90×10^{-01}	2
α 380-500	0.969	0.977	8.35×10^{-01}	2
α 500-870	0.881	0.841	3.52×10^{-01}	2
Nov	G1 (N:142)	G2 (N:88)	P	t
τ500	0.223	0.235	3.04×10^{-01}	2
α 440-870	1.095	1.001	**3.12×10^{-02}**	**2**
α 380-500	1.100	1.026	**1.98×10^{-02}**	**2**
α 500-870	1.081	0.990	5.13×10^{-02}	2
Dec	G1 (N:85)	G2 (N:110)	P	t
τ500	0.210	0.199	3.96×10^{-01}	2
α 440-870	1.028	0.990	4.49×10^{-01}	2
α 380-500	1.058	1.042	6.86×10^{-01}	2
α 500-870	1.004	0.958	3.82×10^{-01}	2

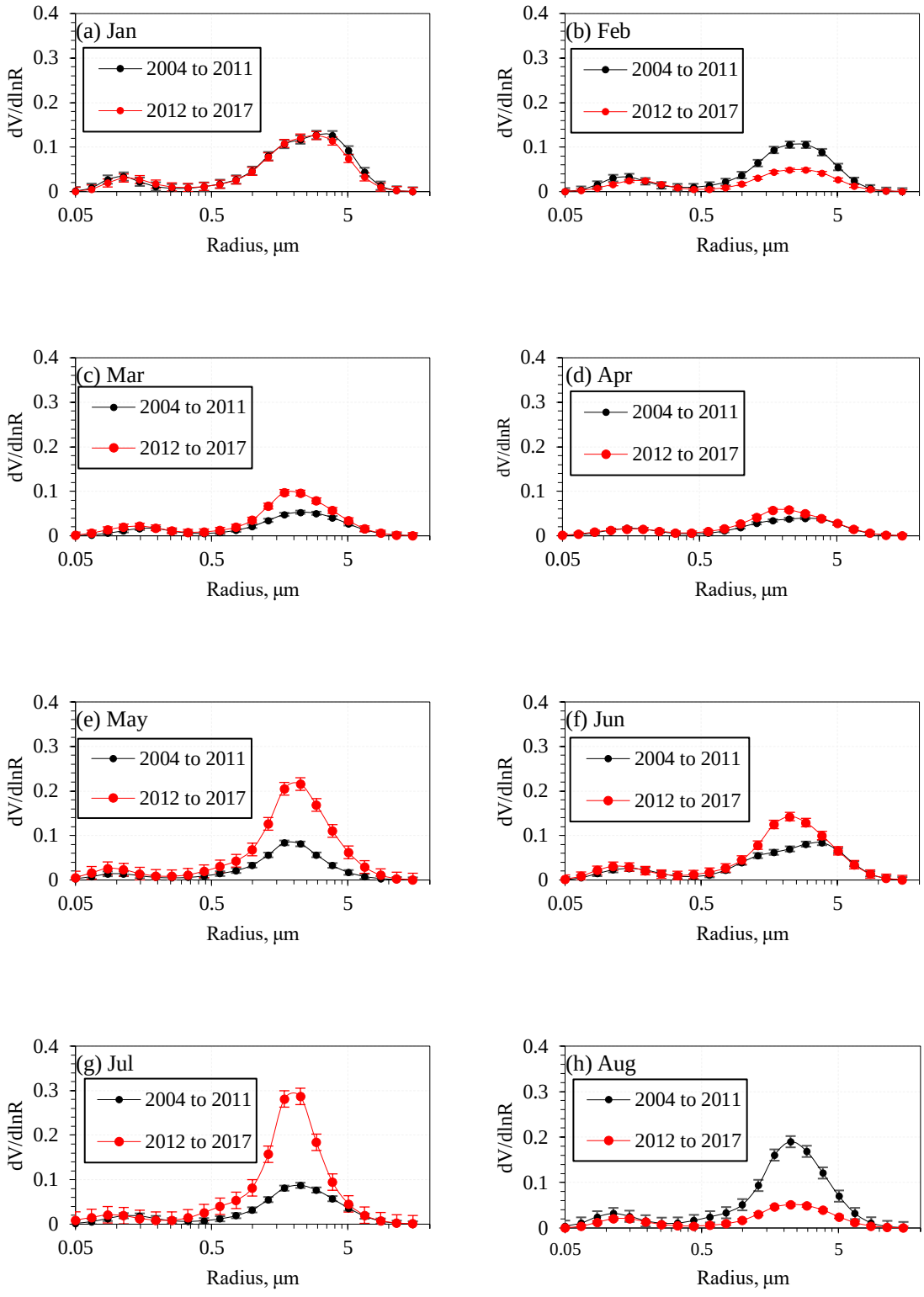
(a) Jan
(b) Feb
(c) Mar
(d) Apr
(e) May
(f) Jun
(g) Jul
(h) Aug
2004 to 2011
2012 to 2017
dV/dlnR
Radius, μm
0.4
0.3
0.2
0.1
0
0.05
0.5
5

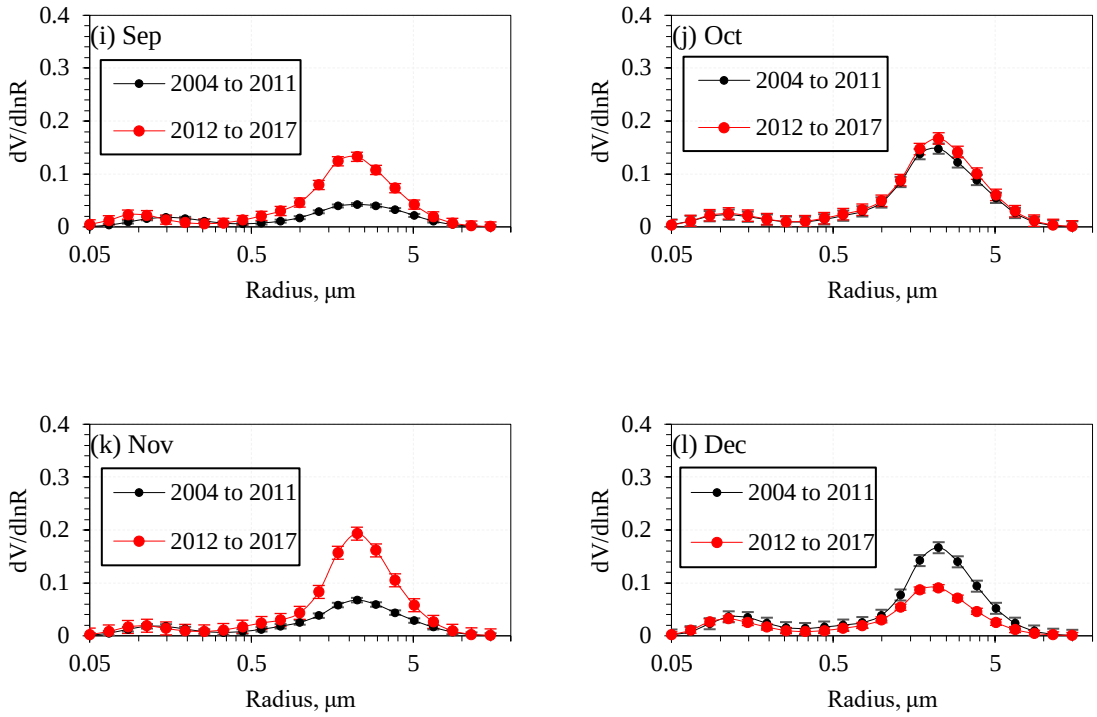

Figure 29. Monthly variation using size distribution data over Mezaira, UAE during the sub-periods 2004 – 2011 (G1) and 2012 -2017 (G2).

Daily values analysis in "Figure 30" "Table 16" showed that there is an overall increasing trend at τ_{500} which was by (6%) with decreasing trends at $\alpha_{440\text{-}870}$, $\alpha_{380\text{-}500,}$ and $\alpha_{500\text{-}870}$ by (5 %), (21%) and (24%), respectively, with a high level of confidence for all results.

However, using the same frequency, we investigated each month separately and the results are represented in "Table 17". The results indicate that the PM_{10} concentration increased in January, April, June, and November. However, only the June value is statistically significant. As for the $\alpha_{440\text{-}870}$ wavelength, the decline in the trend was observed in January, February, March, April, and September. The trend is approximately the same as the trend at $\alpha_{380\text{-}500}$ and $\alpha_{500\text{-}870}$.

The largest decline of PM_{10} concentration in the region was noticed during August, September with associated statistical variations (530%, 287%, and 160%), respectively, while an increase was observed in the month of June. Results also showed a very low level of confidence "Table 17".

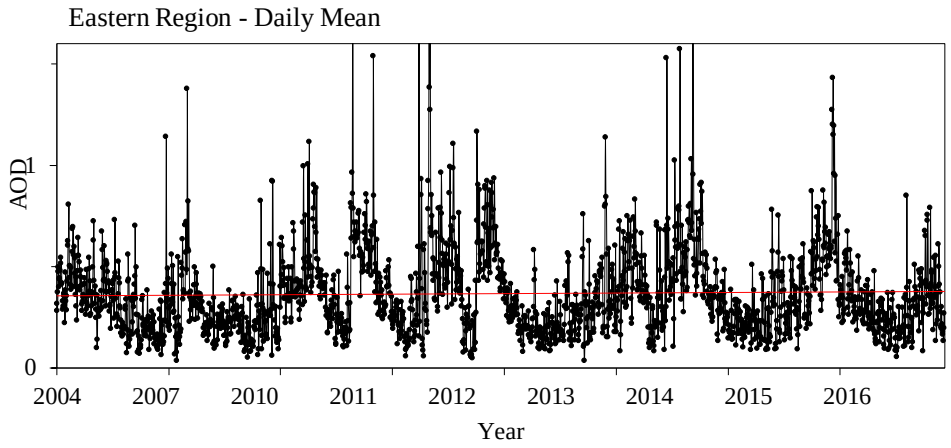

Figure 30. Aerosols Optical Depth over the East of Arabian Peninsula

Table 16. Daily Statistical Comparison over Mezaira, UAE during the periods 2001 and 2017.

	Mean		
N: 2034	Slope	Percentage	P-Value
τ500	0.00001	6	**9.22×10^{-08}**
α 440-870	-0.00007	-21	**1.85×10^{-53}**
α 380-500	-0.00002	-5	**1.28×10^{-72}**
α 500-870	-0.00008	-25	**4.82×10^{-54}**

Table 17. Monthly Statistical Comparison using daily values over Mezaira, UAE during the periods 2001 and 2004 and 2017.

Mean	Jan (N: 169)			Mar (N: 162)		
	Slope	Percentage	P-Value	Slope	Percentage	P-Value
τ500	0.0015	69	2.04×10^{-01}	0.005	214	4.94×10^{-02}
α 440-870	-0.003	-74	4.03×10^{-01}	-0.0036	-87	1.40×10^{-01}
α 380-500	-0.0054	-118	5.97×10^{-02}	-0.0002	-5	9.41×10^{-01}
α 500-870	-0.0024	-136	5.12×10^{-01}	-0.0028	-69	2.17×10^{-01}
Mean	Feb (N: 121)			Apr (N: 147)		
	Slope	Percentage	P-Value	Slope	Percentage	P-Value
τ500	-0.0031	-103	6.77×10^{-02}	0.0013	49	4.94×10^{-01}
α 440-870	-0.003	-53	**6.81×10^{-03}**	-0.0018	-41	4.01×10^{-01}
α 380-500	-0.0054	-84	**1.57×10^{-03}**	0.0018	38	5.13×10^{-01}
α 500-870	-0.0024	-44	**1.39×10^{-02}**	-0.0013	-30	5.26×10^{-01}
Mean	May (N: 107)			Jul (N: 162)		
	Slope	Percentage	P-Value	Slope	Percentage	P-Value
τ500	-0.0032	40	2.21×10^{-01}	-0.0022	-97	3.22×10^{-01}
α 440-870	0.0029	-50	2.59×10^{-01}	-0.001	-24	4.96×10^{-01}
α 380-500	0.0038	-83	2.48×10^{-01}	-0.002	-42	2.76×10^{-01}
α 500-870	0.0036	62	1.51×10^{-01}	-0.0009	-22	5×10^{-01}
Mean	Jun (N: 137)			Aug (N: 208)		
	Slope	Percentage	P-Value	Slope	Percentage	P-Value
τ500	0.007	262	**1.17×10^{-03}**	-0.0094	-534	**2.39×10^{-09}**

α 440-870	0.0039	78	**4.72×10^{-02}**	0.007	214	**7.20×10^{-05}**
α 380-500	0.005	89	5.25×10^{-02}	0.0094	256	**1.59×10^{-06}**
α 500-870	0.0032	65	8.21×10^{-02}	0.0071	221	**4.09×10^{-05}**
Mean	Sep (N: 192)			Nov (N: 230)		
	Slope	Percentage	P-Value	Slope	Percentage	P-Value
τ500	-0.0056	-287	**2.94×10^{-06}**	0.0006	36	3.43×10^{-01}
α 440-870	-0.0007	-20	7.57×10^{-01}	0.0073	262	**3.53×10^{-03}**
α 380-500	0.0013	33	5.96×10^{-01}	0.0041	125	**2.70×10^{-02}**
α 500-870	0.2209	638	6.85×10^{-01}	0.0075	273	**4.75×10^{-03}**
Mean	Oct (N: 204)			Dec (N: 195)		
	Slope	Percentage	P-Value	Slope	Percentage	P-Value
τ500	-0.0031	-166	**4.89×10^{-05}**	-0.0008	-43	2.58×10^{-01}
α 440-870	0.0112	348	**6.78×10^{-07}**	0.0002	6	9.37×10^{-01}
α 380-500	0.0047	128	**1.47×10^{-02}**	0.0003	8	9.01×10^{-01}
α 500-870	0.0116	367	**5.44×10^{-07}**	-0.0003	-9	9.22×10^{-01}

Same as for all locations, we looked at the seasonal variation but starting from 2004 to 2017 over the eastern region. Changes in AOD, Angstrom, and size distribution were calculated during different seasons over the years covered by the study. The results are represented in "Figure 31". During two sub-periods (2004 - 2011 and 2012 - 2017), an increasing trend in PM_{10} concentration was found during the second sub-period (2012 – 2017) in all seasons except in the fall season where a decline was noticed. Trends at $\alpha_{440\text{-}870}$ were decreasing in all seasons as well, but not during the spring season. There was an equality between the two sub-periods which means lower man-made emissions during this season. However, the results (AOD) showed a low level of confidence with ($p < 0.05$) during all seasons except the summer. While at two wavelengths ($\alpha_{440\text{-}870}$ and $\alpha_{500\text{-}870}$) the confidence levels were high during the summer and fall. Lastly, the same was also noticed at $\alpha_{380\text{-}500}$ during the summer and spring "Table 18". Analyzing the size distribution of particulate matter for seasonally "Figure 32" revealed that in general natural emissions slightly increased during the second sub-period (2012- 2017), except during spring and fall.

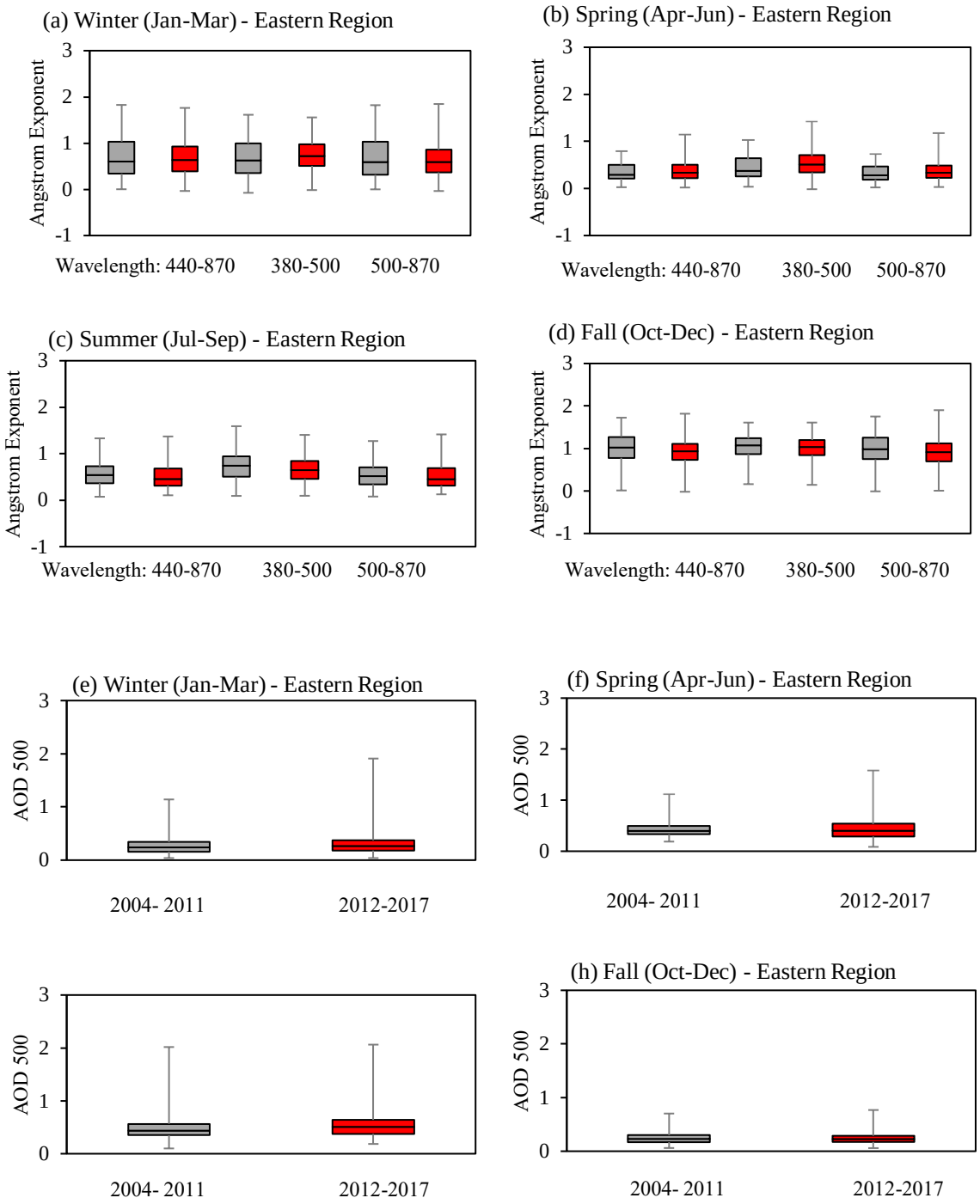

Figure 31. Seasonal Variation using daily mean values of τ_{500}, $\alpha_{440-870}$, $\alpha_{380-500}$ & $\alpha_{500-870}$ over Mezaira, UAE during the sub-periods 2004 – 2011 (G1) and 2012 -2017 (G2).

Table 18. Seasonal Statistical Comparison over Mezaira, UAE during the sub-periods 2004 – 2011 (G1) and 2012 -2017 (G2).

		τ500	α440-870	α380-500	α500-870	N
Winter	p	6.58×10^{-02}	5.24×10^{-01}	2.81×10^{-01}	3.69×10^{-01}	134
	t	2	2	2	2	318
Spring	p	7.36×10^{-01}	2.58×10^{-01}	**7.76×10^{-03}**	**5.24×10^{-02}**	91
	t	2	2	**2**	**2**	311
Summer	p	**6.64×10^{-04}**	**2.36×10^{-02}**	**6.36×10^{-04}**	3.73×10^{-01}	276
	t	**2**	**2**	**2**	2	286
Fall	p	7.07×10^{-01}	1.57×10^{-02}	1.45×10^{-01}	**1.74×10^{-02}**	338
	t	2	2	2	**2**	291

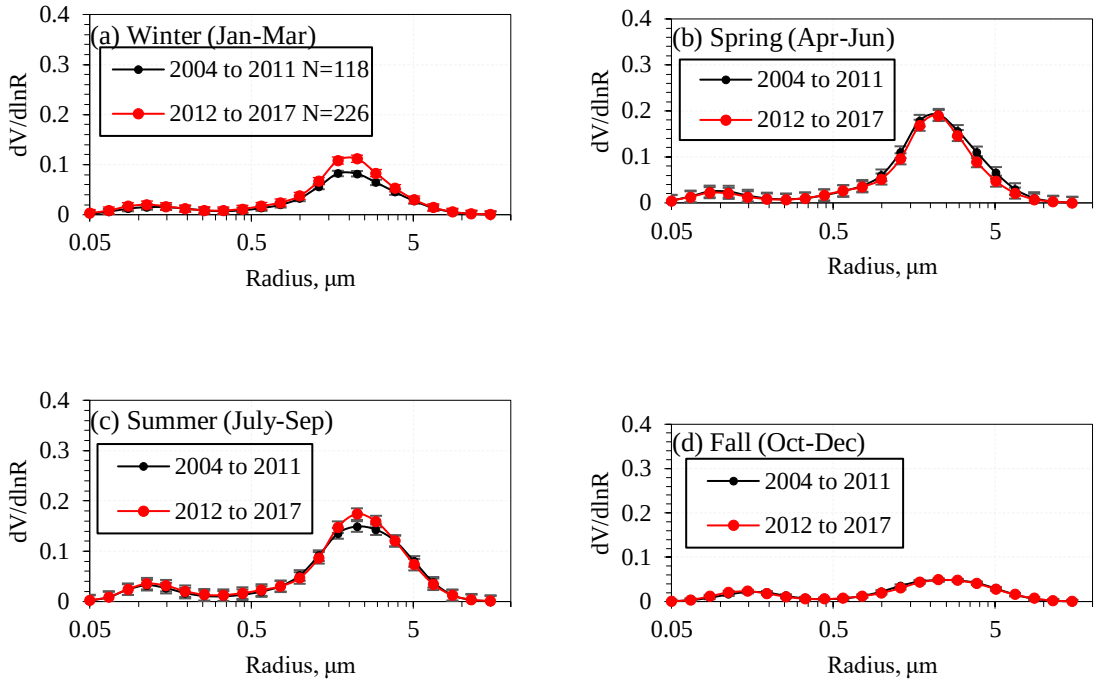

Figure 32. Seasonal Variation using size distribution data over Mezaira, UAE during the sub-periods 2004 – 2011 (G1) and 2012 -2017 (G2).

4.1.3. Western Region - Particulate Matter Trend and Variation Percent

The third area is the western region of the Arabian Peninsula.

The figures in this section show the trends at different frequencies at τ_{500}, $\alpha_{440-870}$, $\alpha_{380-500}$, and $\alpha_{500-870}$. These frequencies are similar to the pervious mentioned frequencies (e.g. daily, monthly, seasonal, and annual). The values were calculated using observations measured over the KAUST_Campus station during the period 2012 to 2018. The number of daily, monthly, and annual values here are 796, 34, and 6, respectively. Mean values corresponding to different frequency variations are represented along with the percentage difference and the p values "Table 19".

The results of the annual mean analysis "Figure 33" show that there is a slight increasing trend of τ_{500} and $\alpha_{440-870}$ and this is not the same as the cases in the Solar Village and the Mezaira analysis results. Such an increasing trend in AE indicates higher anthropogenic emissions over the western region of the Arabian Peninsula.

Moreover, results show that over the KAUST_Campus there is an overall increasing trend in τ_{500} and $\alpha_{440-870}$ by (11%) and (18%) respectively. However, the results are not statistically significant at the 95% confidence level with ($p < 0.05$) where the p values of τ_{500} $\alpha_{440-870}$ are 0.8.

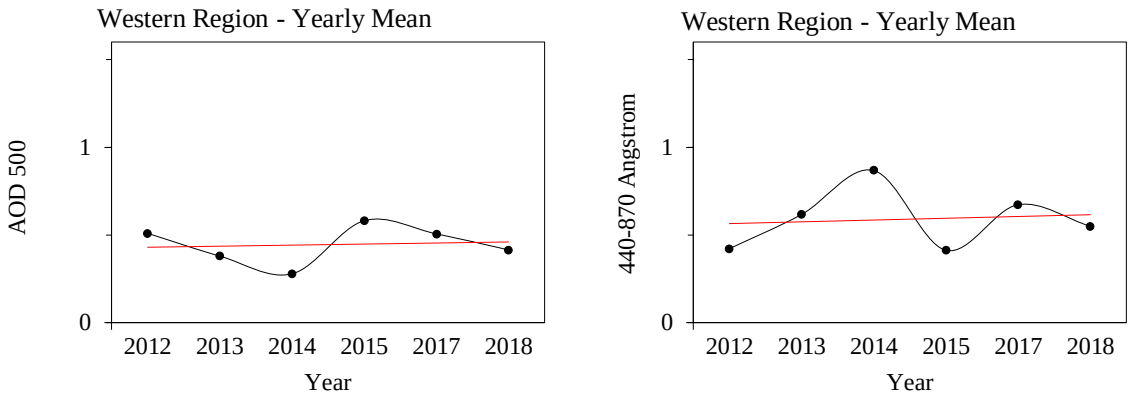

Figure 33. Trend of τ_{500} & $\alpha_{440-870}$ over KAUST_Campus, Saudi Arabia for 2012 to 2018 using annual mean values

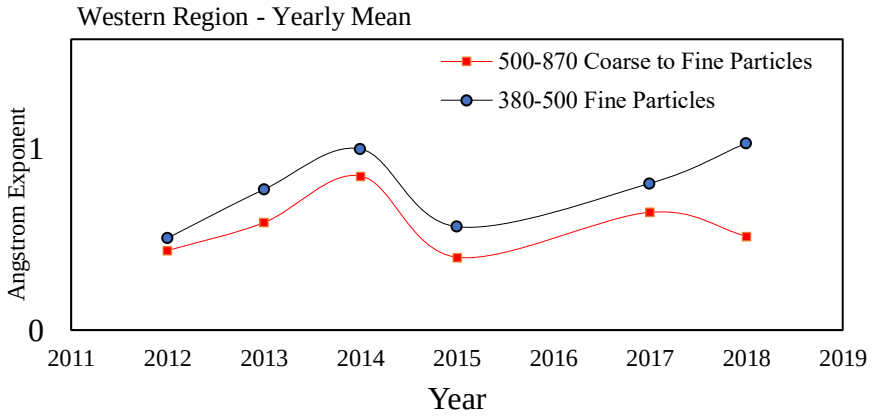

Figure 34. Trend of $\alpha_{380-500}$ & $\alpha_{500-870}$ over KAUST_Campus, Saudi Arabia for 2012 to 2018 using annual mean values

Table 19. Yearly Statistical Comparison over KAUST_Campus, Saudi Arabia during the periods 2012 and 2018.

	Mean			Median		
N: 6	Slope	Percentage	P-Value	Slope	Percentage	P-Value
τ500	0.006	11	8.38×10^{-01}	0.0025	3	8.95×10^{-01}
α 440-870	0.01	18	8.35×10^{-01}	0.0057	10	8.88×10^{-01}
α 380-500	0.0652	106	2.36×10^{-01}	0.0518	84	2.83×10^{-01}
α 500-870	0.0034	6	9.38×10^{-01}	0.0007	1	9.86×10^{-01}

Analysis using monthly mean values "Figure 35" "Table 22" shows a similar trend discussed above of “annual mean values”. The p-valued "Table 20" is not promising because there is only one mean value that is statistically significant (at $\alpha_{380-500}$). "Table 20" and "Figure 36" show that overall there is an increasing trend at $\alpha_{440-870,}$ $\alpha_{380-500}$, and $\alpha_{500-870}$ by 13%, 30%, and 10%, respectively. Also, the same as for $\tau_{500.}$ Results in "Table 21" indicate that an increasing trend τ_{500} was noticed during all months except Feb, Mar, and Jun. However, it is worth mentioning that there is no data after Sep or P-values for Jan and September. This is mainly because of the low number of observations for some months and unavailable data for others. Highest statistical variation was noticed in April (55%), while it varies between 19% and 50% during the other months. An identical trend has also been found between the $\alpha_{440-870}$ and $\alpha_{380-500}$ in each month and the same trend as in $\alpha_{500\text{-}870}$ except during April, and July. This suggests that there is an increasing trend at AE for most of the months, and therefore, higher man-made emissions. P values during all months exceed 0.05, alt-

hough the mean value during April at $\alpha_{440-870}$ is below the significant level and the median value is at the same wavelength during March. The results represented in "Table 21" show that over the west region there is an increasing trend at τ_{500} by (15%) and (72%) at $\alpha_{440-870}$. Also, the variations associated with $\alpha_{380-500}$ and $\alpha_{500-870}$ increased over time by (108%) and (70%), respectively. These variations were greatly increased when compared to other trends associated with other stations mentioned in previous sub-sections. Analyzing the size distribution of particulate matter in every month "Figure 37" shows that natural emissions only increased during the second sub-period (2007- 2012) in Apr, May, June, Aug, and Sep. However, the man-made emissions were higher than in the central and eastern regions, especially in Aug, Sep, Oct, Nov, and Dec.

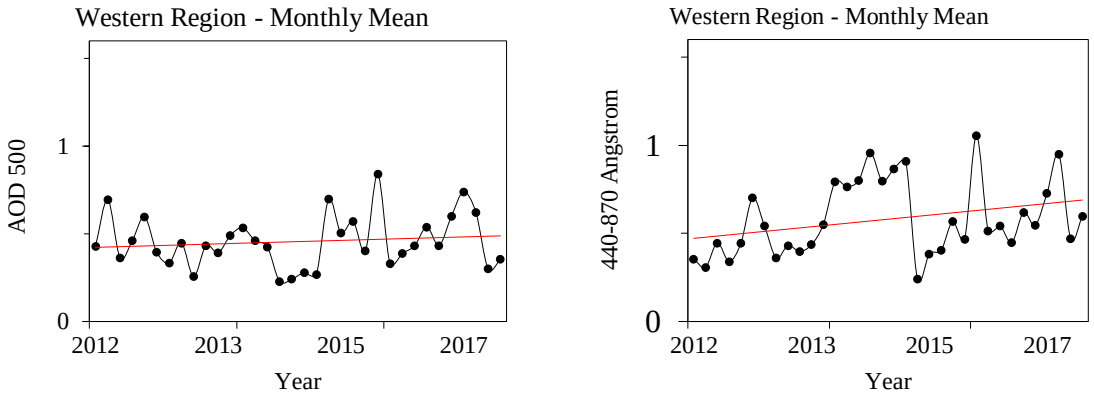

Figure 35. Trend of τ_{500} & $\alpha_{440-870}$ over KAUST_Campus, Saudi Arabia for 2012 to 2018 using monthly mean values

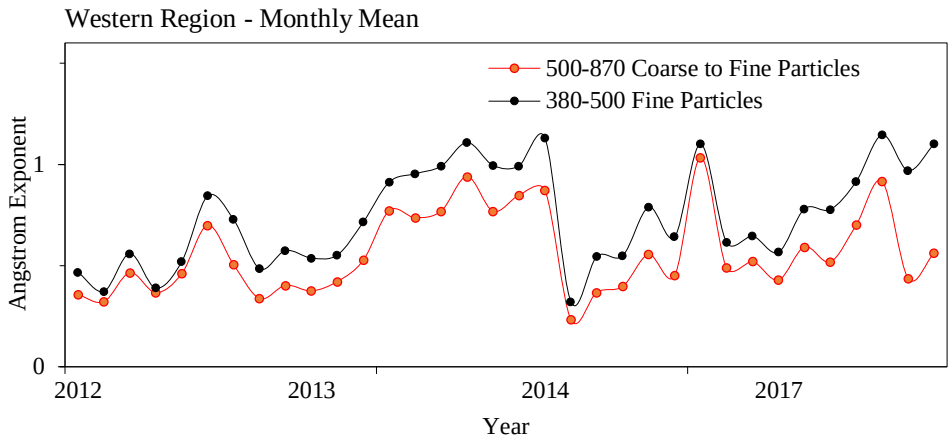

Figure 36. Trend of $\alpha_{380-500}$ & $\alpha_{500-870}$ over KAUST_Campus, Saudi Arabia for 2012 to 2018 using monthly mean values

Table 20. Monthly Statistical Comparison over KAUST_Campus, Saudi Arabia during the periods 2012 - 2018.

	Mean			Median		
N: 34	Slope	Percentage	P-Value	Slope	Percentage	P-Value
τ500	0.0013	8	4.52×10^{-01}	0.0019	12	2.25×10^{-01}
α 440-870	0.0021	13	7.37×10^{-02}	0.0024	15	9.6×10^{-02}
α 380-500	0.0047	30	**2.06×10^{-02}**	0.0047	30	**3.29×10^{-02}**
α 500-870	0.0016	10	7.72×10^{-02}	0.002	13	1.15×10^{-01}

Table 21. Monthly Statistical Comparison over KAUST_Campus, Saudi Arabia during the periods 2012 and 2018.

	Mean			Median		
N: 2 (Jan)	Slope	Percentage	P-Value	Slope	Percentage	P-Value
τ500	0.0104	7	-	0.0171	11	-
α 440-870	0.089	19	-	0.0629	13	-
α 380-500	0.0264	5	-	0.0362	7	-
α 500-870	0.0861	18	-	0.0624	13	-
N: 4 (Feb)	Slope	Percentage	P-Value	Slope	Percentage	P-Value
τ500	-0.0156	19	5.94×10^{-01}	-0.0018	2	9.45×10^{-01}
α 440-870	0.0127	9	8.85×10^{-01}	0.0209	14	8.08×10^{-01}
α 380-500	0.0085	5	9.36×10^{-01}	0.0129	7	9.02×10^{-01}
α 500-870	0.0104	8	9×10^{-01}	0.0178	13	8.26×10^{-01}
N: 3 (Mar)	Slope	Percentage	P-Value	Slope	Percentage	P-Value
τ500	-0.0149	12	2.35×10^{-01}	-0.039	22	5.08×10^{-01}
α 440-870	0.0538	42	2×10^{-01}	0.0463	34	$\mathbf{1.77\times10^{-02}}$
α 380-500	0.0558	34	1.8×10^{-01}	0.0506	30	1.45×10^{-01}
α 500-870	0.05	40	8.3×10^{-02}	0.0414	32	7.64×10^{-02}
N: 4 (Apr)	Slope	Percentage	P-Value	Slope	Percentage	P-Value
τ500	0.0587	55	5.9×10^{-02}	0.0585	50	5.85×10^{-02}
α 440-870	-0.0078	9	$\mathbf{-7.8\times10^{-03}}$	-0.0088	9	$\mathbf{-8.8\times10^{-03}}$
α 380-500	-0.014	12	-1.4×10^{-02}	-0.0121	10	-1.2×10^{-02}
α 500-870	-0.0107	12	-1.1×10^{-02}	-0.0133	14	-1.3×10^{-02}

N: 4 (May)	Slope	Percentage	P-Value	Slope	Percentage	P-Value
τ500	0.0129	12	8.78×10^{-02}	-0.0003	0	9.78×10^{-01}
α 440-870	0.0536	53	1.49×10^{-01}	0.0492	45	1.23×10^{-01}
α 380-500	0.0736	54	4.15×10^{-02}	0.0684	49	6.29×10^{-02}
α 500-870	0.0411	42	2.26×10^{-01}	0.0414	39	1.74×10^{-01}
N: 4 (Jun)	Slope	Percentage	P-Value	Slope	Percentage	P-Value
τ500	-0.0205	20	4.80×10^{-01}	-0.0128	10	6.63×10^{-01}
α 440-870	0.0204	23	4.20×10^{-01}	0.0074	7	4.52×10^{-01}
α 380-500	0.0824	58	1.89×10^{-01}	0.0754	46	9.84×10^{-02}
α 500-870	0.0162	19	4.99×10^{-01}	0.0012	1	8.93×10^{-01}
N: 5 (Jul)	Slope	Percentage	P-Value	Slope	Percentage	P-Value
τ500	0.0099	11	7.33×10^{-01}	0.0083	9	6.98×10^{-01}
α 440-870	-0.0125	11	2.62×10^{-01}	-0.0117	10	4.24×10^{-01}
α 380-500	0.0341	20	2.81×10^{-01}	0.0307	18	3.13×10^{-01}
α 500-870	-0.0158	14	2.21×10^{-01}	-0.0158	14	3.36×10^{-01}
N: 3 (Aug)	Slope	Percentage	P-Value	Slope	Percentage	P-Value
τ500	0.036	16	4.82×10^{-01}	0.0516	22	5.40×10^{-01}
α 440-870	-0.044	20	7.49×10^{-01}	-0.0158	7	8.82×10^{-01}
α 380-500	-0.0221	8	8.65×10^{-01}	0.0008	0	9.93×10^{-01}
α 500-870	-0.0444	21	7.40×10^{-01}	-0.0176	8	8.66×10^{-01}
N: 2 (Sep)	Slope	Percentage	P-Value	Slope	Percentage	P-Value
τ500	0.0427	16	-	0.0405	15	-

α 440-870	0.0646	15	-	0.0456	11	-
α 380-500	0.0507	10	-	0.048	9	-
α 500-870	0.0625	15	-	0.0446	11	-

Table 22. Monthly Statistical Comparison using daily values over KAUST_Campus, Saudi Arabia during the sub-periods 2012 – 2014 (G1) and 2015 -2018 (G2).

Jan	G1 (N:29)	G2 (N:28)	P	t
τ500	0.279	0.330	1.37×10^{-01}	2
α 440-870	0.866	1.055	**1.16×10^{-02}**	**2**
α 380-500	0.992	1.101	1.01×10^{-01}	2
α 500-870	0.847	1.035	**1.39×10^{-02}**	**2**
Feb	G1 (N:23)	G2 (N:20)	P	t
τ500	0.347	0.388	5.87×10^{-01}	2
α 440-870	0.526	0.514	8.75×10^{-01}	2
α 380-500	0.700	0.614	3.43×10^{-01}	2
α 500-870	0.495	0.489	9.37×10^{-01}	2
Mar	G1 (N:58)	G2 (N:24)	P	t
τ500	0.572	0.431	1.95×10^{-01}	2
α 440-870	0.335	0.542	**2.78×10^{-03}**	**2**
α 380-500	0.429	0.646	**6.97×10^{-03}**	**2**
α 500-870	0.330	0.520	**3.97×10^{-03}**	**2**
Apr	G1 (N:58)	G2 (N:50)	P	t

τ500	0.312	0.624	5.46×10^{-02}	2
α 440-870	0.439	0.336	1.12×10^{-01}	2
α 380-500	0.566	0.434	1.48×10^{-01}	2
α 500-870	0.435	0.323	1.90×10^{-01}	2
May	G1 (N:58)	G2 (N:44)	P	t
τ500	0.446	0.482	3.31×10^{-01}	2
α 440-870	0.370	0.464	**9.14×10^{-03}**	**2**
α 380-500	0.466	0.625	**6.02×10^{-03}**	**2**
α 500-870	0.371	0.444	**1.34×10^{-02}**	**2**
Jun	G1 (N:58)	G2 (N:46)	P	t
τ500	0.491	0.524	3.02×10^{-01}	2
α 440-870	0.440	0.434	3.83×10^{-01}	2
α 380-500	0.537	0.700	**1.82×10^{-04}**	**2**
α 500-870	0.440	0.419	6.27×10^{-01}	2
Jul	G1 (N:45)	G2 (N:68)	P	t
τ500	0.457	0.459	8.86×10^{-02}	2
α 440-870	0.604	0.572	5.64×10^{-01}	2
α 380-500	0.761	0.860	**8.73×10^{-04}**	**2**
α 500-870	0.588	0.548	2.70×10^{-01}	2
Aug	G1 (N:13)	G2 (N:46)	P	t
τ500	0.534	0.779	7.60×10^{-01}	2

α 440-870	0.792	0.627	5.64×10^{-02}	2
α 380-500	0.913	0.809	**1.75×10^{-02}**	**2**
α 500-870	0.772	0.603	7.23×10^{-02}	2
Sep	G1 (N:28)	G2 (N:9)	P	t
τ500	0.461	0.623	**2.53×10^{-02}**	**2**
α 440-870	0.766	0.948	**2.54×10^{-04}**	**2**
α 380-500	0.954	1.146	**8.92×10^{-05}**	**2**
α 500-870	0.737	0.915	**4.56×10^{-04}**	**2**

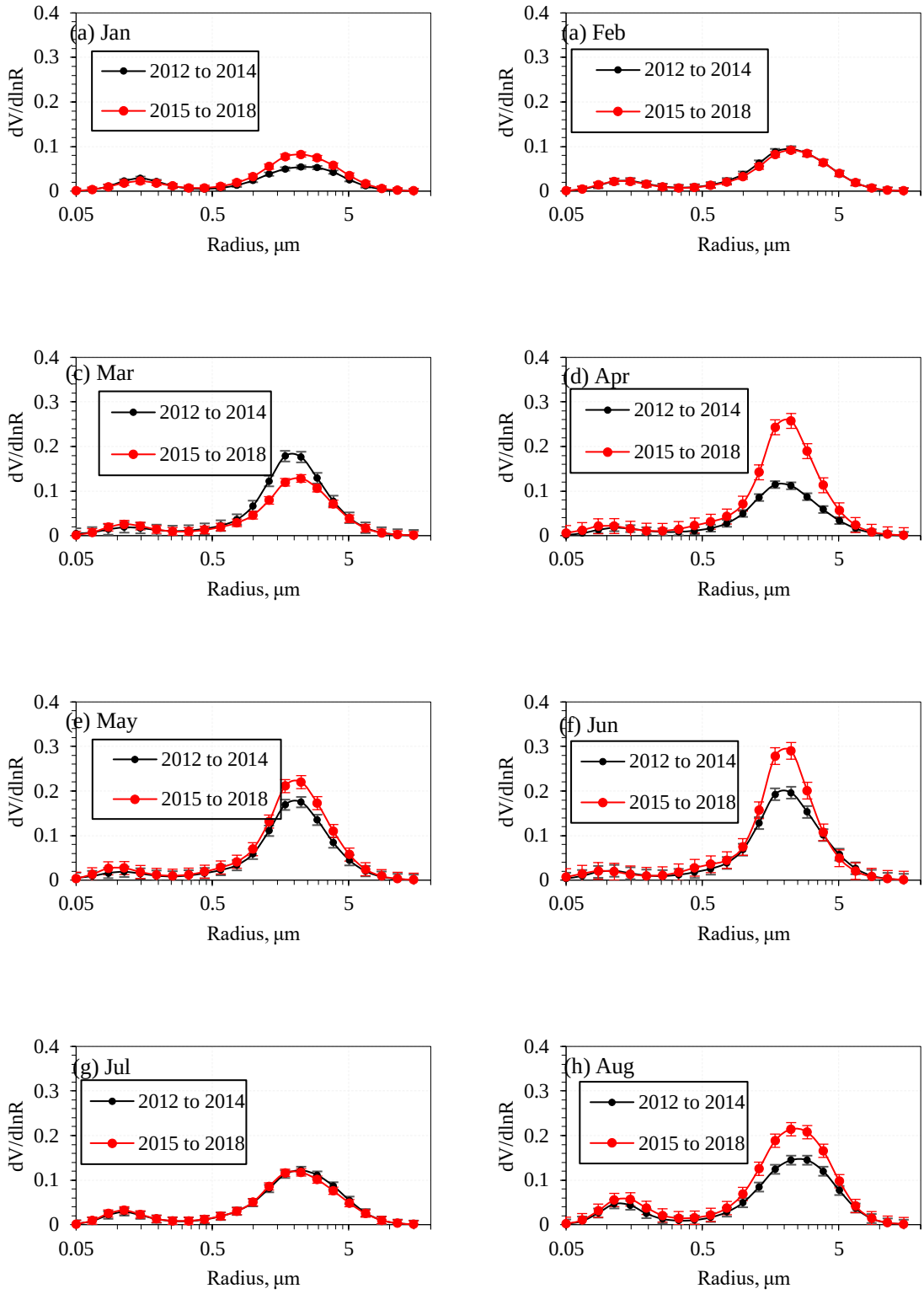
(a) Jan
2012 to 2014
2015 to 2018
dV/dlnR
Radius, μm
(a) Feb
(c) Mar
(d) Apr
(e) May
(f) Jun
(g) Jul
(h) Aug
0.4
0.3
0.2
0.1
0
0.05
0.5
5

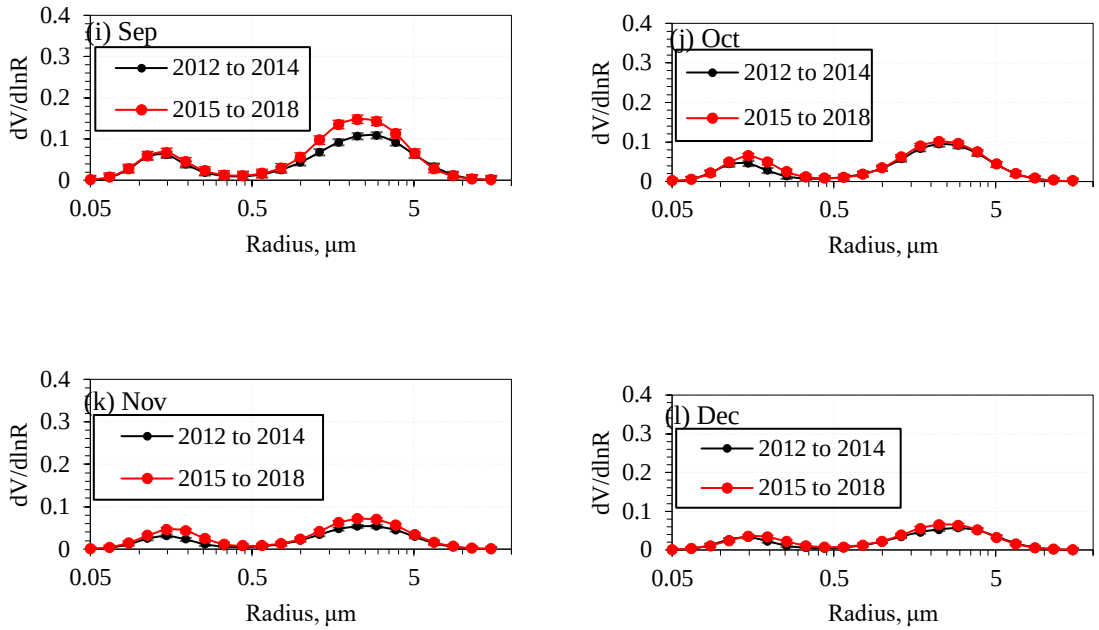

Figure 37. Monthly variation using size distribution data over KAUST_Campus, Saudi Arabia during the sub-periods 2012 – 2014 (G1) and 2015 -2018 (G2).

Analysis of the daily mean values was also preformed "Figure 38" "Table 23". In terms of particulate matter concentration (at τ_{500}), the results show that there was a high variation in the percentage during April, May, and June where the values are 220%, 230%, and 360%, respectively, with lower variations observed from July to December. Readings are range between 70% and 50% "Table 24". The different values of the wavelengths were divided into two clusters: one cluster increased significantly and the other decreased. The agreement in the upward trend between all wavelengths was observed in June, July, August, and October, while a declining trend was noticed from January to May, in addition to the September, November, and December. This can be explained by the levels of pollution resulting from human activity that fall in some months and rise during others.

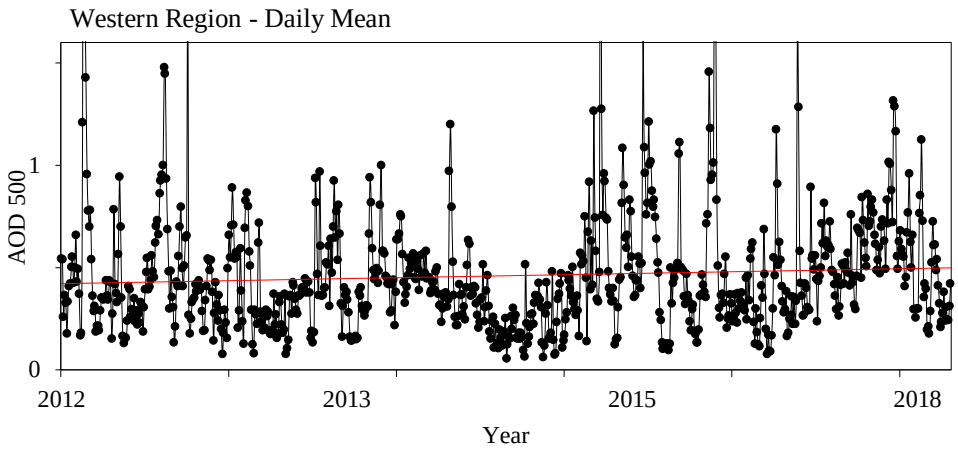

Figure 38. Aerosols Optical Depth over the West of Arabian Peninsula

Table 23. Daily Statistical Comparison over KAUST_Campus, Saudi Arabia during the periods 2012 - 2018.

	Mean		
N: 769	Slope	Percentage	P-Value
τ500	0.0001	15	9.87×10^{-01}
α 440-870	0.0003	72	$\mathbf{1.27\times10^{-11}}$
α 380-500	0.0005	108	$\mathbf{3.22\times10^{-18}}$
α 500-870	0.0003	71	$\mathbf{4.55\times10^{-11}}$

Table 24. Monthly Statistical Comparison using daily values over KAUST_Campus, Saudi Arabia during the periods 2012-2018.

Mean	Jan (N: 57)			Mar (N: 82)		
	Slope	Percentage	P-Value	Slope	Percentage	P-Value
τ500	0.0055	103	**5.36×10^{-03}**	0.0039	60	5.68×10^{-01}
α 440-870	-0.0194	115	**2.23×10^{-06}**	-0.0015	31	6.30×10^{-01}
α 380-500	-0.0177	97	**5.28×10^{-07}**	-0.0029	48	4.35×10^{-01}
α 500-870	-0.0197	120	**2.19×10^{-06}**	-0.0009	19	7.63×10^{-01}
Mean	Feb (N: 43)			Apr (N: 108)		
	Slope	Percentage	P-Value	Slope	Percentage	P-Value
τ500	0.0112	132	**8.79×10^{-03}**	0.0097	229	**1.03×10^{-02}**
α 440-870	-0.0067	55	1.33×10^{-01}	-0.0026	72	2.27×10^{-01}
α 380-500	-0.011	72	**4.28×10^{-02}**	-0.0021	45	4.30×10^{-01}
α 500-870	-0.0055	48	1.97×10^{-01}	-0.0025	70	2.35×10^{-01}
Mean	May (N: 102)			Jul (N: 113)		
	Slope	Percentage	P-Value	Slope	Percentage	P-Value
τ500	0.0105	232	**8.44×10^{-07}**	-0.0014	35	5.50×10^{-01}
α 440-870	-0.0108	268	**2.39×10^{-06}**	0.0034	66	7.14×10^{-02}
α 380-500	-0.0148	282	**3.77×10^{-07}**	0.007	96	**5.05×10^{-03}**
α 500-870	-0.0101	256	**3.32×10^{-06}**	0.003	60	1.15×10^{-01}
Mean	Jun (N: 104)			Aug (N: 59)		
	Slope	Percentage	P-Value	Slope	Percentage	P-Value
τ500	-0.0175	360	**6.56×10^{-06}**	-0.0086	70	9.06×10^{-02}

α 440-870	0.0207	492	**5.78×10^{-10}**	0.0157	140	**1.09×10^{-06}**
α 380-500	0.0251	429	**1.27×10^{-07}**	0.0145	103	**2.57×10^{-05}**
α 500-870	0.0201	485	**7.33×10^{-10}**	0.0157	145	**7.56×10^{-07}**
Mean	Sep (N: 37)			Nov (N: 30)		
	Slope	Percentage	P-Value	Slope	Percentage	P-Value
τ500	-0.007	52	**1.38×10^{-03}**	-0.0081	106	**1.16×10^{-04}**
α 440-870	-0.0107	49	**6.30×10^{-05}**	-0.0084	118	8.45×10^{-02}
α 380-500	-0.0092	34	**3.04×10^{-04}**	-0.0025	7	5.57×10^{-01}
α 500-870	-0.0107	51	**6.30×10^{-05}**	-0.0083	26	9.29×10^{-02}
Mean	Oct (N: 31)			Dec (N: 30)		
	Slope	Percentage	P-Value	Slope	Percentage	P-Value
τ500	-0.0013	9	7.80×10^{-01}	0.0044	55	3.29×10^{-02}
α 440-870	0.0135	52	**4.64×10^{-04}**	-0.0238	89	**4.17×10^{-04}**
α 380-500	0.0103	32	**9.56×10^{-03}**	-0.0223	67	**3.86×10^{-04}**
α 500-870	0.0139	56	**2.98×10^{-04}**	-0.0238	93	**4.17×10^{-04}**

The Solar Village and Mezaira are discussed regarding the seasonal variation starting from 2012 to 2018 over the western region. Changes in AOD, Angstrom, and size distribution were calculated during different seasons over the years covered by the study in this region. The results are shown in "Figure 39."

During two sub-periods (from 2012 to 2014 and from 2015 to 2018), a rise in particulate matter concentration (at τ_{500}) was noticed during the second sub-period in the spring and summer seasons, but not in the winter season in which there was a declining trend. It is important to mention that there was not enough data to investigate the fall season over the region.

At $\alpha_{440-870}$, we noticed an increase of AE values during the winter season, but not in the spring and summer seasons where the values were decreasing (Coarse-mode Particles). However, at $\alpha_{380-500}$ results showed an increasing trend in all seasons, which means that the values during the spring and summer decreased at the $\alpha_{440-870}$ wavelength due to a decrease in the coarse particles over the KAUST_Campus. This reflects higher anthropogenic emissions than the natural one during the three seasons. It has also been confirmed through the results shown at $\alpha_{500-870}$ where the trends during the spring and summer were decreasing.

Considering the P values "Table 25", the results about the winter season trend at $\alpha_{380-500}$ and $\alpha_{500-870}$ are not statistically significant and the same thing is true for the results about the summer season and the spring at $\alpha_{380-500}$. On the other hand, the distribution of the particle's size was also analyzed and plugged "Figure 40". The results indicated that natural particles are higher during the second period of all seasons, except in the winter where the rise of natural particles during the first period is higher.

Anthropogenic aerosols, in general, are lower than the natural during all periods, however, it is noticed that the levels of Anthropogenic particles are higher in the seasons of the fall, summer, winter, and spring, respectively "Figure 40"

By comparing the monthly change between two periods (2012 - 2014) and (2015 - 2018) based on size distribution "Figure 40", natural emission rates are higher than man-made during April, May, June, Augustus, September, October, November, and December, with the predominant type being the natural one. It was higher in ratio during the second period (2015 – 2018) than the first period (2012-2018), and almost equal during February and July. In addition, it was noticed that the highest rate of man-made emissions was during August, September, and October, over the other months.

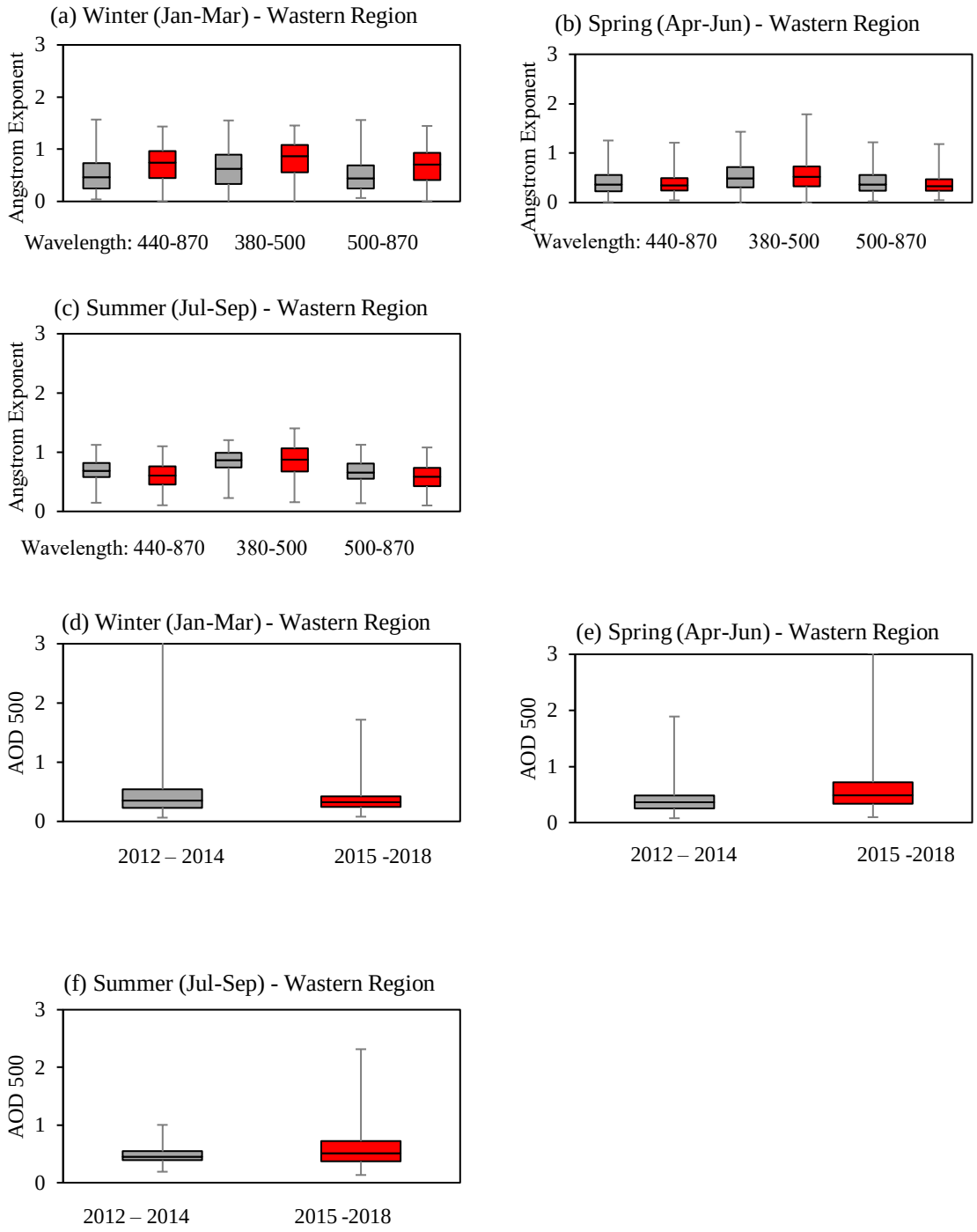

Figure 39. Seasonal Variation using daily mean values of τ_{500}, $\alpha_{440-870}$, $\alpha_{380-500}$ & $\alpha_{500-870}$ over KAUST_Campus, Saudi Arabia during the sub-periods 2012 – 2014 (G1) and 2015 -2018 (G2).

Table 25. Seasonal Statistical Comparison over KAUST_Campus, Saudi Arabia during the sub-periods 2012 – 2014 (G1) and 2015 -2018 (G2).

		τ500	α440-870	α380-500	α500-870	N
Winter	P	2.2×10^{-01}	**6×10^{-05}**	**1.2×10^{-03}**	**9×10^{-05}**	110
	t	2	**2**	**2**	**2**	72
Spring	p	**3×10^{-04}**	8×10^{-01}	1.25×10^{-01}	4.07×10^{-01}	174
	t	**2**	2	2	2	140
Summer	p	**6.4×10^{-03}**	1.3×10^{-01}	**3×10^{-05}**	2.45×10^{-01}	86
	t	**2**	2	**2**	2	123

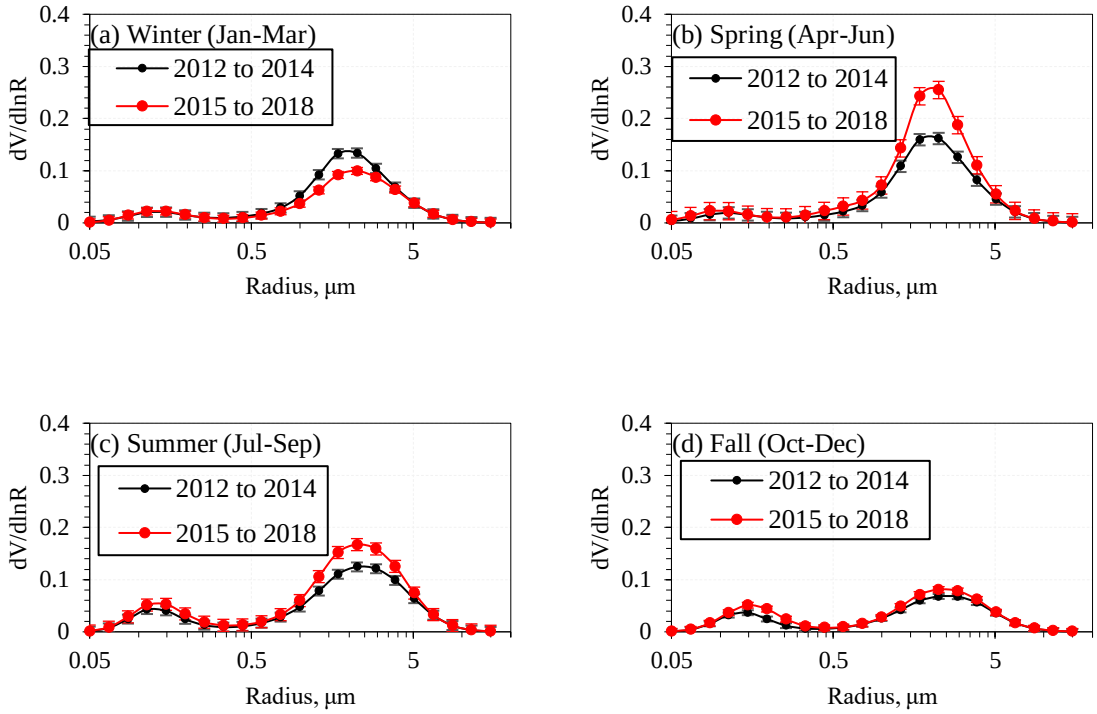

Figure 40. Seasonal Variation using size distribution data over KAUST_Campus, Saudi Arabia during the sub-periods 2012 – 2014 (G1) and 2015 -2018 (G2).

4.1.4. Northern and Southern Regions - Particulate Matter Trend and Variation Percentage

In this section, we discussed the results of the fourth and fifth regions that are supposed to be covered in the study. "Figure 41" shows the trend of mean values in different frequencies at τ_{550} and α_{470}. These frequencies are the same as the previous mentioned frequencies (e.g. daily, monthly, seasonal, and annual). The values were calculated using observations measured using the Terra Satellite (MODIS Sensor) during the period 2000 to 2018. The number of daily, monthly, annual values here are 6212, 255, and 19, respectively. This is the largest number of observations among all the data collected from different stations located in different geographical locations. Mean values corresponding to different frequency variations are represented along with the percentage difference and the p values in many tables and figures in this section. The annual data in "Figure 42" shows that there is an increasing trend at both τ_{550} and α_{470} over the southern region, and this suggests an increase in anthropogenic emissions. In the same talk, as for the northern region, "Figure 42" indicated that there is an increasing trend at τ_{550} and a decrease at α_{470}, which is not the same as happened in the southern. Moreover, the results associated in "Table 26" show that over the two regions there is an overall increasing trend of particulate matter concentration (at τ_{550}) by (1%) in both the south and north, respectively. However, the percentage increases at both τ_{550} and α_{470} are not statistically significant at the 95% confidence level with ($p < 0.05$) where the p values are 0.06 and 0.3. Trends at α_{470} over the south region indicated that the man-made emissions increased by (2%), while it also decreased by (2%) over the north. Results presented are not statistically signifi-

cant at the 95% confidence level with ($p < 0.05$) except the mean and median values over the north area at α_{470}.

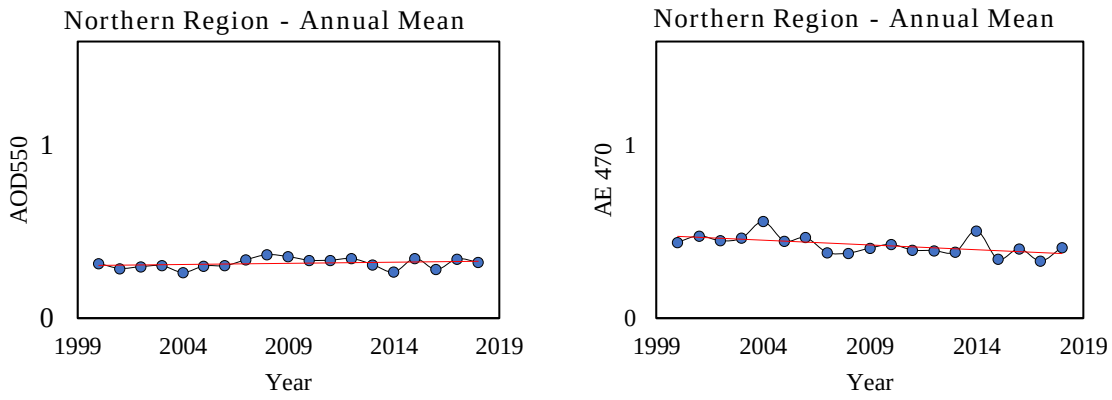

Figure 41. Trend of τ_{550} & α_{470} over Terra North, Saudi Arabia for 2000 to 2018 using annual mean values

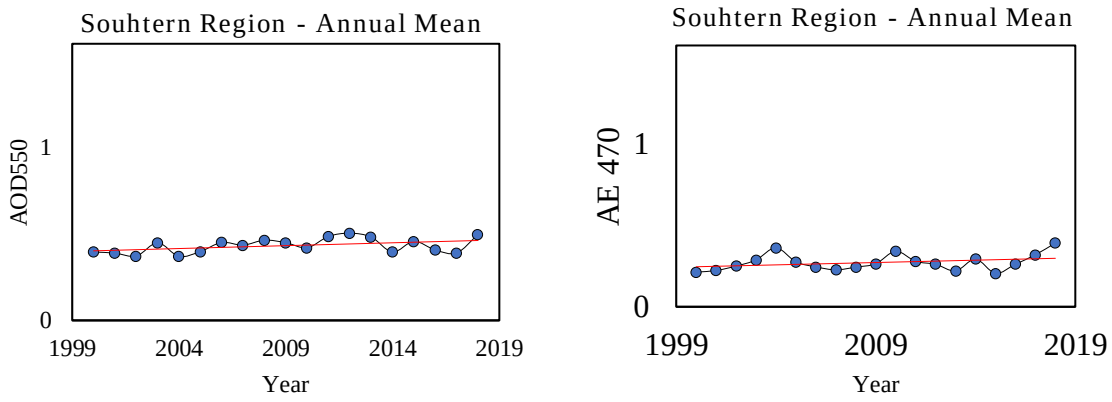

Figure 42. Trend of τ_{550} & α_{470} over Terra South, Saudi Arabia for 2000 to 2018 using annual mean values

Table 26. Yearly Statistical Comparison over Terra south and north of the Arabian Peninsula during the periods 2000 and 2018.

	Mean			Median		
N: 19	Slope	Percentage	P-Value	Slope	Percentage	P-Value
τ550 N	0.0013	1	3.01×10^{-01}	0.0012	1	3.05×10^{-01}
α 470 N	-0.0055	2	**1.40×10^{-02}**	-0.0072	3	**1.34×10^{-02}**
τ550 S	0.0033	1	6.10×10^{-02}	0.0016	1	2.38×10^{-01}
α 470 S	0.0029	2	1.87×10^{-01}	0.0033	2	2.29×10^{-01}

Monthly mean values were also analyzed over the north and south areas of the peninsula. Over the northern region "Figure 43", the trend of particulate matter concentration (at τ_{550}) is showed a slight decreasing trend over time which indicates that there is a slight drop in mean values of the particulate matter present into the atmosphere, while the increase in the same values was noticed over the southern region.

In addition, the other graphs showing the angstrom values "Figure 44" also represent the same trend mentioned about particulate matter concentration (at τ_{550}) in the two regions. This suggests that there is an increase in the anthropogenic emissions over the southern region and a decrease over the northern region.

However, unlike other stations, we did not analyze the data at $\alpha_{380-500}$ and $\alpha_{500-870}$ because the Terra Satellite (MODIS Sensor) only offered Angstrom information at $\alpha_{470,}$ unlike the ground-based stations (AERONET).

Probability tests in the section "Table 27" showed that the results are statistically significant. The test results also showed that all of the results presented in the below

graphs "Figure 45", "Figure 46" , and "Figure 47" are statistically significant except the results at α_{470} over the north area.

Focusing on each month separately, we also started looking at the variation and trend for each specific month over the period mentioned. The results in "Table 28" indicated that the trends for aerosols in both regions (north and south) rise in some months and fall in others. The observed increase was in March, May, June, October, November, and December, while no declining trend was observed in the same month over the two areas at all.

Over the course of several months, there was a marked increase in the concentration over the southern region and a decreasing trend during the same months over the northern region. These months include February, April, July, and October. Also, there was an increasing trend of the concentration over the northern region during September, while it was lower in the southern region.

The analysis of α_{470} confirmed that in the southern region, and during all months without exception, there was a continuous increase in the trend, which means that there was an increase in fine particles. This suggests that emissions resulting from human activities increased over time. The same rise in manmade emissions was observed in the northern region, but only in three months - April, August, and December. However, regarding the probability test, we can see the low level of confidence in more than 79% of the values listed "Table 29".

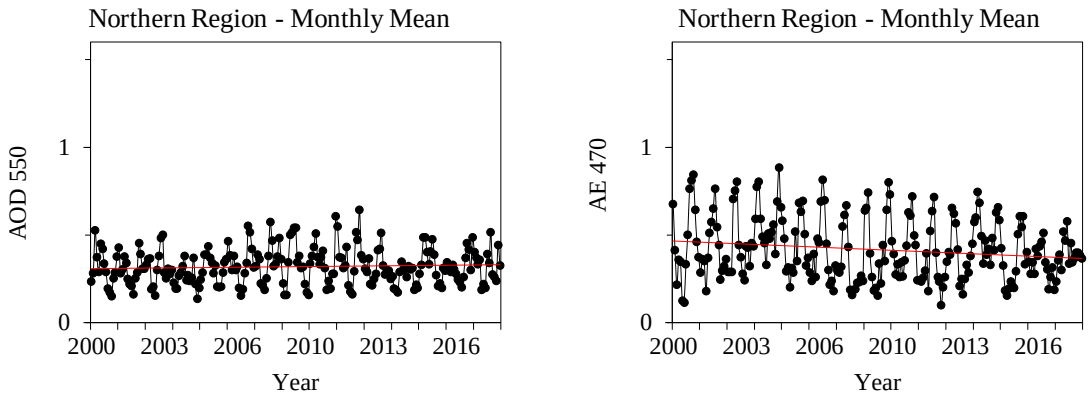

Figure 43. Trend of τ_{550} & α_{470} over Terra North, Arabian Peninsula for 2000 to 2018 using monthly mean values

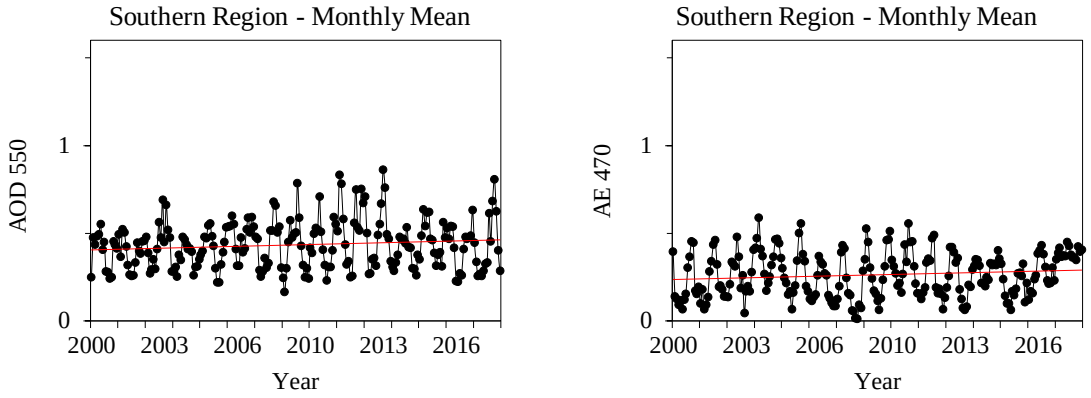

Figure 44. Trend of τ_{550} & α_{470} over Terra South, Arabian Peninsula for 2000 to 2018 using monthly mean values

Table 27. Monthly Statistical Comparison over Terra (north & south), Arabian Peninsula during the periods 2000 - 2018.

	Mean			Median		
N: 255	Slope	Percentage	P-Value	Slope	Percentage	P-Value
τ550 N	0.0001	7	**2.24×10^{-02}**	0.00009	7	1.88×10^{-01}
α 470 N	-0.0004	28	1.53×10^{-01}	-0.0007	56	2.12×10^{-01}
τ550 S	0.0003	21	**3.07×10^{-04}**	0.0002	16	**4.17×10^{-03}**
α 470 S	0.0002	14	**1.17×10^{-03}**	0.0002	16	**1.09×10^{-03}**

Table 28. Monthly Statistical Comparison over Terra (north & south), Arabian Peninsula during the periods 2000 and 2018.

	Mean			Median		
N: 18 (Jan)	Slope	Percentage	P-Value	Slope	Percentage	P-Value
τ550 N	0.0029	27	**1.61×10^{-02}**	0.0023	24	**1.24×10^{-02}**
α 470 N	-0.0165	43	**2.48×10^{-05}**	-0.0182	49	**9.23×10^{-05}**
τ550 S	0.0022	13	4.08×10^{-01}	0.0006	4	8.13×10^{-01}
α 470 S	-0.0071	32	7.28×10^{-02}	-0.0093	51	9.55×10^{-02}
N: 19 (Feb)	Slope	Percentage	P-Value	Slope	Percentage	P-Value
τ550 N	-0.0019	14	3.29×10^{-01}	-0.0014	11	4.06×10^{-01}
α 470 N	-0.0059	22	1.76×10^{-01}	-0.0069	27	1.50×10^{-01}
τ550 S	0.0002	1	5.01×10^{-01}	-0.0017	10	5.79×10^{-01}

α 470 S	0.0015	9	6.00×10^{-01}	0.0018	14	7.02×10^{-01}
N: 19 (Mar)	Slope	Percentage	P-Value	Slope	Percentage	P-Value
τ550 N	0.0042	23	1.82×10^{-01}	0.0035	21	1.65×10^{-01}
α 470 N	-0.0068	36	6.78×10^{-02}	-0.0112	67	**1.42×10^{-02}**
τ550 S	0.0026	10	5.44×10^{-01}	0.0012	5	7.43×10^{-01}
α 470 S	0.0034	29	5.44×10^{-01}	0.0038	54	3.87×10^{-01}
N: 19 (Apr)	Slope	Percentage	P-Value	Slope	Percentage	P-Value
τ550 N	-0.0029	13	4.74×10^{-01}	-0.0025	12	4.53×10^{-01}
α 470 N	0.0003	2	9.36×10^{-01}	-0.0008	6	8.65×10^{-01}
τ550 S	0.0064	24	**2.13×10^{-02}**	0.0047	19	5.65×10^{-02}
α 470 S	0.0026	25	3.52×10^{-01}	0.0022	34	4.23×10^{-01}
N: 19 (May)	Slope	Percentage	P-Value	Slope	Percentage	P-Value
τ550 N	0.0026	11	4.69×10^{-01}	0.0017	7	6.47×10^{-01}
α 470 N	-0.0015	11	4.69×10^{-01}	-0.0020	16	6.38×10^{-01}
τ550 S	0.0009	3	7.72×10^{-01}	0.0014	5	6.85×10^{01}
α 470 S	0.0059	77	9.35×10^{-01}	0.0060	124	**3.58×10^{02}**
N: 19 (Jun)	Slope	Percentage	P-Value	Slope	Percentage	P-Value
τ550 N	0.0012	7	6.98×10^{-01}	0.0009	5	7.38×10^{-01}

α 470 N	-0.0041	27	3.15×10^{-01}	-0.0069	54	1.35×10^{-01}
τ550 S	0.0103	35	9.28×10^{-02}	0.0083	30	1.22×10^{-01}
α 470 S	0.0049	58	1.52×10^{-01}	0.0041	81	1.88×10^{-01}
N: 19 (Jul)	Slope	Percentage	P-Value	Slope	Percentage	P-Value
τ550 N	-0.0001	1	9.62×10^{-01}	0.0016	10	5.02×10^{-01}
α 470 N	-0.0015	9	6.95×10^{-01}	-0.0045	31	2.95×10^{-01}
τ550 S	0.01	30	**3.43×10^{-02}**	0.0069	23	**5.73×10^{-02}**
α 470 S	0.006	81	8.31×10^{-02}	0.0041	92	2.13×10^{-01}
N: 19 (Aug)	Slope	Percentage	P-Value	Slope	Percentage	P-Value
τ550 N	-0.0014	8	5.30×10^{-01}	-0.0014	8	5.46×10^{-01}
α 470 N	0.0028	19	4.42×10^{-01}	-0.0006	6	8.73×10^{-01}
τ550 S	0.0041	15	4.42×10^{-01}	0.0032	12	2.53×10^{-01}
α 470 S	0.0107	98	4.42×10^{-01}	0.0104	131	**9.08×10^{-03}**
N: 19 (Sep)	Slope	Percentage	P-Value	Slope	Percentage	P-Value
τ550 N	0.0035	19	2.25×10^{-01}	0.0028	16	2.90×10^{-01}
α 470 N	-0.002	10	6.05×10^{-01}	-0.0057	29	1.80×10^{-01}
τ550 S	-0.0011	5	5.55×10^{-01}	-0.0003	1	9.06×10^{-01}
α 470 S	0.0072	53	6.60×10^{-02}	0.0068	63	1.21×10^{-01}
N: 19	Slope	Percentage	P-Value	Slope	Percentage	P-Value

(Oct)						
τ550 N	0.0008	5	7.32×10^{-01}	0.0006	4	7.46×10^{01}
α 470 N	-0.0039	20	2.88×10^{-01}	-0.0081	45	6.43×10^{02}
τ550 S	0.0002	1	9.00×10^{-01}	0.0002	1	8.94×10^{01}
α 470 S	0.0003	1	9.27×10^{-01}	-0.0035	26	2.40×10^{01}
N: 18 (Nov)	Slope	Percentage	P-Value	Slope	Percentage	P-Value
τ550 N	0.0043	34	**1.52×10^{-02}**	0.0033	28	**1.17×10^{-02}**
α 470 N	-0.0143	43	**1.17×10^{-03}**	-0.0174	54	**1.28×10^{-03}**
τ550 S	9.66×10^{05}	1	9.53×10^{-01}	0.0011	8	4.13×10^{-01}
α 470 S	-0.0023	11	5.03×10^{-01}	-0.0034	19	4.56×10^{-01}
N: 18 (Dec)	Slope	Percentage	P-Value	Slope	Percentage	P-Value
τ550 N	0.0017	16	1.61×10^{-01}	0.0016	16	1.35×10^{-01}
α 470 N	-0.0149	40	**8×10^{-04}**	-0.0158	44	**2.19×10^{-03}**
τ550 S	4.07×10^{06}	0	10×10^{-01}	-0.0006	4	8.33×10^{-01}
α 470 S	-0.0040	17	2.48×10^{-01}	-0.0049	26	2.59×10^{-01}

Table 29. Monthly Statistical Comparison using daily values over Terra (north & south), Arabian Peninsula during the sub-periods 2000 – 2009 (G1) and 2010 -2018 (G2).

Jan	G1 (N:264)	G2 (N:269)	P	t
τ550 N	0.179	0.199	**9.94×10^{-03}**	**2**
α 470 N	0.748	0.622	**5.49×10^{-08}**	**2**
τ550 S	0.314	0.313	9.34×10^{-01}	2
α 470 S	0.420	0.388	2.54×10^{-01}	2
Feb	G1 (N:247)	G2 (N:228)	P	t
τ550 N	0.280	0.257	8.29×10^{-02}	2
α 470 N	0.514	0.487	3.10×10^{-01}	2
τ550 S	0.399	0.389	6.46×10^{-01}	2
α 470 S	0.310	0.324	5.98×10^{-01}	2
Mar	G1 (N:271)	G2 (N:246)	P	t
τ550 N	0.345	0.365	2.66×10^{-01}	2
α 470 N	0.379	0.344	1.38×10^{-01}	2
τ550 S	0.459	0.505	**5.24×10^{-02}**	**2**
α 470 S	0.216	0.234	4.72×10^{-01}	2
Apr	G1 (N:251)	G2 (N:219)	P	t
τ550 N	0.455	0.422	1.21×10^{-01}	2
α 470 N	0.288	0.294	8.07×10^{-01}	2
τ550 S	0.488	0.528	**7.75×10^{-02}**	**2**
α 470 S	0.187	0.218	1.20×10^{-01}	2

May	G1 (N:272)	G2 (N:239)	P	t
τ550 N	0.443	0.475	8.34×10^{-02}	2
α 470 N	0.282	0.271	5.67×10^{-01}	2
τ550 S	0.500	0.519	2.75×10^{-01}	2
α 470 S	0.123	0.178	**1.13×10^{-03}**	**2**
Jun	G1 (N:254)	G2 (N:232)	P	t
τ550 N	0.356	0.342	3.43×10^{-01}	2
α 470 N	0.301	0.276	2.16×10^{-01}	2
τ550 S	0.519	0.629	**1.06×10^{-04}**	**2**
α 470 S	0.139	0.183	**2.13×10^{-02}**	**2**
Jul	G1 (N:274)	G2 (N:248)	P	t
τ550 N	0.319	0.329	3.96×10^{-01}	2
α 470 N	0.352	0.309	3.71×10^{-02}	2
τ550 S	0.577	0.675	**6.53×10^{-05}**	**2**
α 470 S	0.115	0.174	**4.20×10^{-04}**	**2**
Aug	G1 (N:276)	G2 (N:254)	P	t
τ550 N	0.341	0.332	3.52×10^{-01}	2
α 470 N	0.283	0.296	5.53×10^{-01}	2
τ550 S	0.495	0.533	**5.98×10^{-02}**	**2**
α 470 S	0.161	0.264	**3.20×10^{-07}**	**2**
Sep	G1 (N:290)	G2 (N:261)	P	t
τ550 N	0.333	0.355	5.21×10^{-02}	2

α 470 N	0.403	0.377	1.91×10^{-01}	2
τ550 S	0.438	0.427	4.01×10^{-01}	2
α 470 S	0.217	0.305	**1.85×10^{-05}**	**2**
Oct	G1 (N:300)	G2 (N:251)	P	t
τ550 N	0.334	0.332	9.20×10^{01}	2
α 470 N	0.386	0.366	3.54×10^{01}	2
τ550 S	0.296	0.302	5.64×10^{01}	2
α 470 S	0.355	0.340	5.48×10^{01}	2
Nov	G1 (N:296)	G2 (N:237)	P	t
τ550 N	0.214	0.243	**2.51×10^{-03}**	**2**
α 470 N	0.650	0.533	**1.29×10^{-06}**	**2**
τ550 S	0.273	0.281	3.59×10^{-01}	2
α 470 S	0.407	0.375	2.09×10^{-01}	2
Dec	G1 (N:294)	G2 (N:239)	P	t
τ550 N	0.182	0.208	**6.70×10^{-04}**	**2**
α 470 N	0.744	0.59	**1.68×10^{-11}**	**2**
τ550 S	0.294	0.294	9.93×10^{-01}	2
α 470 S	0.438	0.392	**9.11×10^{-02}**	**2**

The results presented in "Table 30" (daily mean values) demonstrate that, over the north and south regions, there was an overall increase in the particulate matter trend (at τ_{550}). These increased trends are not strong compared to other trends associated with other stations mentioned in the previous sub-sections above.

However, a deeper analysis of the daily mean values was carried out as presented in "Table 31". Over several months, data has been analyzed and the results found are that there was an increase in particulate matter concentration during several months over the southern and northern regions. These months include January, March, May, June, July, August, October and November. While a decreasing trend in the northern region was observed during April and two more in September and December.

Based on the value of α_{470}, we can say that there was a noticeable rise in fine particles over the southern region, more than in the northern region. It was between January and September and a drop in the trend was started from October until December. In contrast, the northern region was also encountered a decreasing trend in the particle's concentration for the same months (Oct to Dec).

The P-Values in "Table 31" show that the confidence level is higher than the confidence levels associated with the monthly mean analysis in which more than 40% of the data has a p-value less than 0.05.

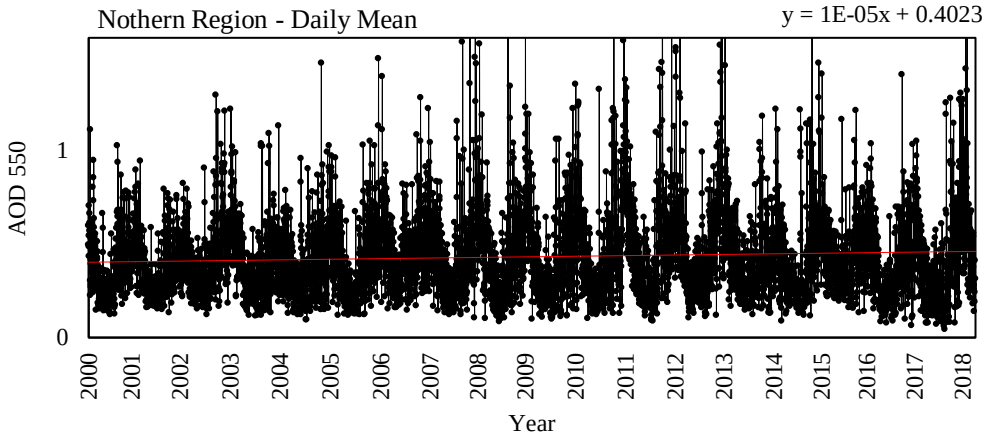

Figure 45. Aerosols Optical Depth over the North of Arabian Peninsula

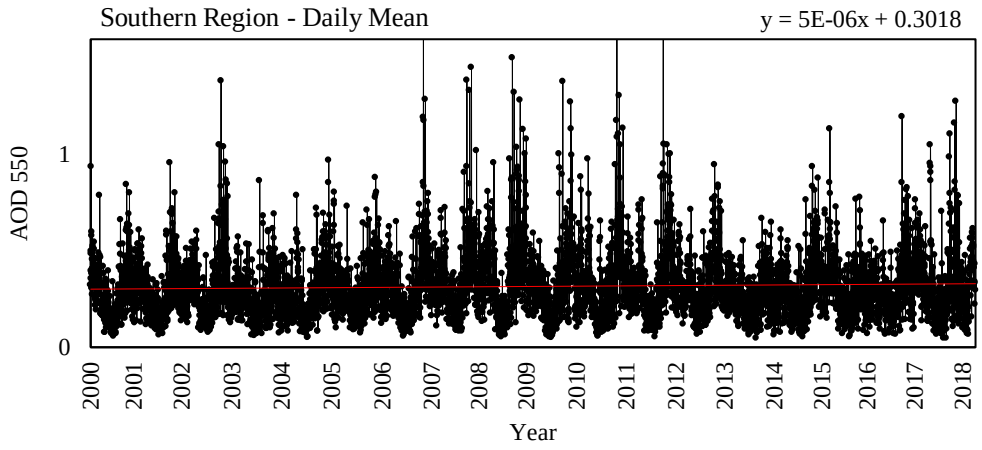

Figure 46. Aerosols Optical Depth over the South of Arabian Peninsula

Table 30. Daily Statistical Comparison over Terra (north & south), Arabian Peninsula during the periods 2000 – 2018.

	Mean		
N: 6212	Slope	Percentage	P-Value
τ550 N	0.000004	8	1.22×10^{-13}
α 470 N	-0.00002	29	1.39×10^{-06}
τ550 S	0.000009	13	5×10^{-33}
α 470 S	0.000008	18	1.41×10^{-14}

Table 31. Monthly Statistical Comparison using daily values over Terra (north & south), Arabian Peninsula during the periods 2000 – 2018.

Mean	Jan (N: 533)			Mar (N: 517)		
	Slope	Percentage	P-Value	Slope	Percentage	P-Value
τ550 N	0.0001	28	9.37×10^{-02}	0.0002	29	**4.89×10^{-06}**
α 470 N	-0.0006	47	2.08×10^{-01}	-3×10^{04}	43	**1.12×10^{-03}**
τ550 S	0.00009	15	8.29×10^{-02}	0.0001	11	**2.06×10^{-04}**
α 470 S	-0.0003	40	2.93×10^{-01}	0.0001	23	1.69×10^{-01}
Mean	Feb (N: 475)			Apr (N: 470)		
	Slope	Percentage	P-Value	Slope	Percentage	P-Value
τ550 N	-0.00007	12	**4.24×10^{-09}**	-0.0001	11	**8.04×10^{-03}**
α 470 N	-0.0002	19	**1.69×10^{-05}**	2×10^{05}	3	5.30×10^{-01}
τ550 S	-0.00004	5	**5.10×10^{-05}**	0.0002	19	2.51×10^{-01}
α 470 S	0.00009	14	5.57×10^{-02}	0.0001	23	6.55×10^{-01}
Mean	May (N: 511)			Jul (N: 522)		
	Slope	Percentage	P-Value	Slope	Percentage	P-Value
τ550 N	0.0001	11	**2.16×10^{-02}**	3×10^{05}	5	4.03×10^{-01}
α 470 N	-0.00006	11	5.58×10^{-01}	-1×10^{04}	16	9.77×10^{-01}
τ550 S	0.00004	4	6.97×10^{-01}	0.0004	34	1.42×10^{-01}
α 470 S	0.0002	69	6.22×10^{-02}	0.0002	73	2.59×10^{-01}
Mean	Jun (N: 486)			Aug (N: 530)		
	Slope	Percentage	P-Value	Slope	Percentage	P-Value
τ550 N	0.00003	4	**4.10×10^{-09}**	0.0104	1637	6.57×10^{-01}

α 470 N	-0.0002	34	**9.87×10^{-06}**	-3×10^{05}	6	7.04×10^{-01}
τ550 S	0.0004	34	1.68×10^{-01}	6×10^{05}	6	**4.61×10^{-18}**
α 470 S	0.0002	61	**7.99×10^{-03}**	0.0001	25	**1.47×10^{-06}**
Mean	Sep (N: 551)			Nov (N: 533)		
	Slope	Percentage	P-Value	Slope	Percentage	P-Value
τ550 N	0.0001	16	7×10^{-01}	0.0001	24	**3.14×10^{-14}**
α 470 N	-0.00007	10	4.84×10^{-01}	-5×10^{04}	45	**2.59×10^{-09}**
τ550 S	-0.00005	6	**3.41×10^{-10}**	5×10^{06}	1	4.45×10^{-01}
α 470 S	0.0003	64	1.06×10^{-01}	-8×10^{05}	11	3.67×10^{-01}
Mean	Oct (N: 511)			Dec (N: 533)		
	Slope	Percentage	P-Value	Slope	Percentage	P-Value
τ550 N	0.00003	5	3.53×10^{-01}	6×10^{05}	17	4.12×10^{-01}
α 470 N	-0.0001	15	**9.11×10^{-05}**	-0.0005	40	2.11×10^{-01}
τ550 S	0.000002	0	**3.76×10^{-12}**	-9×10^{07}	0	6.08×10^{-01}
α 470 S	-4×10^{06}	1	**5.38×10^{-04}**	-0.0001	13	5.35×10^{-01}

By studying the seasonal variation "Figure 47", we noticed that the particulate matter concentration increased in the second sub-period during the winter and fall months, while it decreased in the summer and did not change in value during the spring season. Given an Angstrom value of α_{470}, the values decreased in all seasons except in the spring season, where the values are equal in the two sub-periods.

Moreover, the fine particles increased in the second sub-period during the winter and fall, and during the first sub-period in the summer. In addition, the coarse particles al-

so increased during the summer and winter, while they declined during the fall, and did not change in value during the spring season in the two sub-periods. The P-Values of these results are shown in "Table 32". However, the values indicated that the results over the south region have a high level of confidence except for the value of τ_{550} during the fall. On the other hand, the values over the northern are not statistically significant except for the results at α_{470} during the winter and fall.

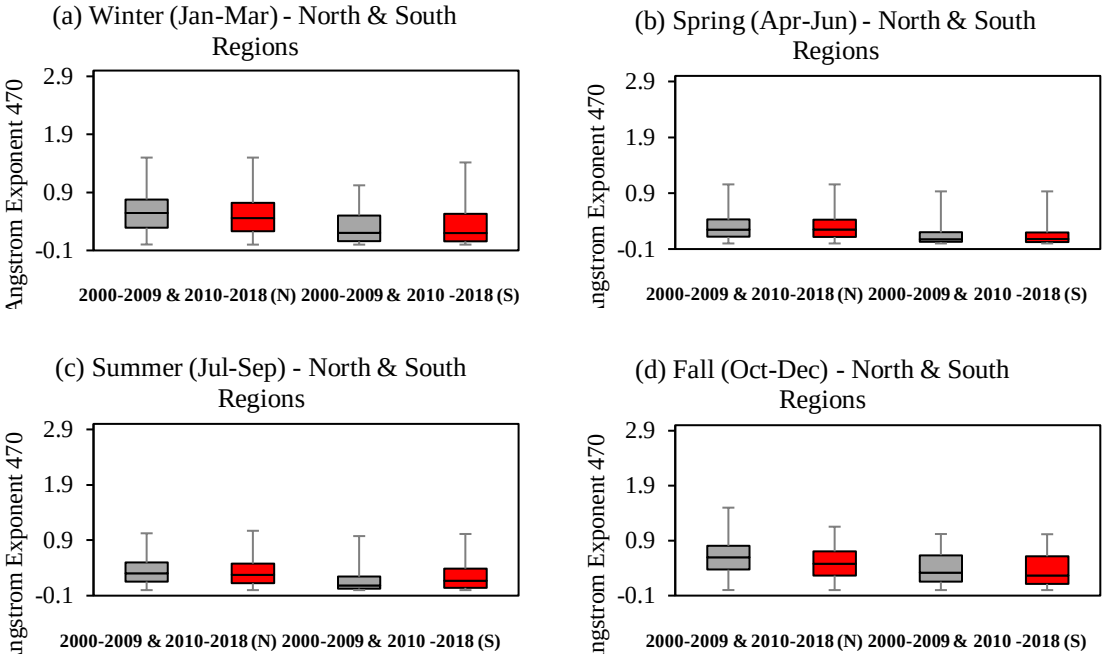

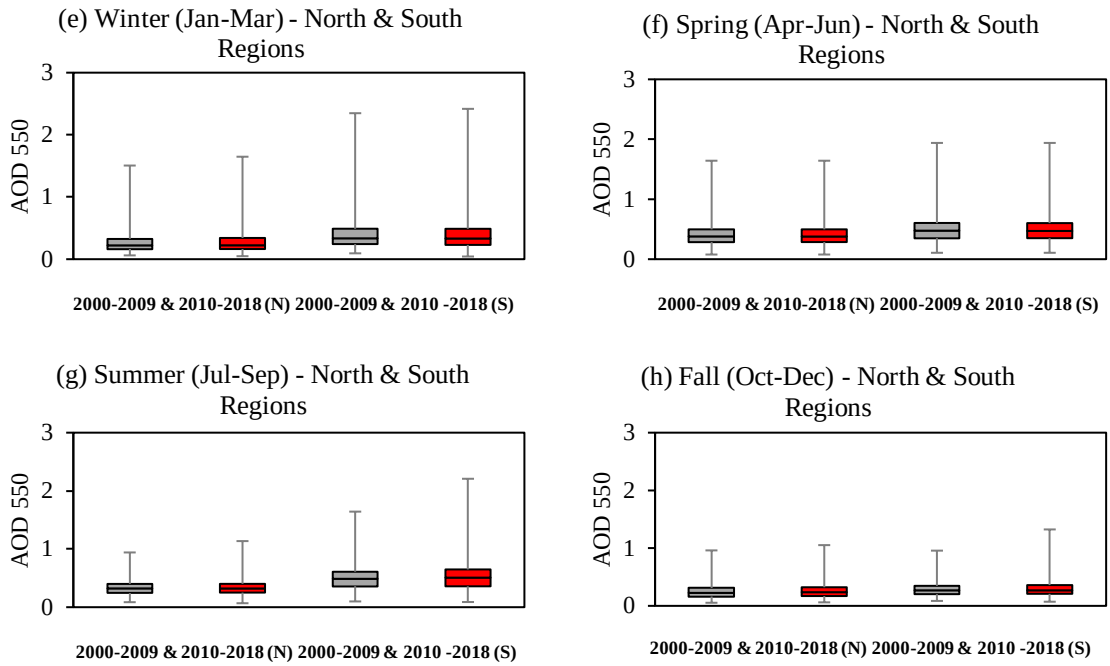

Figure 47. Seasonal Variation using daily mean values of τ_{550} & α_{470} over Terra south and north of the Arabian Peninsula during the sub-periods 2000 – 2009 (G1) and 2010 -2018 (G2)

Table 32. Seasonal Statistical Comparison over Terra south and north of the Arabian Peninsula during the sub-periods 2000 – 2009 (G1) and 2010 -2018 (G2).

		τ500	α440-870	α380-500	α500-870	N
Winter	p	6.68×10^{-01}	**2.24×10^{-04}**	4.66×10^{-01}	8.7×10^{-01}	782
	t	2	**2**	2	2	743
Spring	p	6.43×10^{-01}	3.83×10^{-01}	**2.71×10^{-05}**	**5.86×10^{-05}**	777
	t	2	2	**2**	**2**	690
Summer	p	2.52×10^{-01}	1.16×10^{-01}	**7.08×10^{-04}**	**2.21×10^{-13}**	840
	t	2	2	**2**	**2**	763
Fall	p	**3.8×10^{-03}**	**1.34×10^{-11}**	4.09×10^{-01}	**3.7×10^{-02}**	890
	t	**2**	**2**	2	**2**	727

4.1.5 Jubail City - Particulate Matter Trend

4.1.5.1 Particulate Matter Trend

In addition to the chemical characterization that was set as one of the thesis objectives and because of the presence of an advanced instrument (Synchronized Hybrid Ambient Real-time Particulate Monitor - Thermo Scientific 5030i), the level of PM_{10} on an hourly basis over the monitoring period was successfully recorded and obtained for discussion in this sub-section. By looking at the concentration of PM_{10}, the average continuously fluctuated around 75 $\mu g/m^3$, except on the second day of the monitoring where it suddenly peaked until it reached 300 $\mu g/m^3$. However, the slope was noticed to decrease insignificantly over the monitoring period. The regulatory authority in Jubail did not set and regulate hourly PM_{10} concentrations and just restricted the annual and daily levels, and the same thing for the other standards. "Table 33" show the limits on an annual and daily basis.

Table 33 PM_{10} limits in different standards

Organization	Annual ($\mu g/m^{3)}$)	Daily ($\mu g/m^{3)}$)
World Health Organization (WHO)	20	50
United. States. Environmental protection Agency (U.S.EPA)	50	150
Royal Commission (RC)	50	150
Presidency of Meteorology and Environment (PME)	80	340

Based on the hourly values in "Figure 48", the daily average of PM_{10} was calculated as shown in "Figure 49". This kind of calculation helps to compare the PM_{10} levels with lo-

cal and international standards. Over eleven (11) days of monitoring, the levels of PM_{10} decreased as denoted previously in the hourly monitoring results. The results show that the concentration was below the allowable limits of several standards, including RCER-2015, PME, and U.S. EPA. However, the concentration did not abide by the WHO limit, except on day (28/5/2018) when it reached 50 µg/m3.

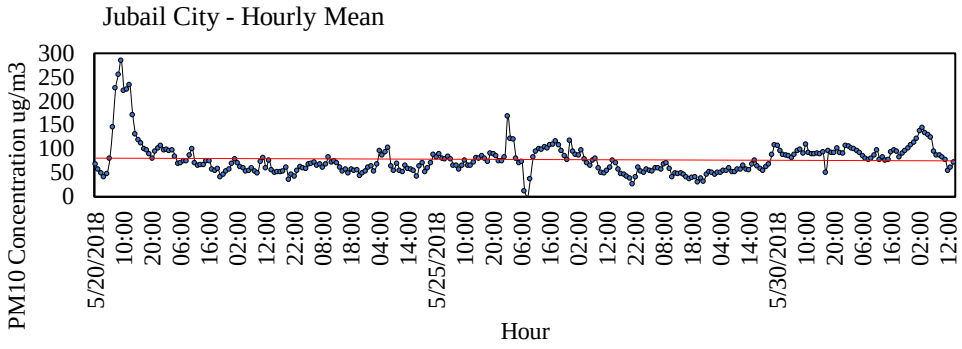

Figure 48. Hourly trend of PM_{10} levels in Jubail during the last 10 days of May 2018 and the first day of June 2018

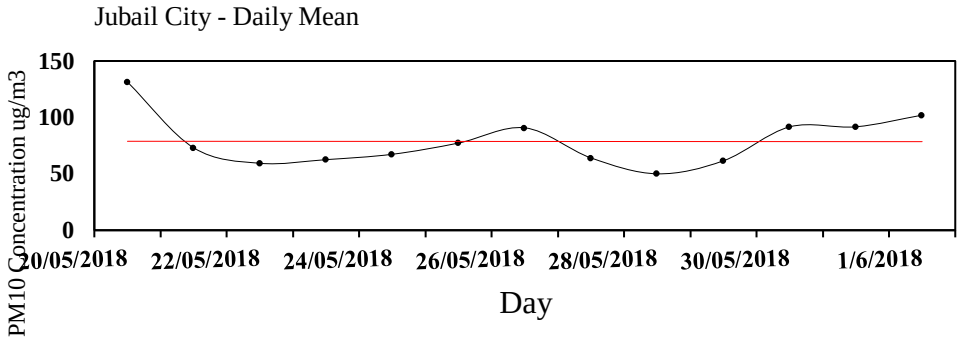

Figure 49. Daily trend of PM_{10} levels in Jubail during the last 10 days of May 2018 and the first day of June 2018

4.2 Morphological Characteristics of PM_{10} Samples

This section is totally related to the second objective of the study namely: “Assessing morphological and mineralogical characteristics of the Airborne Particulate Matter over two different cities within the Arabian Peninsula”.

4.2.1 Morphological Characteristics of PM_{10} in Jubail and Ras Tanura

As part of chemical characterization work, and due to a lack of knowledge about the size and shape of PM_{10} over the Arabia Peninsula, samples over two locations in the Eastern Region were obtained to be analyzed and discussed. Areas which underwent sampling were selected based on the presence of industrial activities as the possibility of generating man-made particles is higher than for any other location. Starting with the Jubail area:

Field-Emission Scanning Electron Microscopy (FESEM) images "Figures 50 and 51" present the shape and size of the particles taken from Jubail and Ras Tanura at a magnification scale of 2300X. Both figures show that most particles are very small in size and have an irregular shape. For the Jubail sample, most dispersed particles were between 1.4 and 2.8 µm, while some particles were very small reaching a size of less than 1.4 µm. Agglomerated particles found at different spots had sizes up to 17 µm "Figure 50". Such agglomerated particles could be as result of the deposition process that does not reflect the real size and shape. On the other hand, particles of sizes between 1.4 and 2.8 µm denote the presence of combustion products, sea salts, and dust. However, smaller particles reflect the effects of ongoing industry and the anthropogenic activities in Jubail on the atmosphere.

On the other hand, the particles collected from Ras Tanura "Figure 51" were larger in size than the particles collected over Jubail industrial city. On average, the size of the particles varied between 5 and 7 µm and had irregular, and spherical shapes with less dispersion. Clustered particles were not noticed at any spot on the filter, although the sampling period was twice as high as the sampling period in Jubail. It supports the possibility that the emission sources of particles in Ras Tanura differ from the sources in Jubail. However, the significant number of small particles found in different spots at the filter signifies that there is a significant environmental impact because of anthropogenic activities (mainly refinery operations).

"Table 34" shows the characteristics of particulate matter in these two cities including size, shape, and classification based on Morphology).

Table 34 Jubail and Ras Tanura PM_{10} size, shape, and classification based on Morphology

	Jubail	Ras Tanura
Size	1.4 - 2.8 µm	5 - 7 µm
Shape	Irregular	Irregular
	Clustered	
Classification	Quartz/ Silica.	Calcium rich particles
	Aluminosilicates	

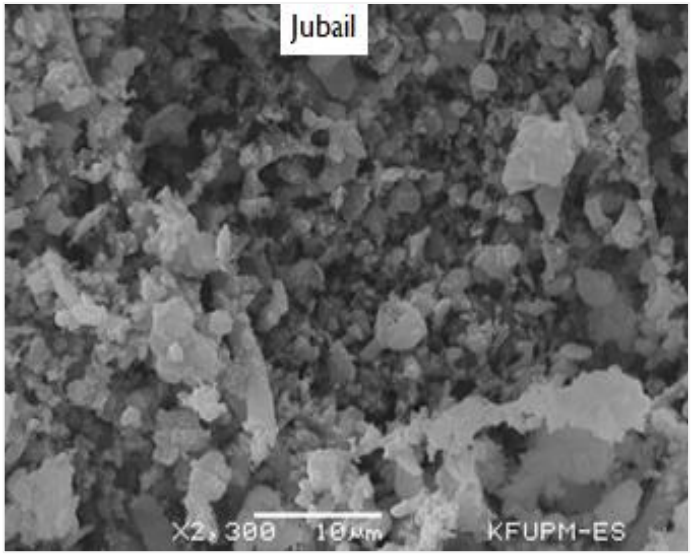

Figure 50. Field-Emission Scanning Electron Microscopy (FESEM) images of PM_{10} collected from Jubail.

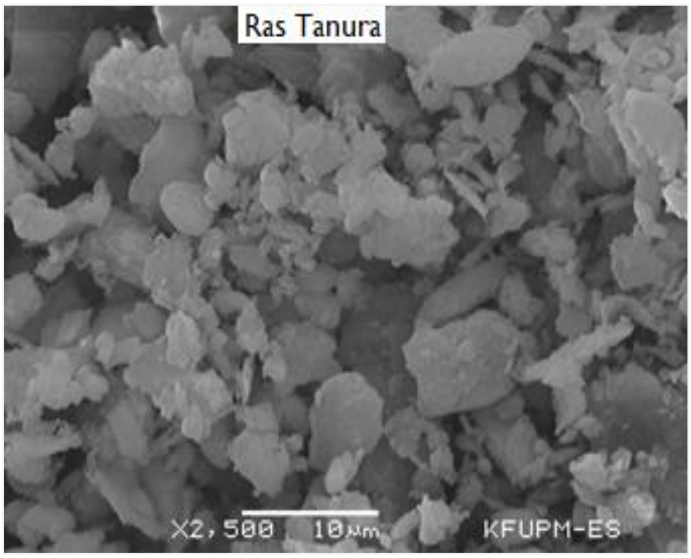

Figure 51. Field-Emission Scanning Electron Microscopy (FESEM) images of PM_{10} collected Ras Tanura.

4.3 Elemental Composition of PM_{10} Samples using XRF

Figure 52 shows the levels of the elemental composition of PM_{10} samples obtained from Jubail and Ras Tanura. Starting from 20/05/2018, 11 samples were collected from the Jubail area and each sample represents 24 hours of particulate matter collection, while the samples taken from Ras Tanura (5) represent 48 to 72 hours of monitoring. Each bar in the figure represents the elements present for each sample (percent by weight). The elements found were zinc, magnesium, sodium , aluminum, silicon, sulfur, chlorine, potassium, calcium, iron, strontium, zirconium and barium. Many of these elements have an impact on hydrogen ion concentration. Hence, the need to reduce the emission of such elements into the atmosphere is important. Zinc, barium, sulfur, sodium, and potassium show a higher percentage in the Jubail samples compared with Ras Tanura, meanwhile, calcium, chlorine, aluminum, iron, and magnesium were higher in the Ras Tanura samples. The main source of zinc in the Jubail could include road transport and the steelmaking process. This is because zinc acts as a corrosion resistant agent and is used as an alloy during the melting and coating of steel coils surfaces, while the barium is likely produced from sea water. Jubail is, by nature, rich in sulfide, especially in soil and groundwater. In addition, it hosts a desalination plant and heavy industry that relies mainly on fossil fuel-based energy, which is one of the biggest sources that releases sulfur. Like the zinc levels, and although the percentage was lower than other elements, aluminum levels were close to the zinc levels in Jubail and higher in Ras Tanura. It is worth mentioning that the concentration of the calcium in the Ras Tanura samples was higher than the Jubail samples. This may be due to construction in residential and manufacturing industries, in addi-

tion to the extraction of stone and other earth material which could have occurred during the sampling period.

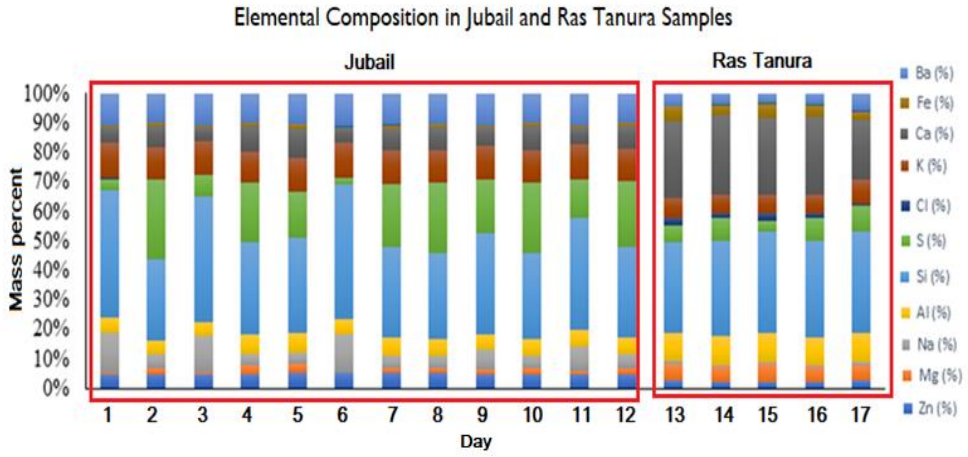

Figure 52. Elemental composition of PM_{10} samples collected from Jubail and Ras Tanura

4.4 Mineralogical Characteristics of PM_{10} Samples using XRD

4.4.1 Mineralogical Characteristics of PM in Jubail and Ras Tanura

Figure 53 represents a dendrogram generated to display all clusters that appeared after the analysis. However, more details are listed in "Table 35", which shows info about the sampling date and duration in both cities, days involved in each appeared cluster and all minerals identified.

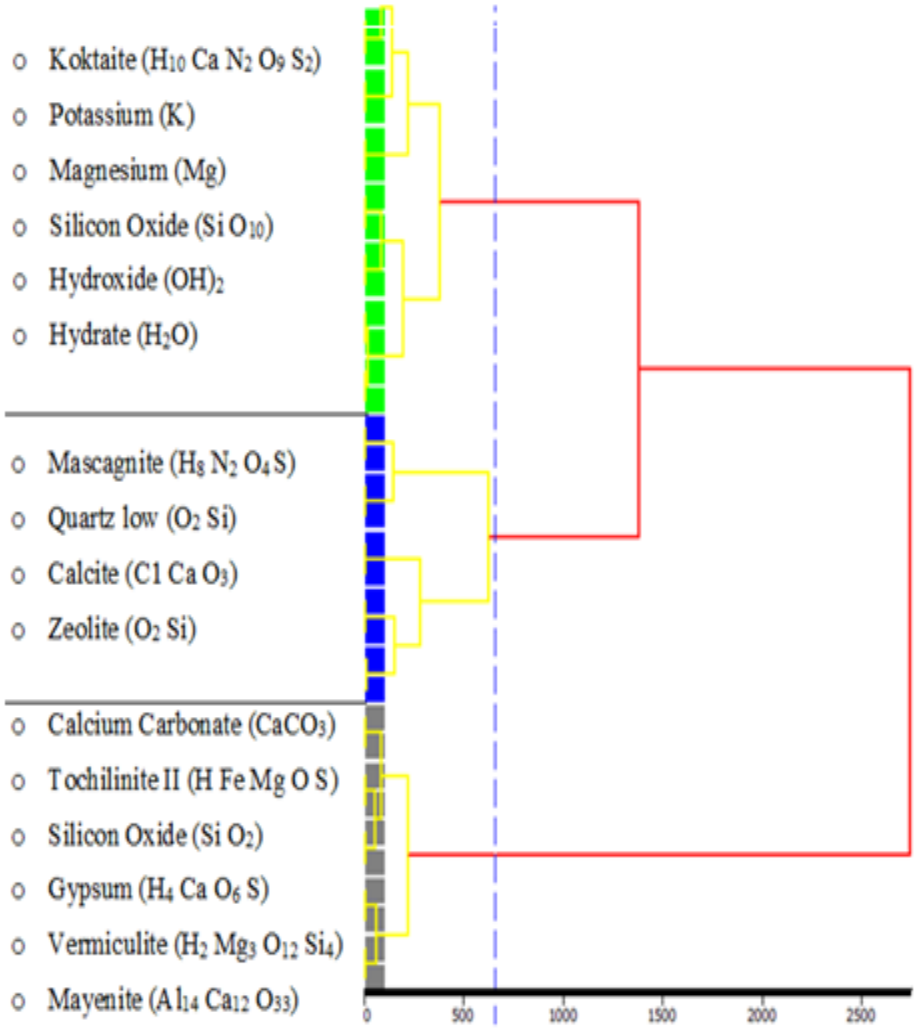

Figure 53. Types of Clusters generated based on the Mineral Composition of the Sample

Table 35. Samples Information

Cluster Number	Involved Samples	Sampling date	duration	Mineral name & formula
#1 (Green)	Jubail_6	21/05/2018	24 h	Koktaite (H_{10} Ca N_2 O_9 S_2) Potassium (K) Magnesium (Mg) Silicon Oxide (Si O_{10}) Hydroxide $(OH)_2$ Hydrate (H_2O)
	Jubail_8	23/05/2018	24 h	
	Jubail_9	24/05/2018	24 h	
	Jubail_12	27/05/2018	24 h	
	Jubail_13	28/05/2018	24 h	
	Jubail_14	29/05/2018	24 h	
	Jubail_15	30/05/2018	24 h	
	Jubail_17	1/06/2018	24 h	
#2 (Blue)	Jubail_5	20/05/2018	24 h	Mascagnite (H_8 N_2 O_4 S) Quartz low (O_2 Si) Calcite (C1 Ca O_3) Zeolite (O_2 Si)
	Jubail_7	22/05/2018	24 h	
	Jubail_10	25/05/2018	24 h	
	Jubail_11	26/05/2018	24 h	
	Jubail_16	31/05/2018	24 h	
#3 (Grey)	Ras Tan._1	21-23/06/2018	48 h	Calcium Carbonate ($CaCO_3$) Tochilinite II (H Fe Mg O S) Silicon Oxide (Si O_2) Gypsum (H_4 Ca O_6 S) Vermiculite (H_2 Mg_3 O_{12} Si_4) Mayenite (Al_{14} Ca_{12} O_{33})
	Ras Tan._2	23-25/06/2018	48 h	
	Ras Tan._3	25-28/06/2018	72 h	
	Ras Tan._4	28-30/06/2018	48 h	
	Ras Tan._5	30-2/07/2018	48 h	

Results showed that clusters #1 and #2 are a bit close to each other, while cluster #3 differs. Cluster #3 includes all of the Ras Tanura samples only reflecting the differences between the Jubail and Ras Tanura samples about the mineral composition. In cluster #1, Koktaite was one of the minerals present in a very low percent (1.6 %). It consists of a hydrous sulfate of calcium and ammonium. Other minerals detected were Silicon Oxide, Hydroxide, and Hydrate. Silicon Oxide is most commonly found in nature as quartz and in many living organisms. It is used commercially as an electrical insulator and semiconductor (MOS) devices. Inhalation of such minerals could lead to severe inflammation of the lung tissue, and could even cause lung cancer. Cluster #2 holds other minerals; one of them called “Mascagnite” is in a higher percentage; about 24.1%. It is a mineral that consists of Ammonium Sulfate and is usually associated with natural burning of an outcrop or underground coal seam. Such condition is not a part of the industries in Jubail and it makes the estimation of the emission source difficult to calculate, however, it can be linked with oil exploration activities near the area. In the same cluster, Quartz low, Calcite, and Zeolite were also detected but in very small quantities. About Cluster #3, there were many other minerals including Calcium Carbonate, Tochilinite II (acicular variety), Silicon Oxide, Gypsum, Vermiculit, and Mayenite. The Calcium Carbonate is most commonly found in rocks and it is made of Calcite. The rock is widely/ naturally available in the eastern province of KSA. Quartz is another mineral found in about 3.8% and it is mainly composed of Oxygen and Silicon atoms. It is the second most abundant mineral in the Earth's continental crust and expected so there is no concern about its presence in the sampled area. "Figures 54, 55 and 56" shows the analysis result of XRD for all samples collected.

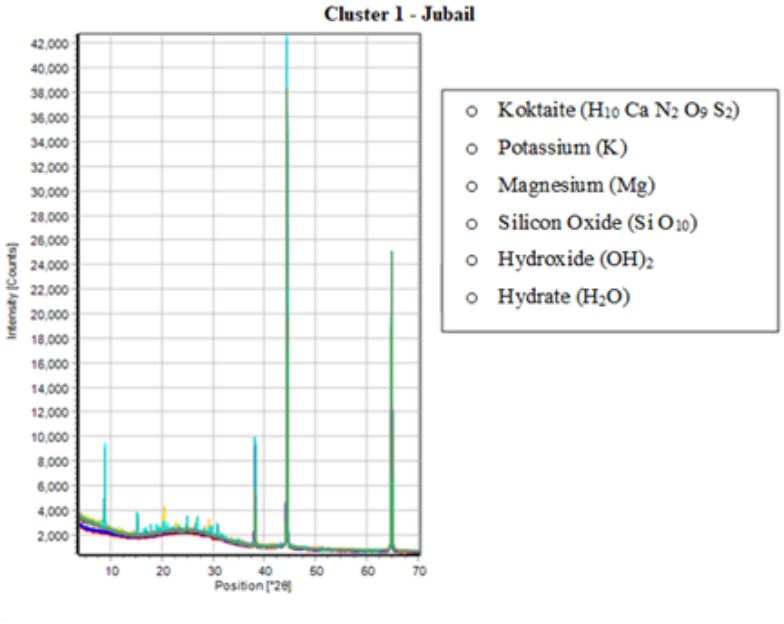

Figure 54. Percentage of Minerals in Cluster 1

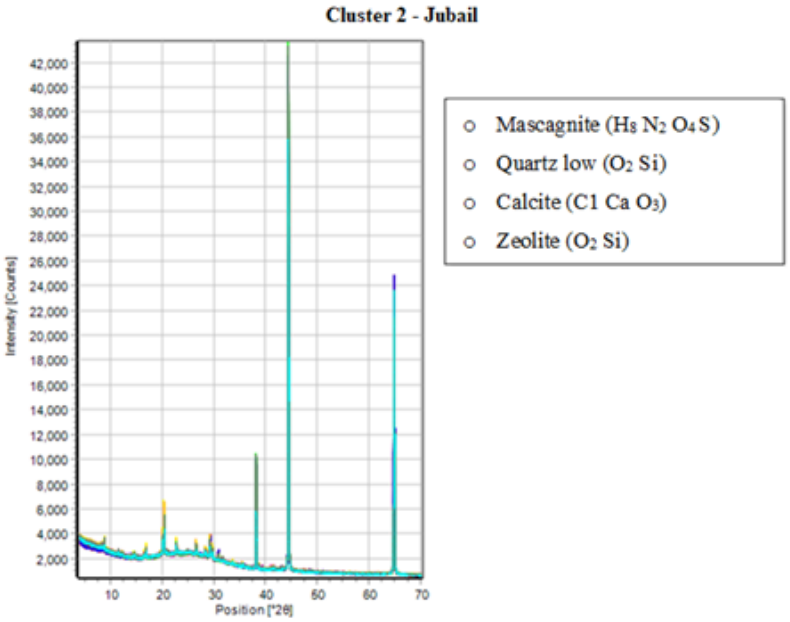

Figure 55. Percentage of Minerals in Cluster 2

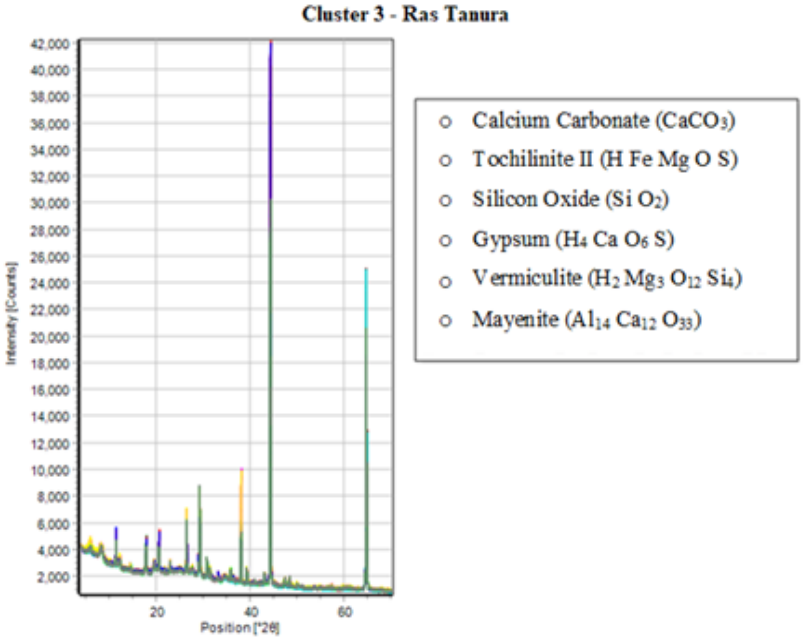

Figure 56. Percentage of Minerals in Cluster 3

To make an appropriate explanation regarding the differences in mineral composition between the first and second clusters which contain only the Jubail samples, we looked at weather conditions during the period that the ground monitoring took place from 20/5/2018 to 1/6/2018 to determine the main causes for these differences. The weather data includes information about temperature, humidity, wind speed, and direction. The "Tables 36 and 37" show these data.

In "Tables 36 and 37" and for arrangement purposes, and since all Jubail samples are separated into two different clusters by the XRD, we separated the weather data exactly the same as the arrangement of the first and second clusters.

According to the weather data plugged into the tables, the reasons behind the separation of the Jubail samples into two different groups are not directly linked with the changes in

weather conditions, as the differences in weather conditions between the two groups are very similar and there is no significant change that could explain the change in the mineral composition. However, the segregation between samples into different clusters could be traced back to natural geological processes, the precipitation of vapor and water, and the presence of living organisms. The change could also occur because the mineral tends to change to a more stable state continually through natural weathering processes and the formation of metamorphic rocks.

Table 36. Data of Jubail monitoring including the Meteorological information – provided by the SHARP monitor

	Date	Average PM (μg/m³)	Ambient RH (%)	Ambient (°C)	Wind Speed (km/h)
Cluster 1	21/5/18	73	39	31	14
	23/5/18	63	38	32	13
	24/5/18	67	35	32	9
	27/5/18	64	40	34	10
	28/5/18	50	48	33	9
	29/5/18	62	45	35	14
	30/5/18	92	38	34	13
	1/6/2018	102	41	35	17
Cluster 2	20/5/18	131	43	33	12
	22/5/18	59	38	32	10
	25/5/18	77	47	34	10
	26/5/18	91	51	35	13
	31/5/18	92	44	36	13

Table 37. Wind speed and direction in Jubail city – (TimeandDate.com)

	Date	Time	Wind Direction		Date	Time	Wind Direction
Cluster 1	21-May-18	24:00	S	Cluster 2	20-May-18	24:00	WW
		6:00	N			6:00	W
		12:00	N			12:00	N
		18:00	E			18:00	ENE
	23-May-18	24:00	SSW		22-May-18	24:00	SSW
		6:00	NNE			6:00	N
		12:00	NNE			12:00	E
		18:00	E			18:00	E
	24-May-18	24:00	N		25-May-18	24:00	S
		6:00	N			6:00	SE
		12:00	E			12:00	ESE
		18:00	E			18:00	E
	27-May-18	24:00	WNW		26-May-18	24:00	N
		6:00	WNW			6:00	NE
		12:00	N			12:00	NE
		18:00	N			18:00	NNE
	28-May-18	24:00	S		31-May-18	24:00	SSW
		6:00	NE			6:00	SSW

		12:00	NNE			12:00	ENE
		18:00	NNE			18:00	ENE
	29-May-18	24:00	SSW				
		6:00	N				
		12:00	ENE				
		18:00	N				
	30-May-18	24:00	S				
		6:00	NNW				
		12:00	E				
		18:00	ENE				
	1-Jun-18	24:00	S				
		6:00	S				
		12:00	E				
		18:00	E				

4.5 Trace Metal Levels in PM Samples

4.5.1 Trace Metal Levels in PM collected from Jubail and Ras Tanura

Using inductively coupled plasma mass spectrometry (ICP-MS), the samples were analyzed/investigated. Eleven (11) particulate matter samples from Jubail and one (1) sample from Ras Tanura were analyzed for trace metals. "Figure 57" presents the ICP/MS results for trace metals. Lithium, cobalt, vanadium, arsenic, silver, manganese, nickel molybdenum, copper, chromium, cadmium, and lead with a concentration between 0.001 and 0.06 µg/m^3 were identified. Other metals with a higher concentration include boron, zinc, aluminum and these range between 4 and 10 µg/ m^3 in most of the samples (Jubail and Ras Tanura), whereas, iron (Fe) was also detected in all samples but in smaller concentrations where it reached up to 1.6 µg/m^3. Trace metals with a high level of toxicity which can introduce a severe risk to human health include lithium, cobalt, vanadium, arsenic, silver, manganese, nickel molybdenum, copper, chromium, cadmium, and lead. They can cause damage to the kidneys, lungs, liver, heart and bones and many other organs in our bodies and may cause death. The results comparing their levels with the Royal Commission Environmental Regulation-2015 "Table 38" showed that all of the regulated metals within the mentioned group are within the allowable limits. Boron is usually found to naturally occur in boron-containing rocks through the weathering process that takes place in seawater. Mining activities may also generate boron. As mentioned earlier, the potential sources of the zinc in the Jubail area could include road and steelmaking process where the zinc is used as an alloy that is needed during the melting

process and the coating of steel coil surfaces since it is widely used as corrosion resistant agent in many products.

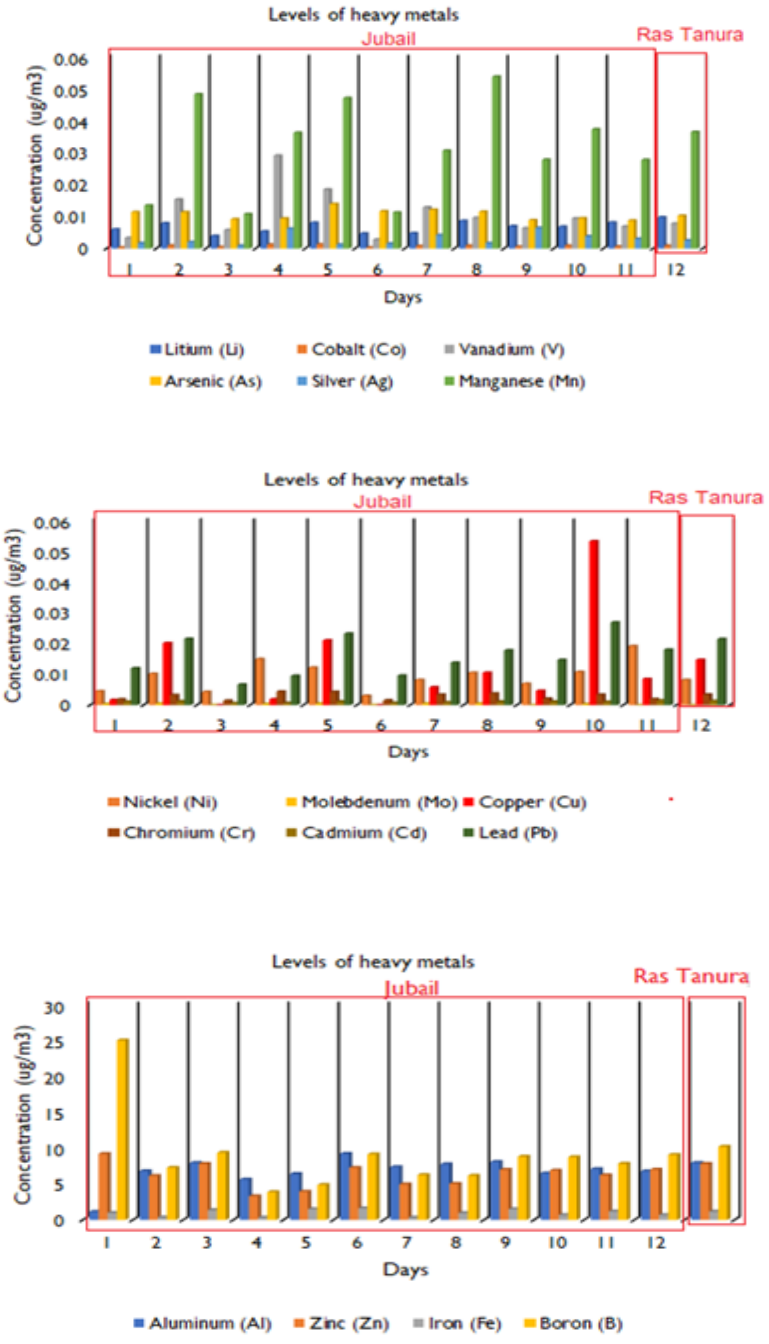

Figure 57. Concentration (µg/m^3) of Trace Metals in PM_{10} samples collected from Jubail and Ras Tanura

Table 38: RCER-2015, Allowable Limit of Trace Metal in the Air

Trace Metal	RCER-2015, µg/m^3 (24h)
Lead	0.5
Nickel	0.1
Cadmium	0.0025
Vanadium	1

To identify the relationship between the ground-based monitoring by the Thermo Scientific 5030i and the Satellite observation using the MODIS Sensor, we extracted satellite observation data at the same time as the ground-based monitoring in Jubail and Ras Tanura "Figures 58 and 59". Further, "Figure 60" presents the concentration of three selected metals (Al, Fe, Zn) and the Angstrom Exponent at 470 that identifies the particles' size. It showed that on 24/05/2018 there was a decrease in the AE 470 value (fine particles) and in the concentration of the above-mentioned heavy metals. Moreover, on 29/05/ 2018 and 20/05/ 2018 there was an increase in the concentration of the metals, while we still can see a high Angstrom Exponent value, which indicates that there is no (or neglected) relationship between them and that any increase in the value of one of them is not accompanied by a decrease in the other.

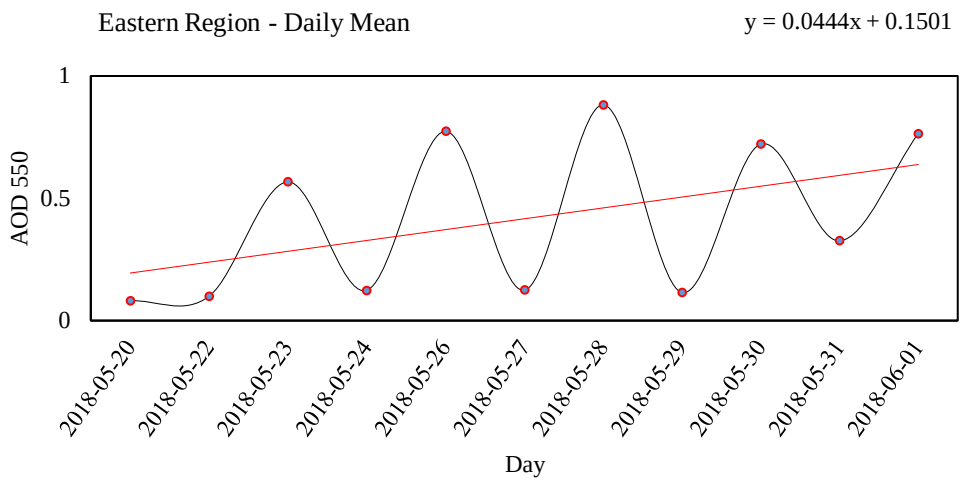

Figure 58. AOD Trend over the Eastern Region during the Period of Real-Time Monitoring

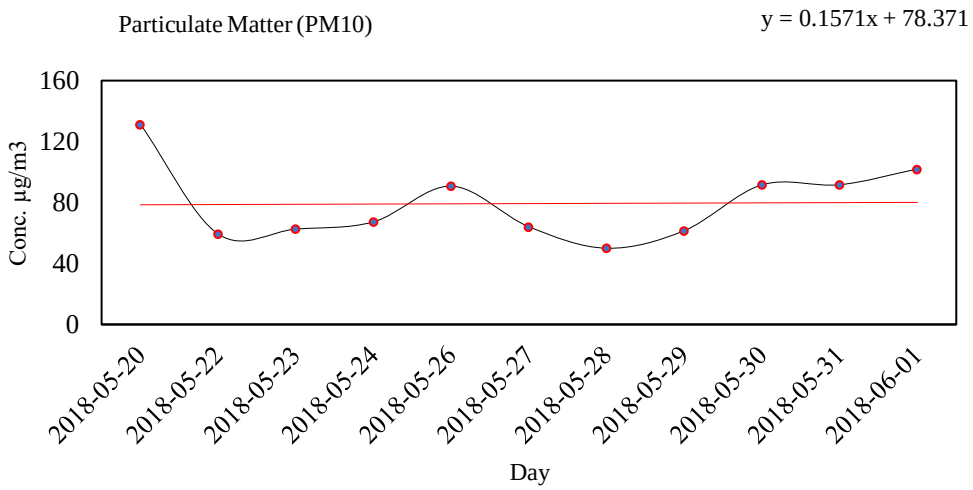

Figure 59. PM Trend over the Eastern Region during the Period of Real-Time Monitoring

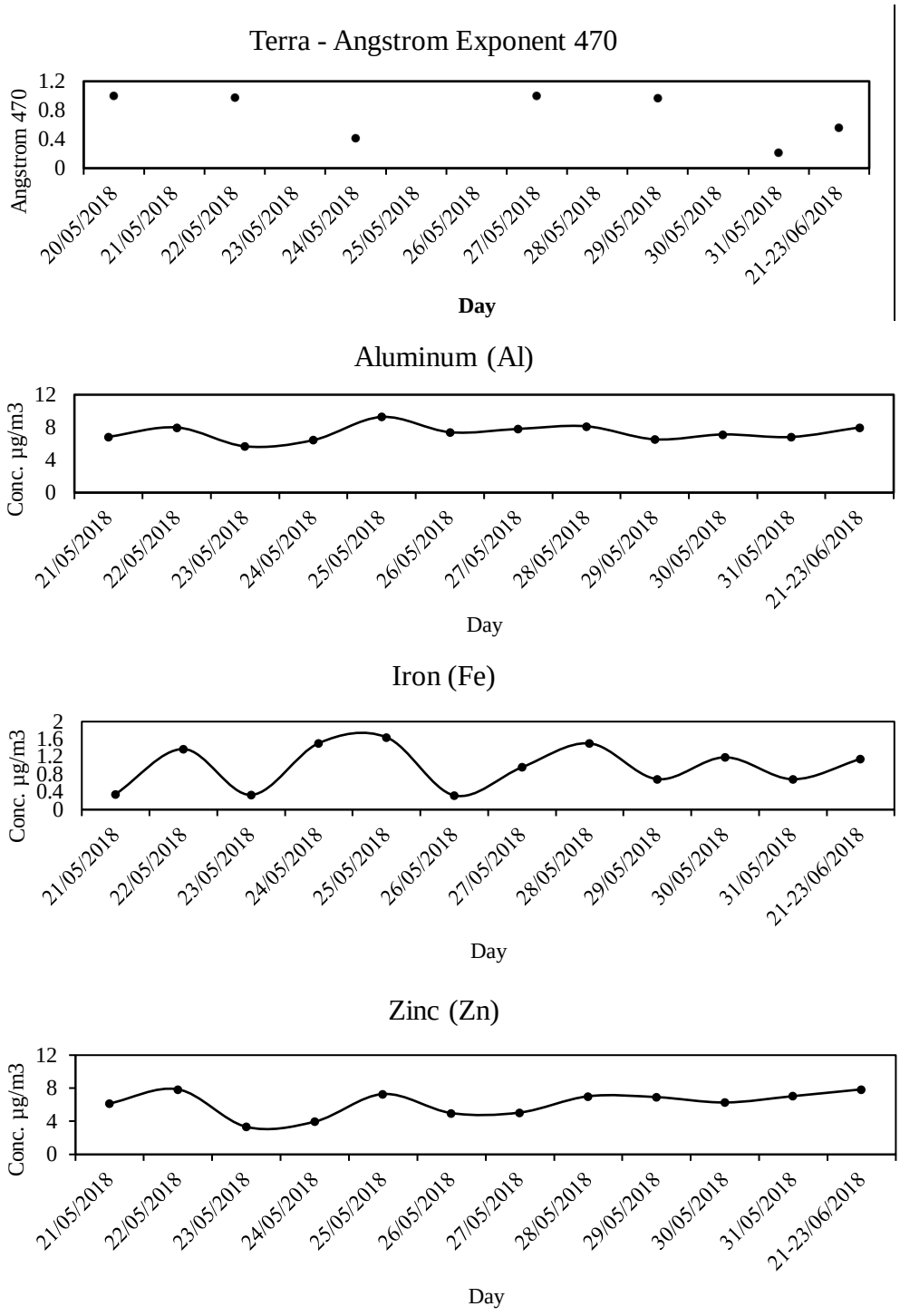

Figure 60. Comparison between the Highest Level of Trace Metals Elements (Real-Time Monitoring) and the Angstrom Values from Terra

4.6 Prediction of Future Trend over the Arabian Peninsula:

To achieve the third objective mentioned in this research, we established the work in this sub-section. The third objective is "Predicting the future trend of Airborne Particulate Matter using historical data gathered from Space-Borne and Ground-Based Stations".

As mentioned earlier, and to predict the PM_{10} values for the upcoming period, monthly observation values of $AOD_{500\&550}$ were chosen instead of daily trends for this section. However, as stated, the prediction was performed using data collected over Solar Village, Terra South, and Terra North. This is basically because the data gathered from Mezaira and the KAUST_Campus were plagued by numerous missing values. This hampers the ability to come up with a reliable model for these data.

4.6.1 Central of Arabian Peninsula

With the central region of Arabian Peninsula, the steps listed in procedure # 3.4.6.1 were followed and applied using the Solar Village historical data.

Before building the ARIMA model, several tests and exploratory procedures were carried out to ensure that the appropriate model was selected to make predictions with the highest possible accuracy and to avoid generating incorrect prediction results.

At first, we saved 10% of the latest data and used the previous 90% of the data to predict the saved 10% but known data. This procedure provided a practical cross-validation impact to make sure we use an appropriate model that fits our time series. However, to begin, we will make the frequent differencing process so that an appropriate differencing frequency is recognized and selected, as the time series data from the central region in-

cludes seasonal variations and trend components that might have a significant effect on the prediction results. "Figure 61" shows the time series without any differencing, the time series with one differenced process, and with two differenced processes. However, according to rule #2 for identifying ARIMA models, “If the lag-1 autocorrelation is -0.5 or more negative, the series may be over differenced” which was shown clearly in the second differences series (below graphs). In this light, the first difference process was selected and this indicates the required number of differences which fit the time series data.

An additional procedure was applied to the differenced series, which helped in the model selection process. The test is called “eacf” and its results are given in "Figure 62" below. It suggests that the AR is zero (0) and the MA is also zero (0), therefore, the model that fits the series will be the ARIMA(0,1,0), which is going to be used on the 90% of the time series, as stated previously, to compare the produced forecasting results with the 10% of the actual data that were saved (the remaining 10%). "Figure 63" show the forecasting results.

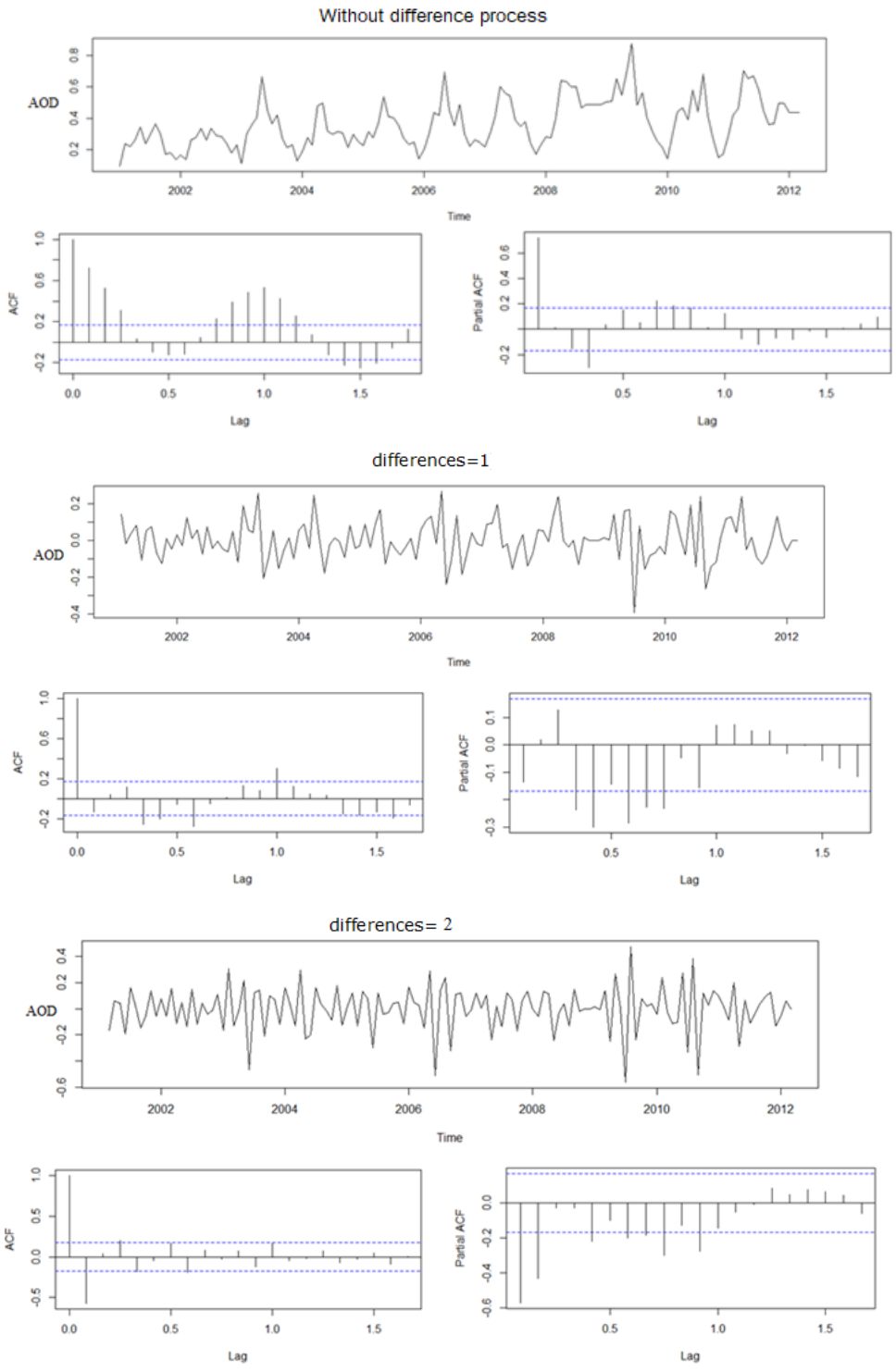

Figure 61. Results of acf & pacf Tests on Central Region Time Series Data with and without Differentiations

```
AR/MA
  0 1 2 3 4 5 6 7 8 9 10 11 12 13
0 o o o x x o x o o o o  x  o  o
1 o o o x o o x o o o o  x  o  o
2 o x o o o o x o o o o  x  o  o
3 x x x o x o x o o o o  x  o  o
4 x x x x x o x o o o o  o  o  o
5 x x o o x o o o o o o  o  o  o
6 x x x o x o o o o o o  o  o  o
7 x o x x x o o o o o o  o  o  o
```

Figure 62. Results of eacf test on Central Region Time Series Data after Applying first Differencing

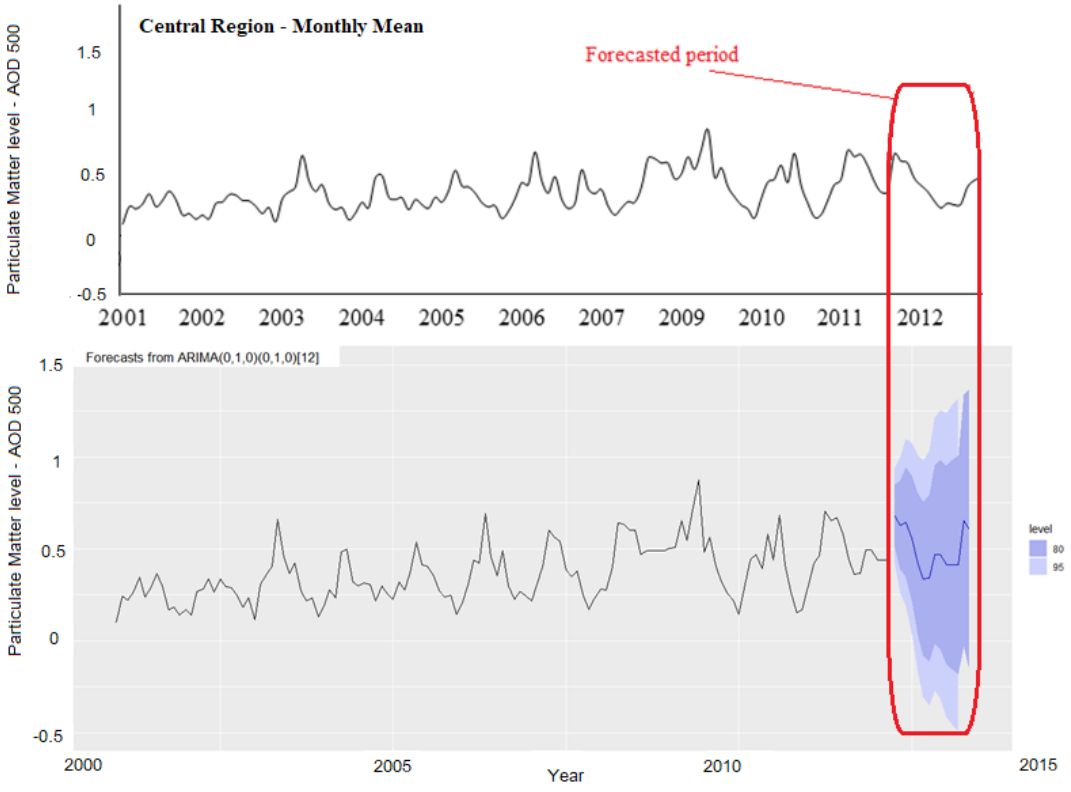

Figure 63. Result of Forecasted Values using 90% of Solar Village Data

As shown in "Figure 63" there is almost a major convergence of both the actual and predicted results, which confirms that this model can be used on the data we have to produce reliable predicted results for the upcoming years. Since the result was satisfactory, we made the prediction for the upcoming period using this model. "Figures 64, 65, and 66" below show the predicted values that represent the particulate matter mean concentration in the central region of the Arabian Peninsula. Further predictions were shown in three graphs; up to 2014, 2025, and 2030 with different confidence levels at both 80 and 95 %. Values in the first graph below show the highest confidence level and show that particulate matter increased followed by a decrease until 2014. The other two graphs have a very low level of confidence; however, they indicate that the particulate matter decreases over time.

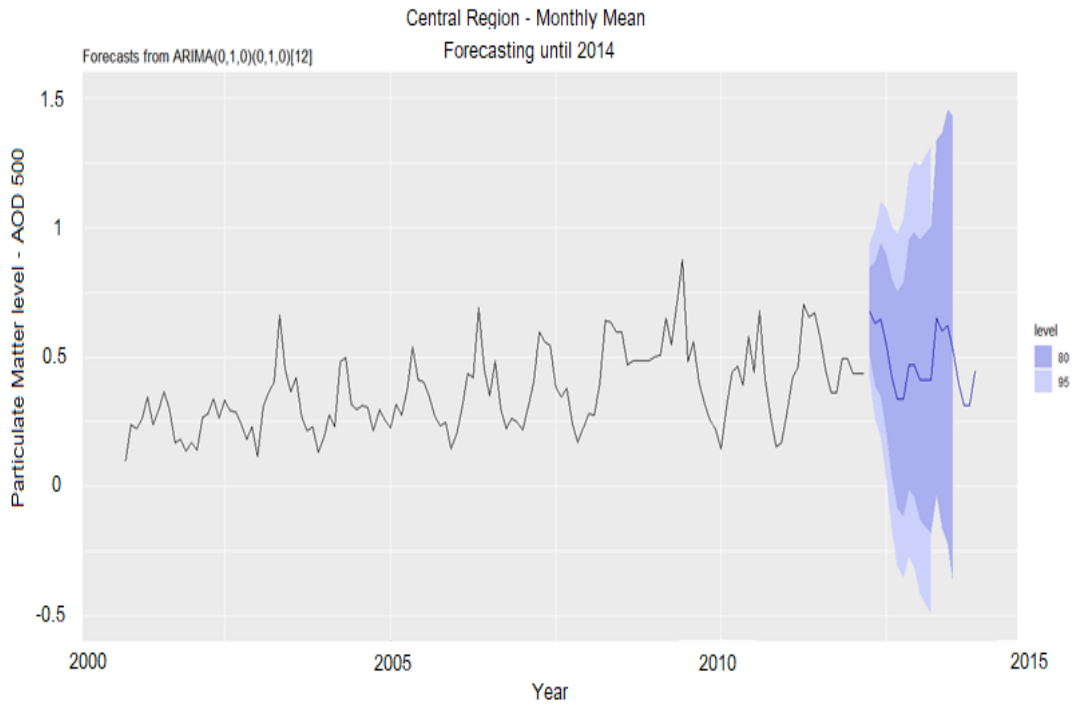

Figure 64. Predicted Mean Values of PM_{10} over the Central of Arabian Peninsula using ARIMA (0,1,0) Model until 2014

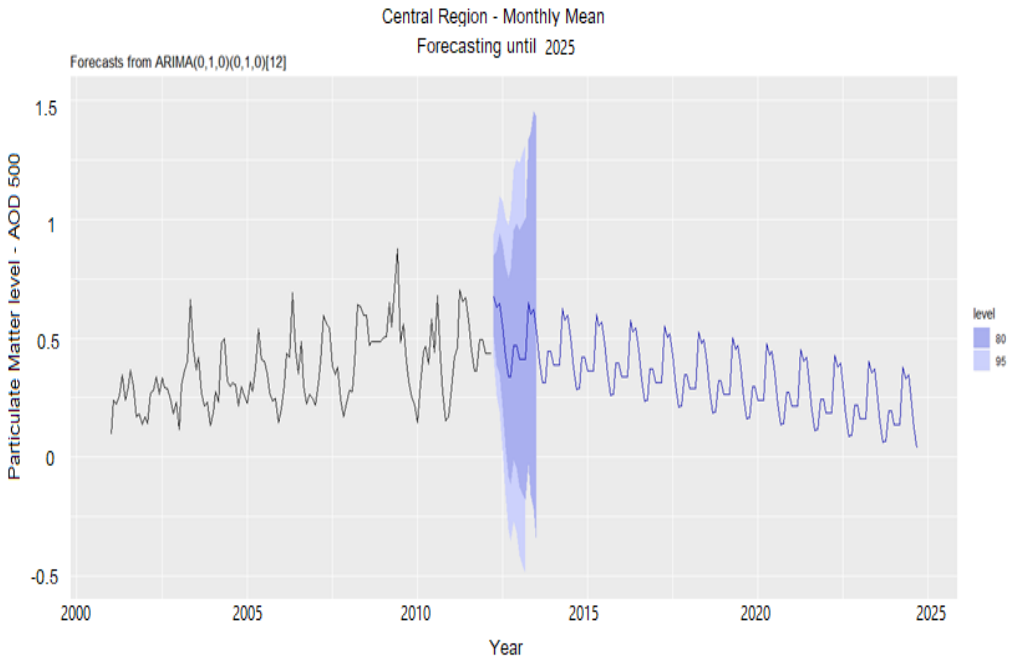

Figure 65. Predicted Mean Values of PM_{10} over the Central of Arabian Peninsula using ARIMA (0,1,0) Model until 2025

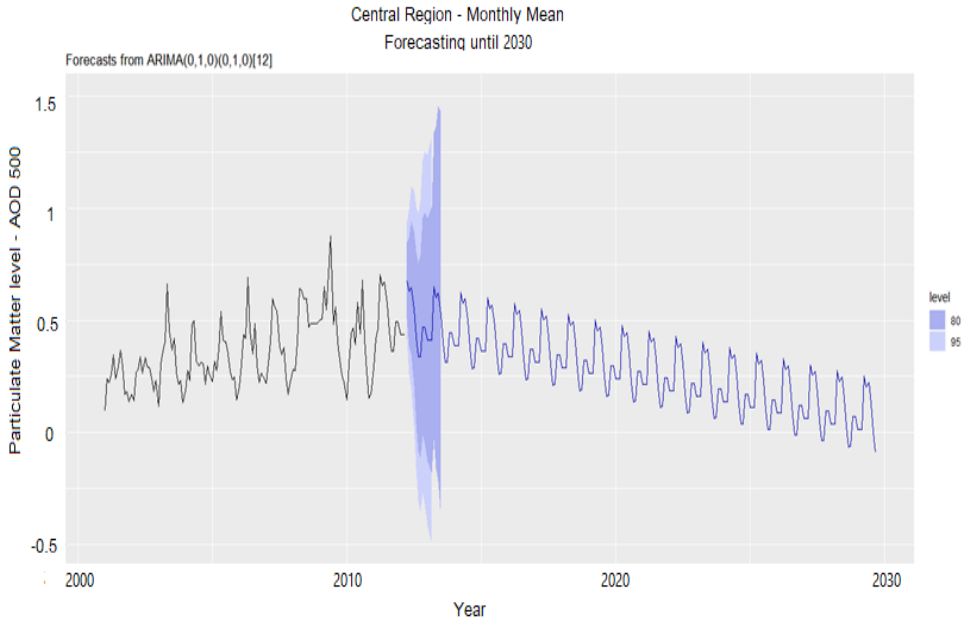

Figure 66. Predicted Mean Values of PM_{10} over the Central of Arabian Peninsula using ARIMA (0,1,0) Model until 2030

4.6.2 North of the Arabian Peninsula

As for the north region of the Peninsula, the steps listed in the procedure under section 3.4.6.2 were followed and applied using the Terra/ MODIS historical data.

However, in addition to the test performed on the Solar Village data, we also applied more tests to come up with a suitable model that fits the time series data of the northern region of the Peninsula, as the process of model selection is varied from one set of data to another.

In the beginning, as in the previous section, we made several differencing processes to determine the number of differences required for the north region time series data. "Figure 67" shows the results of the first and second difference processes. However, to ensure that we select a suitable model, we examine different models through their AIC value. This value helps select a proper model, where the more negative the value, the better the model that fits the time series. "Table 39" shows the results from all of the models tested and is based on the selection of the model with a more negative value (i.g. 2,1,2).

Besides that, we also applied the auto. arima test to get a suggestion. The following was typed: Series: N1seriesdiff1 ARIMA (3,0,0) (2,0,0) [12] with zero mean AIC=-477.4

Based on this, we can say that the best model that fits the time series data for the north region is the ARIMA (2,1,2) (2,1,0)[12] or ARIMA(3,0,0)(2,1,0)[12]. Therefore, a trial using 90% of the time series data has been established. The results are shown in "Figure 68"

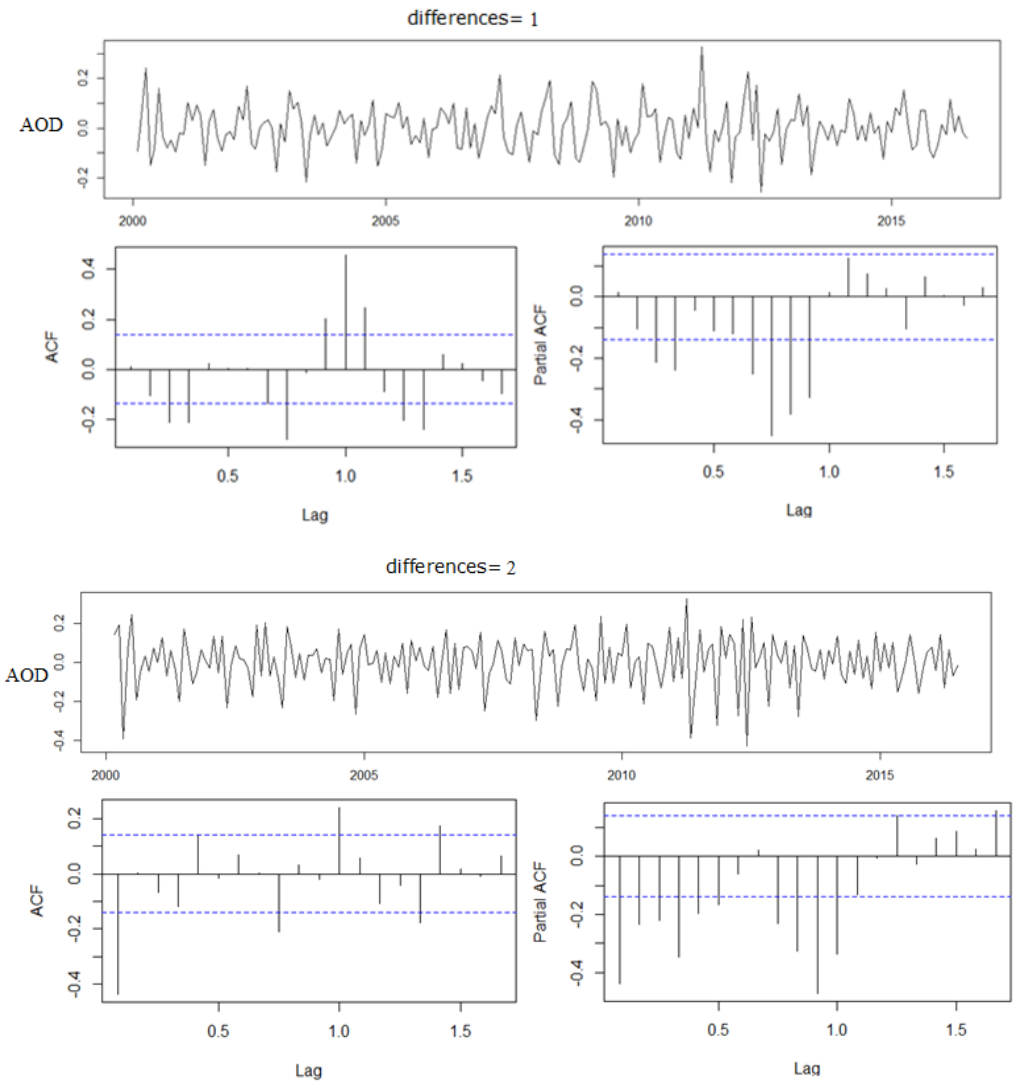

Figure 67. Results of acf & pacf tests on Northern Region Time Series Data with and without Differencing

Table 39. AIC Results of Different ARIMA Models

ARIMA model	AIC value	ARIMA model	AIC value
(0,1,0)	-385.37	(2,2,2)	-369.61
(1, 1, 0)	-383.4	(2,1,2)	-445.99
(1,1,1)	-381.72	(3,0,0)	-445.87
(2,1,1)	-432.87	(1,1,2)	-427.55
(2,2,1)	-373.2	(0,1,2)	-412.01
(0,0,2)	-437.01	(2,2,2)	-369.61
(0,0,1)	-419.53	(0,0,0)	-340.36

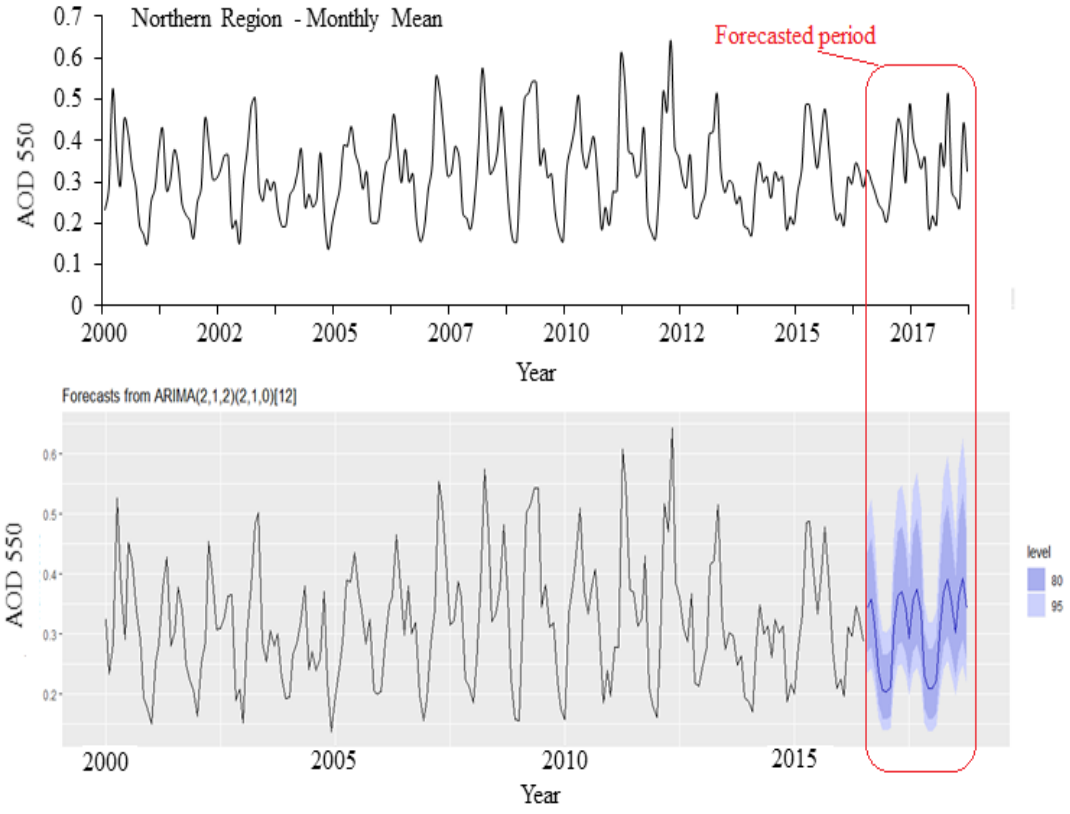

Figure 68. Result of Forecasted Values using 90% of Terra Northern Region Data

Figure 68" show the great accuracy of a selected model that fits the time series, thus, we will be relying on the ARIMA ((2,1,2) (2,1,0) [12] model to produce the future mean values of the particulate matter after 2018. Actual forecasted values are presented in "Figures 69, 70 and 71".

In general, during the prediction periods, the values indicated that there is an increase in the particulate matter concentration followed by a significant drop in 2020. After that, the means will be decreased slightly over time until 2030.

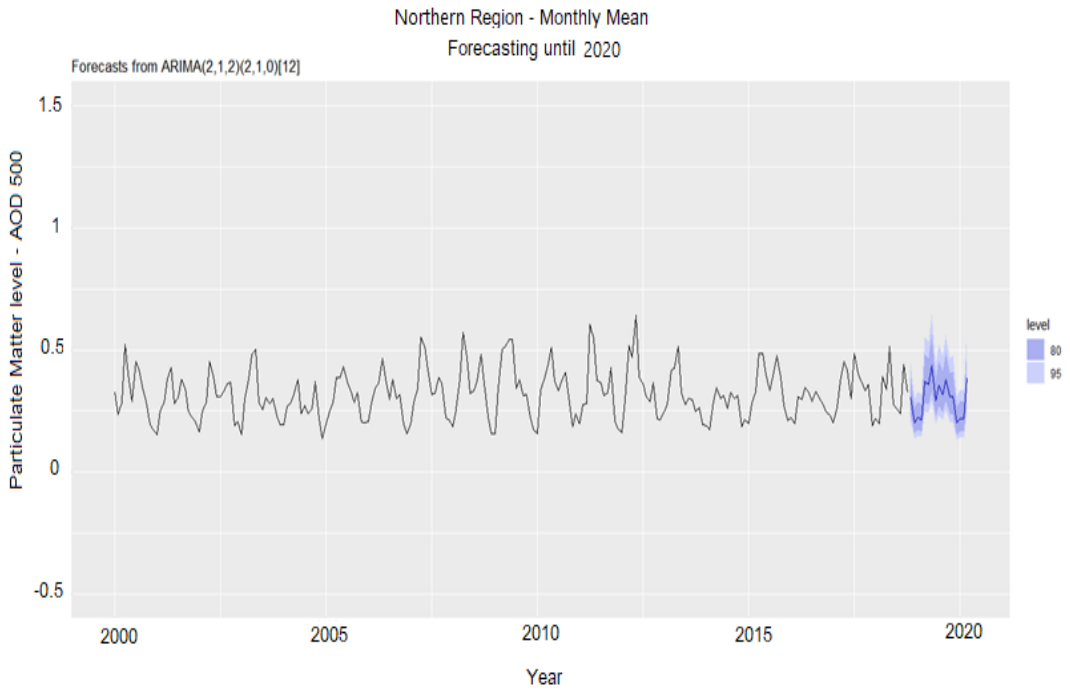

Figure 69. Predicted values/trend of PM_{10} over the North of Arabian Peninsula using ARIMA ((2,1,2) (2,1,0)[12] model until 2020

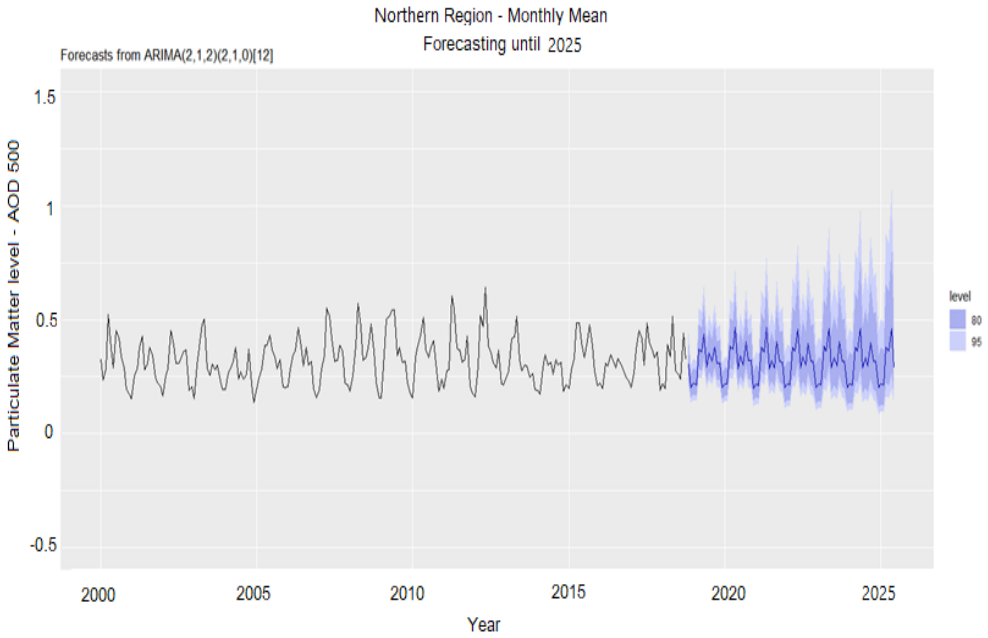

Figure 70. Predicted values/trend of PM_{10} over the North of Arabian Peninsula using ARIMA ((2,1,2) (2,1,0)[12] model

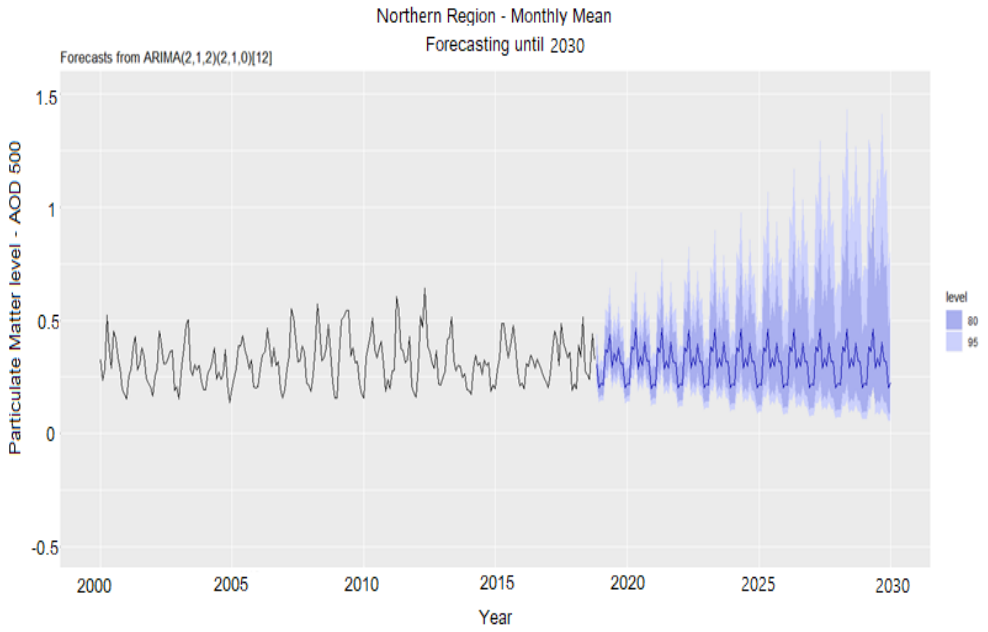

Figure 71. Predicted Values/Trend of PM_{10} over the North of Arabian Peninsula using ARIMA ((2,1,2) (2,1,0)[12] Model until 2030

4.6.3 South of Arabian Peninsula

Lastly, regarding the south region of the Arabian Peninsula, the steps listed in procedure # 3.4.6.3 were followed and applied using the historical data obtained from Terra/ MODIS. This is the same as what happened with the north region.

The steps before forecasting are the same as the other regions' processes. Tests using auto. arima were performed and the results are shown in "Table 40". Based on the values of the AIC, we chose the ARIMA (2,0,0) (0,1,1) [12] to start forecasting the future values using the southern region time series data. Using 90% of the data a trial was made and the results shown in "Figure 72",

As shown in "Figure 73", the line in dark blue is a predicted mean value up to 2020. It indicates that during 2019 there will be a rise in particulate matter concentration over the southern region followed by a decrease starting from mid-2019 until the fourth quarter of the same year. After that, the mean values will keep fluctuating up and down as we move forward until 2030 as reflected in "Figures 74 and 75".

Table 40. Suggested Models using auto.arima

Series Name	Differencing	Suggested Model	AIC value
TS1timeseries	0	ARIMA (2,0,0) (0,1,1) [12] with drift	-411.03
TS1seriesdiff1	1	ARIMA (2,0,0) (2,0,0) [12] with zero mean	-379.89
TS1seriesdiff2	2	ARIMA (1,0,0) (0,0,2)[12] with non-zero mean	-242.95

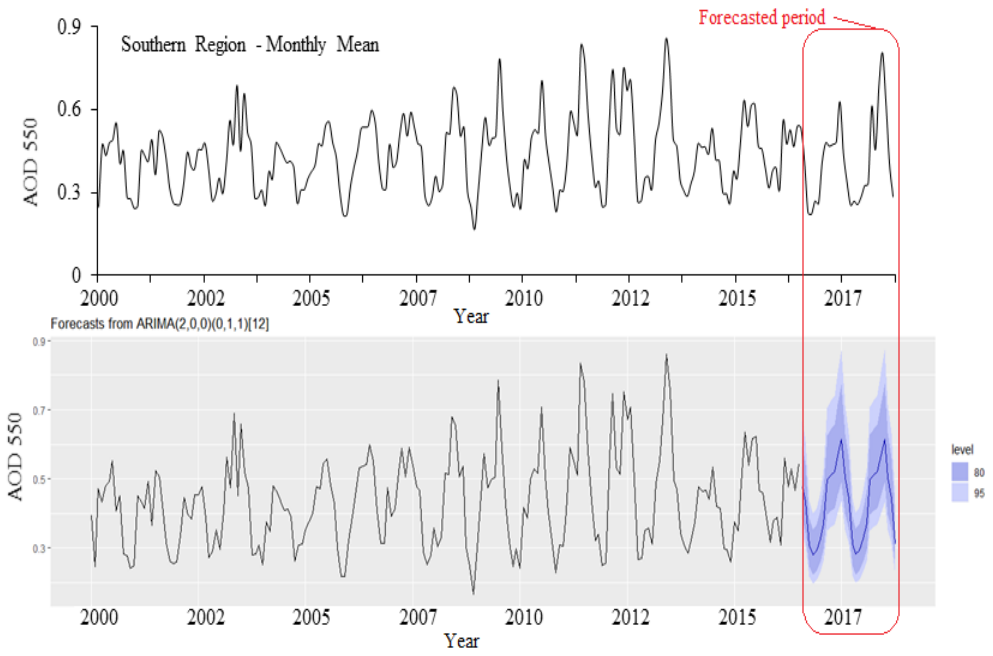

Figure 72. Result of Forecasted Values using 90% of Terra Sothern Region Data

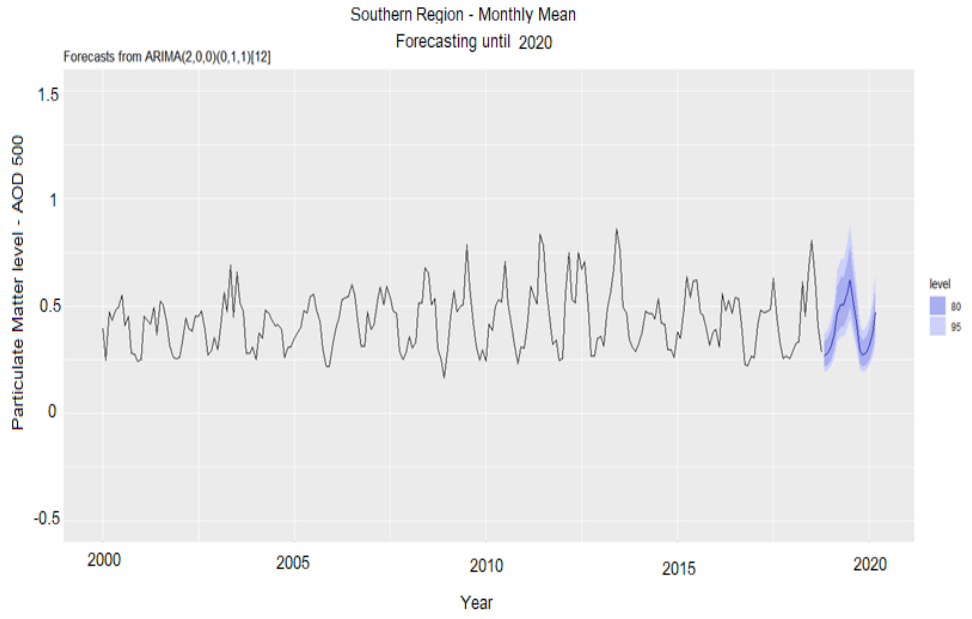

Figure 73. Predicted Values of PM_{10} over the South of Arabian Peninsula using ARIMA ((2,0,0)(0,1,1))[12] Model until 2020

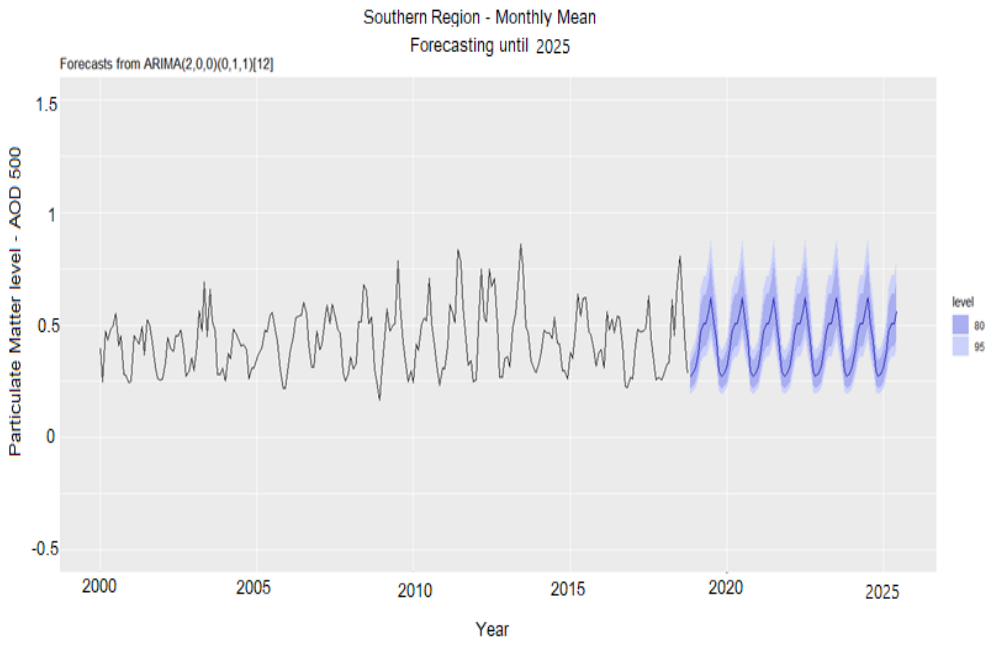

Figure 74. Predicted Values of PM_{10} over the South of Arabian Peninsula using ARIMA ((2,0,0)(0,1,1))[12] Model until 2025

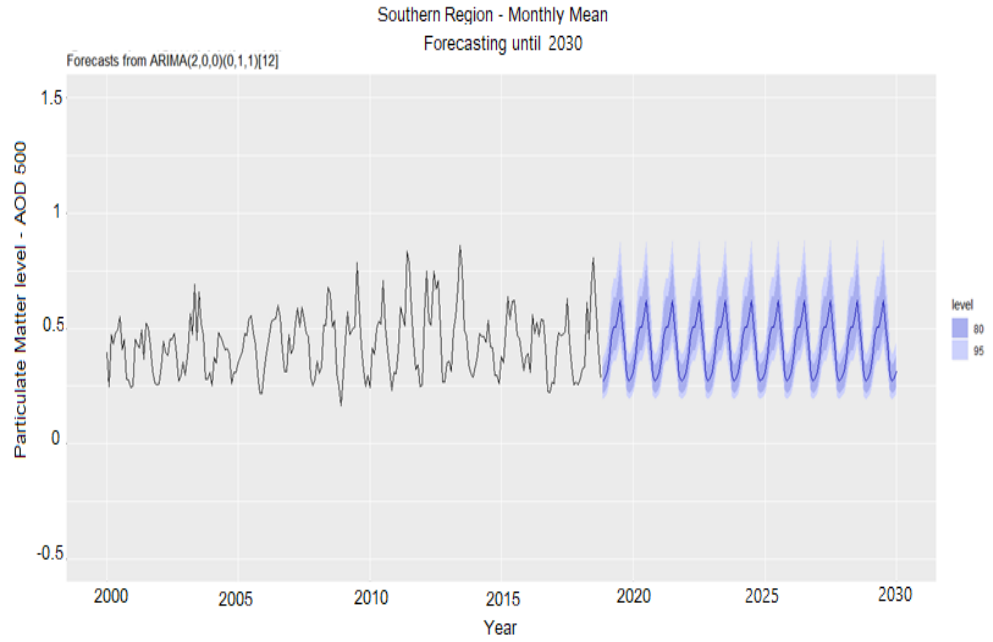

Figure 75. Predicted Values of PM_{10} over the South of Arabian Peninsula using ARIMA ((2,0,0)(0,1,1))[12] Model until 2030

CHAPTER 5

CONCLUSIONS AND RECOMMENDATIONS

5.1. Conclusions

The following conditions have been reached in the present research:

I. The AERONET) and satellite (Terra/ MODIS) analysis showed that the trend of the particulate matter concentration over the five regions has increased with time, although in uneven percentages. The percentages are 58%, 15%, 13%, 8%, 6% in the Central, Western, Southern, Northern and Eastern regions, respectively. However, the same results also showed that the trend for manmade particulate matter is a decrease over time by 29%, 28% and 21% in the Northern, Central and Eastern Regions, respectively, while it significantly increased in the Western (72%) and Southern (18%) Regions.

II. The confidence level of the daily mean values analysis is the highest from among the others, however, the results of the particulate matter concentration over the Western, Northern and Southern Regions were not statistically significant as denoted by the probability test.

III. Analysis of seasonal and specific month data revealed that, over the Central Region, the particulate matter concentration increased during all of the seasons, while the man-made particulates significantly decreased during the winter season,

as well as in the last month of summer and the first and last months in the fall season. By contrast, it increased significantly over the Eastern Region during the first two months of the fall season. However, it also increased in the same region during the other seasons, although at a lower rate with a significant decrease in man-made particles, except during May and August. As for the Western Region, the concentration decreased during all of the seasons, except during the beginning and the middle of the summer season, in addition to the month of December.

IV. The size of PM_{10} is generally small, especially in Jubail city. In both Jubail and Ras Tanura, the particle shape is irregular and more spherical, accompanied by many clusters deposited in different spots on the Jubail filters. This finding indicates that the industries in both cities have a significant impact on air quality and the chemical composition of it.

V. The Jubail PM samples contain zinc, barium, sulfur, sodium, and potassium in higher concentrations than in the Ras Tanura samples. However, the Ras Tanura samples showed higher concentrations of calcium, chlorine, aluminum, iron, and magnesium.

VI. The XRD result showed that the mineral compositions are classified into three stand-alone clusters. Clusters #1 and #2 were close to each other, while cluster #3 was not. However, the segregation between samples into different clusters, especially between the Jubail samples, could be traced back to the natural geological processes and the precipitation of vapor, water, and living organisms. The changes could also occur because the mineral tends to change into a more stable state

continually through natural weathering process, and the metamorphic rocks formation.

VII. ICP-MS showed that the levels of lithium, cobalt, vanadium, arsenic, silver, manganese, nickel molybdenum, copper, chromium, cadmium, and lead, are within the regulatory authority limits.

VIII. The *R-Studio model* showed that, over the Central region, the particulate matter concentration increased, to be followed by a decrease until the last of 2030. Over the North area, the predicated values indicated that there is an overall increase in the particulate matter concentration, to be followed by a significant drop in 2020 which continued until 2030. Lastly, over the South area during 2019, there will be a rise in particulate matter concentration followed by a decrease starting from mid-2019 until the fourth quarter of the same year. After that, the mean values will keep fluctuating up and down as we move forward to 2030.

5.2. Recommendations

In view of the results and limitations in this research work, the following recommendations can be made:

- Size distribution over the south and north of the Arabian Peninsula should be studied.
- At the Gulf Cooperation Council (GCC) level, cooperation should be made to reduce the emissions of man-made particles over the Arabian Peninsula.
- More research work should be established over the West and South areas of the Arabian Peninsula to understand the reasons behind the increase in man-made particles.
- Chemical characterization of the long-term particulate matter over the Arabian Peninsula is highly recommended.
- Chemical characterization of particulate matter should be extended to cover more areas within the Arabian Peninsula.

REFERENCES

Aher, G., Pawar, G., Gupta, P. and Devara, P. (2014). Effect of a major dust storm on optical, physical, and radiative properties of aerosols over coastal and urban environments in Western India. International Journal of Remote Sensing, 35(3), pp.871-903., doi:10.1080/01431161.2013.873153

Aina, Y., van der Merwe, J. and Alshuwaikhat, H., (2014). Spatial and Temporal Variations of Satellite-Derived Multi-Year Particulate Data of Saudi Arabia: An Exploratory Analysis. International Journal of Environmental Research and Public Health, 11(11), doi: 10.3390/ijerph111111152.

Alam, K., Trautmann, T., Blaschke, T., and Subhan, F. (2014). Changes in aerosol optical properties due to dust storms in the Middle East and Southwest Asia. Remote Sensing of Environment, 143, pp.216-227., doi: 10.1016/j.rse.2013.12.021

Alharbi, B., Maghrabi, A. and Tapper, N. (2013). The March 2009 Dust Event in Saudi Arabia: Precursor and Supportive Environment. Bulletin of the American Meteorological Society, 94(4), pp.515-528., doi: 10.1175/BAMS-D-11-00118.1

Alharbi, B., Pasha, M. and N, T., 2014, Assessment of Ambient Air Quality in Riyadh City, Saudi Arabia. Current World Environment, 9(2), p.227, doi:10.12944/cwe.9.2.01.

Ali, M., Assiri, M., and Dambul, R. (2017). Seasonal Aerosol Optical Depth (AOD) Variability Using Satellite Data and its Comparison over Saudi Arabia for the Period 2002–2013. Aerosol and Air Quality Research, 17(5), pp.1267-1280., doi: 10.4209/aaqr.2016.11.0492

Al-Jeelani, H. (2013). The Impact of Traffic Emission on Air Quality in an Urban Environment. Journal of Environmental Protection, 04(02), p.205, doi: 10.4236/jep.2013.42025

Awal, M., Rabbi, J., Hossain, S. and Hashem, M. (2016). Using linear regression to forecast future trends in the crime of Bangladesh. 2016 5th International Conference on Informatics, Electronics, and Vision (ICIEV), doi: 10.1109/ICIEV.2016.7760021.

Badoghpour, S., Hashemi Monfared, S. and Haghshenas, S. (2009). Prediction of Air Pollution Due to Traffic by Means of Artificial Neural Network. world Applied Sciences Journal, [online] (1), pp.156-158.

Bahari, R., Abbaspour, R. and Pahlavani, P. (2014). prediction of PM2.5 concentrations using temperature inversion effects based on an artificial neural network. ISPRS - International Archives of the Photogrammetry, Remote Sensing and Spatial Information Sciences, XL-2/W3, pp.73-77, doi: 10.5194/isprsarchives-XL-2-W3-73-2014

Basha, G., Phanikumar, D., Kumar, K., Ouarda, T. and Marpu, P. (2015). Investigation of aerosol optical, physical, and radiative characteristics of a severe dust storm ob-

served over UAE. Remote Sensing of Environment, 169, pp.404-417., doi: 10.1016/j.rse.2015.08.033

Boman, J., Shaltout, A., Abozied, A. and Hassan, S. (2013). On the elemental composition of PM2.5 in central Cairo, Egypt. X-Ray Spectrometry, 42(4), pp.276-280., doi: 10.1002/xrs.2464

Braga, C. F., Teixeira, E. C., Meira, L., Wiegand, F., Yoneama, M. L., & Dias, J. F. (2005). Elemental composition of PM10 and PM2. 5 in an urban environment in South Brazil. *Atmospheric Environment*, *39*(10), 1801-1815.

Cachorro, V., Toledano, C., Vergaz, R., de Frutos, A., Sorribas, M., Vilaplana, J., and de la Morena, B. (2005). The PHOTONS - AERONET Network Stations in Spain. Recent Advances in Multidisciplinary Applied Physics, pp.173-177, doi: 10.1016/B978-008044648-6.50028-8

Chen, H., Cheng, T., Gu, X., Li, Z. and Wu, Y. (2016). Characteristics of aerosols over Beijing and Kanpur derived from the AERONET dataset. Atmospheric Pollution Research, 7(1), pp.162-169, doi: 10.1016/j.apr.2015.08.008

Clements, N., Hannigan, M. P., Miller, S. L., Peel, J. L., & Milford, J. B. (2016). Comparisons of urban and rural PM 10− 2.5 and PM 2.5 mass concentrations and semi-volatile fractions in northeastern Colorado. *Atmospheric Chemistry and Physics*, *16*(11), 7469-7484.

Daly, A., & Zannetti, P. (2007). Air pollution modeling–An overview. *Ambient air pollution*, 15-28.

Dayou, J., Chang, J. and Sentian, J. (2014). Ground-Based Aerosol Optical Depth Measurements. Ground-Based Aerosol Optical Depth Measurement Using Sunphotometers, p.7, DOI: 10.1007/978-981-287-101-5_2.

Dye, T. (2003). Guidelines for developing an air quality (ozone and PM2.5) forecasting program. Research Triangle Park, N.C.: U.S. Environmental Protection Agency, Office of Air Quality Planning and Standards, Information Transfer and Program Integration Division, AIRNow Program.

Engel, M; Bruckner, H, and Messenzehl, K. (2011). Natural Environment of the Arabian Peninsula.

Farahat, A. (2016). Air pollution in the Arabian Peninsula (Saudi Arabia, the United Arab Emirates, Kuwait, Qatar, Bahrain, and Oman): causes, effects, and aerosol categorization. Arabian Journal of Geosciences, 9(3), p.196., doi: 10.1007/s12517-015-2203-y

Farahat, A., El-Askary, H. and Al-Shaibani, A. (2015). Study of Aerosols' Characteristics and Dynamics over the Kingdom of Saudi Arabia Using a Multisensor Approach Combined with Ground Observations. Advances in Meteorology, pp.1-12, doi: 10.1155/2015/247531

Farahat, A., El-Askary, H. and Dogan, A. (2016). Aerosols Size Distribution Characteristics and Role of Precipitation during Dust Storm Formation over Saudi Arabia. Aerosol and Air Quality Research, 16(10), pp.2523-2534, doi:10.4209/aaqr.2015.11.0656

Farahat, A., El-Askary, H., Adetokunbo, P. and Fuad, A. (2016). Analysis of aerosol absorption properties and transport over North Africa and the Middle East using AERONET data. Annales Geophysicae, 34(11), pp.1031-1044, doi: 10.5194/angeo-34-1031-2016

Feng, X., Li, Q., Zhu, Y., Hou, J., Jin, L. and Wang, J. (2015). Artificial neural networks forecasting of PM2.5 pollution using air mass trajectory based geographic model and wavelet transformation. Atmospheric Environment, 107, pp.118-128, doi: 10.1016/j.atmosenv.2015.02.030

Furman, H. (2003). Dust Storms in the Middle East: Sources of Origin and Their Temporal Characteristics. Indoor and Built Environment, 12(6), pp.419-426, doi: 10.1177/1420326x03037110

García, R., García, O., Cuevas, E., Cachorro, V., Barreto, A., Guirado-Fuentes, C., Kouremeti, N., Bustos, J., Romero-Campos, P., and de Frutos, A. (2016). Aerosol optical depth retrievals at the Izaña Atmospheric Observatory from 1941 to 2013 by using artificial neural networks. Atmospheric Measurement Techniques, 9(1), pp.53-62, doi:10.5194/amt-9-53-2016

Grandey, B., Stier, P. and Wagner, T. (2013). Investigating relationships between aerosol optical depth and cloud fraction using satellite, aerosol reanalysis, and general circulation model data. Atmospheric Chemistry and Physics, 13(6), pp.3177-3184, doi: 10.5194/acp-13-3177-2013

Gupta, P., & Christopher, S. A. (2009). Particulate matter air quality assessment using integrated surface, satellite, and meteorological products: Multiple regression approach. *Journal of Geophysical Research: Atmospheres*, *114*(D14).

Hamdan, N. M., Alawadhi, H., & Jisrawi, N. (2015). Elemental and Chemical Analysis of PM_{10} and PM2. 5 Indoor and Outdoor Pollutants in the UAE. *International Journal of Environmental Science and Development*, *6*(8), 566.

Han, S., Zhang, Y., Wu, J., Zhang, X., Tian, Y., Wang, Y. & Cai, Z. (2015). Evaluation of regional background particulate matter concentration based on vertical distribution characteristics. *Atmospheric Chemistry and Physics*, *15*(19), 11165-11177.

Hasan, F. and Sabbah, I. (2007). Atmospheric Aerosols Optical Properties and Climate over Solar Village, KSA. Nucleation and Atmospheric Aerosols, pp.1155-1158, doi: 10.1007/978-1-4020-6475-3_229

Hashim, S. A. Alsultan, Sultan. MatJafri, M. Z. Abdullah, K. and Salleh, N. M. (2001). The Measurement of Aerosol Optical Thickness in Mina During the Hajj Season 1426H." ISPRS Journal of Photogrammetry and Remote Sensing 26, 241-244.

Higgs, G., Sterling, D. A., Aryal, S., Vemulapalli, A., Priftis, K. N., & Sifakis, N. I. (2015). Aerosol optical depth as a measure of particulate exposure using imputed censored data, and relationship with childhood asthma hospital admissions for 2004 in Athens, Greece. *Environmental health insights*, *9*, EHI-S15665.

Holben, B., Eck, T., Slutsker, I., Smirnov, A., Sinyuk, A., Schafer, J., Giles, D. and Dubovik, O. (2006). Aeronet's Version 2.0 quality assurance criteria. Remote Sensing of the Atmosphere and Clouds., doi:10.1117/12.706524

Holben, B., Eck, T., Slutsker, I., Tanré, D., Buis, J., Setzer, A., Vermote, E., Reagan, J., Kaufman, Y., Nakajima, T., Lavenu, F., Jankowiak, I. and Smirnov, A. (1998). AERONET—A Federated Instrument Network and Data Archive for Aerosol Characterization. Remote Sensing of Environment, 66(1), pp.1-16, doi: 10.1016/S0034-4257(98)00031-5

Hurtado, J., Agarwal, A. and Zhu, X. (2016). Topic discovery and future trend forecasting for texts. Journal of Big Data, 3(1), doi: 10.1186/s40537-016-0039-2

K. M. Hamasha, H. M. Abu Mostafaa, and L. T. Alexander. (2012). Aerosol Optical Thickness at Tabuk City, SAUDI ARABIA. International Journal of Applied Science and Technology, vol. 2, no. 10, p. 69.

Khalil, M., Butenhoff, C., Porter, W., Almazroui, M., Alkhalaf, A. and Al-Sahafi, M. (2015). Air quality in Yanbu, Saudi Arabia. Journal of the Air & Waste Management Association, 66(4), pp.341-355, doi: 10.1080/10962247.2015.1129999.

Khodeir, M., Shamy, M., Alghamdi, M., Zhong, M., Sun, H., Costa, M., Chen, L. and Maciejczyk, P. (2012). Source apportionment and elemental composition of PM2.5 and PM_{10} in Jeddah City, Saudi Arabia. Atmospheric Pollution Research, 3(3), pp.331-340, doi: 10.5094/APR.2012.037

Klingmüller, K., Pozzer, A., Metzger, S., Stenchikov, G. and Lelieveld, J. (2016). Aerosol optical depth trend over the Middle East. Atmospheric Chemistry and Physics, 16(8), pp.5063-5073, doi: 10.5194/acp-16-5063-2016

Kumar, A. and Goyal, P. (2011). Forecasting of air quality in Delhi using principal component regression technique. Atmospheric Pollution Research, 2(4), pp.436-444. doi: 10.5094/APR.2011.050

Kunte, P. and M.A., A. (2015). Detection and monitoring of super sandstorm and its impacts on the Arabian Sea—Remote sensing approach. Atmospheric Research, 160, pp.109-125, doi: 10.1016/j.atmosres.2015.03.003

Lihavainen, H., Alghamdi, M., Hyvärinen, A., Hussein, T., Aaltonen, V., Abdelmaksoud, A., Al-Jeelani, H., Almazroui, M., Almehmadi, F., Al Zawad, F., Hakala, J., Khoder, M., Neitola, K., Petäjä, T., Shabbaj, I. and Hämeri, K. (2016). Aerosols physical properties at Hada Al Sham, western Saudi Arabia. Atmospheric Environment, 135, pp.109-117., doi: 10.1016/j.atmosenv.2016.04.001

Liu, D. J., & Li, L. (2015). Application study of comprehensive forecasting model based on entropy weighting method on the trend of PM2. 5 concentration in Guang-

zhou, China. *International journal of environmental research and public health*, *12*(6), 7085-7099.

Maghrabi, A., Alharbi, B. and Tapper, N. (2011). Impact of the March 2009 dust event in Saudi Arabia on aerosol optical properties, meteorological parameters, sky temperature, and emissivity. Atmospheric Environment, 45(13), pp.2164-2173, doi: 10.1016/j.atmosenv.2011.01.071

McCarthy, N. (2016). Infographic: The 20 Worst Cities Worldwide for Air Pollution. [online] Statista Infographics. Available at: https://www.statista.com/chart/4887/the-20-worst-cities-worldwide-for-air-pollution/ [Accessed 22 Dec. 2017].

Mehdi, J., Reza, G., Ahmad, H., & Omid, N. (2016). Finding the best locations for establishment of solar-wind power stations in Middle-East using GIS: A Review. Renewable and Sustainable Energy Reviews, 66, 38–52. Retrieved from https://www.sciencedirect.com/science/article/pii/S1364032116304105

Mills, T. (1991). Time series techniques for economists. Cambridge: Cambridge University Press.

Mohalfi Saad, Bedi, H. S. Krishnamurti, H. S. and Cocke, Steven D. (1998). Impact of shortwave radiative effects of dust aerosols on the summer season heat low over Saudi Arabia. Monthly weather review 126.12, 3153-3168, doi:10.1175/1520-0493

Mohammed, A. M., Munir, S. A. I. D., & Habeebullah, T. M. (2015). Characterization of atmospheric aerosols in Makkah. *Int. J. Agric. Environ. Res, 1*, 1-18.

Munir, S., Gabr, S., Habeebullah, T. and Janajrah, M. (2016). Spatiotemporal analysis of fine particulate matter (PM2.5) in Saudi Arabia using remote sensing data. The Egyptian Journal of Remote Sensing and Space Science, 19(2), p.195., doi: 10.1016/j.ejrs.2016.06.001

N. Cumberlidge. (2015). Arabian Peninsula Report.

Oamen Festus, I. (2019). Fossil Fuels and the Current Fuel Reserve in Developed and Developing Countries. Science, Technology & Public Policy, 2(1), 5. https://doi.org/10.11648/j.stpp.20180201.12

Pease, P., Tchakerian, V. and Tindale, N. (1998). Aerosols over the Arabian Sea: geochemistry and source areas for aeolian desert dust. Journal of Arid Environments, 39(3), pp.477-496., doi: 10.1006/jare.1997.0368

Percival, D. and Walden, A. (1993). Spectral analysis for physical applications. Cambridge: Cambridge University Press.

Pipal, A., Kulshrestha, A. and Taneja, A. (2011). Characterization and morphological analysis of airborne PM2.5 and PM_{10} in Agra located in north central India. Atmospheric Environment, 45(21), pp.3621-3625, doi: 10.1016/j.atmosenv.2011.03.062

Royal Commission for Jubail and Yanbu (RCJY). (2015). ROYAL COMMISSION ENVIRONMENTAL REGULATIONS 2015 Volume I Regulations and Standards.

Rushdi, A. I., Al-Mutlaq, K. F., Al-Otaibi, M., El-Mubarak, A. H., & Simoneit, B. R. (2013). Air quality and elemental enrichment factors of aerosol particulate matter in Riyadh City, Saudi Arabia. *Arabian Journal of Geosciences, 6*(2), 585-599.

Rushdi, A., Al-Mutlaq, K., Al-Otaibi, M., El-Mubarak, A. and Simoneit, B. (2011). Air quality and elemental enrichment factors of aerosol particulate matter in Riyadh City, Saudi Arabia. Arabian Journal of Geosciences, 6(2), pp.585-599, doi:10.1007/s12517-011-0357-9

Saeed, T., Al-Dashti, H. and Spyrou, C. (2014). Aerosol's optical and physical characteristics and direct radiative forcing during a shamal dust storm, a case study. Atmospheric Chemistry and Physics, 14(7), pp.3751-3769., doi: 10.5194/acp-14-3751-2014

Salinas, S., Chew, B. and Liew, S. (2009). Retrievals of aerosol optical depth and Ångström exponent from ground-based Sun-photometer data of Singapore. Applied Optics, 48(8), p.1473, doi: 10.1364/AO.48.001473

Saudi Arabian Government. (2016) An Industrial Investors Guide. Saudi Arabia; A Land of Opportunities. Retrieved from:

Shalaby, A., Rappenglueck, B. and Eltahir, E. (2015). The climatology of dust aerosol over the Arabian Peninsula. Atmospheric Chemistry and Physics Discussions, 15(2), pp.1523-1571, doi: 10.5194/acpd-15-1523-2015

Sigrid M. Hohle, and Karl H. Teigen. (2015). Forecasting forecasts: The trend effect. Judgment and Decision Making, 10(5), pp.416-428.

Soltani, S., Modarres, R. and Eslamian, S. (2007). The use of time series models for the determination of rainfall climates of Iran. International Journal of Climatology, 27(6), pp.819-829, dio: 10.1002/joc.1427

Soni, K., Parmar, K. and Kapoor, S. (2014). Time series model prediction and trend variability of aerosol optical depth over coal mines in India. Environmental Science and Pollution Research, 22(5), pp.3652-3671, doi: 10.1007/s11356-014-3561-9

Soni, K., Singh, S., Bano, T., Tanwar, R. and Nath, S. (2011). Wavelength Dependence of the Aerosol Angstrom Exponent and Its Implications Over Delhi, India. Aerosol Science and Technology, 45(12), pp.1488-1498, doi: 10.1080/02786826.2011.601774

Souza, D. Z., Vasconcellos, P. C., Lee, H., Aurela, M., Saarnio, K., Teinilä, K., & Hillamo, R. (2014). The composition of $PM_{2.5}$ and PM_{10} collected at urban sites in Brazil. *Aerosol Air Qual. Res*, *14*, 168-176.

TAIWO, L. (2016). Levels and characteristic of airborne particulate matter in Dammam, Dhahran and Khobar, Saudi Arabia. MSc. King Fahd University of Petroleum &

Minerals. Available at: http://eprints.kfupm.edu.sa/140015/1/LAWAL_TAOREED_TAIWO_MS_THESIS.pdf [Accessed 1 Oct. 2017].

Taneja, S., Sharma, N., Oberoi, K. and Navoria, Y. (2016). Predicting trends in air pollution in Delhi using data mining. 2016 1st India International Conference on Information Processing (IICIP), doi:10.1109/IICIP.2016.7975379

Tatem, A., Goetz, S. and Hay, S. (2004). Terra and Aqua: new data for epidemiology and public health. International Journal of Applied Earth Observation and Geoinformation, 6(1), pp.33-46, doi: 10.1016/j.jag.2004.07.001

Teller, A., D. Axisa, D. W. Breed, D. R. Collins, R. T. Bruintjes, and R. Burger. (2008). Aerosol-cloud interactions over Istanbul, Turkey, and central Saudi Arabia. National Center for Atmospheric Research (NCAR).

US Environmental Protection Agency (EPA). (2010) Particulate Matter Urban-Focused Visibility Assessment.

Van Donkelaar, A., Martin, R. V., Brauer, M., & Boys, B. L. (2015). Use of satellite observations for long-term exposure assessment of global concentrations of fine particulate matter. *Environmental health perspectives*, *123*(2), 135.

WHO (2005). WHO Air quality guidelines for particulate matter, ozone, nitrogen dioxide, and sulfur dioxide.

WHO Global Urban Ambient Air Pollution Database (update 2016)", World Health Organization, 2017.

Wilson, W. and Suh, H. (1997). Fine Particles and Coarse Particles: Concentration Relationships Relevant to Epidemiologic Studies. Journal of the Air & Waste Management Association, 47(12), p.1241, doi: 10.1080/10473289.1997.10464074

World Health Organization. (2016). Ambient air pollution: A global assessment of exposure and burden of disease.

Yu, Y., Notaro, M., Liu, Z., Kalashnikova, O., Alkolibi, F., Fadda, E. and Bakhrjy, F. (2013). Assessing temporal and spatial variations in atmospheric dust over Saudi Arabia through satellite, radiometric, and station data. Journal of Geophysical Research: Atmospheres, 118(23), pp.13,253-13,264.

Zhao, C., van Heeswijk, M. and Karhunen, J. (2016). Air quality forecasting using neural networks. 2016 IEEE Symposium Series on Computational Intelligence (SSCI), doi:10.1109/ssci.2016.7850128

Zhao, X. (2015). Satellite Observed Aerosol Optical Thickness and Trend around Megacities in the Coastal Zone. Advances in Meteorology, 2015, pp.1-7, doi: 10.1155/2015/170672

Websites

- NASAUDI ARABIA. 2017. AERONET. Retrieved from https://aeronet.gsfc.naSaudi Ara-bia.gov/new_web/Documents/Aerosol_Optical_Depth.pdf
- NASAUDI ARABIA. 2017 FSF Sun Photometer manual Retrieved from https://aeronet.gsfc.naSaudi Arabia.gov/new_web/man_data.html

  http://fsf.nerc.ac.uk/instruments/cimel.shtml

- MODIS (or Moderate Resolution Imaging Spectroradiometer)

  https://modis.gsfc.naSaudi Arabia.gov/about/

- https://terra.naSaudi Arabia.gov/
- https://modis.gsfc.naSaudi Arabia.gov/about/media/modis_brochure.pdf
- https://en.wikipedia.org/wiki/Convection%E2%80%93diffusion_equation
- https://www.mathworks.com/help/nnet/gs/neural-network-time-series-prediction-and-modeling.html
- https://en.wikipedia.org/wiki/Artificial_neural_network

http://elte.prompt.hu/sites/default/files/tananyagok/AtmosphericChemistry/ch09s02.html

American Environmental Protection Agency (EPA). (2018). What are the Air Quality Standards for PM? Accessed on https://www3.epa.gov/region1/airquality/pm-aq-standards.html

Australian Government. Department of the Environment and Energy. (2018) accessed on 20/06/2018 on http://www.npi.gov.au/resource/particulate-matter-pm10-and-pm25

Google Maps. (2018). https://www.google.com/maps

http://eprints.kfupm.edu.sa/140015/1/LAWAL_TAOREED_TAIWO_MS_THESIS.pdf [Accessed 1 Oct. 2017].

https://www.ic.gov.sa/media/1294/industrial_investor_guide.pdf

Wikipedia. (2018). Jubail. Retrieved from https://en.wikipedia.org/wiki/Jubail

Wikipedia. (2018). King Abdullah University for Science and Technology. Retrieved from:https://en.wikipedia.org/wiki/King_Abdullah_University_of_Science_and_Technology

Wikipedia. (2018). Solar Power in Saudi Arabia. Retrieved from https://en.wikipedia.org/wiki/Solar_power_in_Saudi_Arabia

VITAE

Name :Mohammed Hamoud Al-Otaibi

Nationality :Saudi

Date of Birth :4/5/2019

Email :mood1408@hotmail.com

Address :Jubail 31961, Saudi Arabia

Education

- Master's Degree: Environmental Science. GPA 3.29/4

  King Fahd University of Petroleum and Minerals, KSA

- Bachelor's Degree: Chemical Engineering GPA 4.29/5

  Riyadh Collage of Technology, KSA

Publications and presentations at conferences

- Morphological, Mineralogical and Elemental Characteristics of Particulate Matter (PM10) over the Industrial Zone in the Eastern Province of Saudi Arabia. (Accepted by in European Geosciences Union Conference 2019)
- Analysis of the Long Rang Seasonal Variability of Aerosol Optical Properties over United Arab Emirates (UAE) using Satellites and Weather Stations Measurements. (Submitted).
- Integrated Meteorological and Space-borne analysis of Aerosols Long-term variability and Optical Properties over the United Arab Emirates (UAE). (Submitted).
- Statistical analysis of aerosols trends and characteristics over central Saudi Arabia using Solar Village AERONET data (1999-2014). (Prepared)

Work Experience

- Working at Saudi Iron & Steel Company (HADEED / SABIC) as Environment, Health & Safety Engineer. February, 2013- Present

Certifications:

- NEBOSH International General Certificate in Occupational Safety & Health with CREDIT grade. Aug 2018
- Certified trainer of defensive driving course by National Safety Council (NSC). Mar 2017
- Radiation Safety Officer (RSO) License by King Abdullah City for Atomic and Renewable Energy (KACARE). Jan 2017
- IEMA Practitioner Certificate with DISTINCTION grade by Institute of Environmental Management and Assessment. Jun 2016
- Advanced Safety Certificate by National Safety Council (NSC). Dec 2014
- Engineering Accreditation Certificate by Saudi Council of Engineers. Jan 2013